# Third Korea-Japan Mini-Symposium on Modeling and Measurement of Hydraulic Flows

Presentation Material

Department of Civil Engineering
Kobe University,

March 16, 2012

Program

# Third Korea-Japan Mini-Symposium on Modeling and Measurement of Hydraulic Flows

March 16, 2012
Room 125, Natural Science Building No.3, Kobe University

9：40— 9：50 Opening

9：50—10:25 Choi, S.-U., Yonsei University
Numerical prediction of sediment load in a river using the lateral distribution method

10：25—10:50 Kawahara, Y., Hiroshima University
Effects of vegetation over floodplain on flow resistance and velocity distribution in a compund channel

10：50—11:15 Uchiyama, Y. and Ishii, T., Kobe University
Nearshore dispersion of the radioactive cesium 137 leaked from the Fukushima I Power Plant

11：15—11:50 Hwang, J. H., Dongguk University
Energy growth and anisotropic characteristics in a buoyancy activating turbulence

11：50—13:00 Lunch Break

13：00—13:25 Wells, J.C., Ritsumeikan University
Estimating subsurface flow fields from surface flow quantities

13：25—13:50 Nakayama, A., Kobe University
Kobe University LES Code (KULES) - its capabilities and applications

13：50—14:25 Paik, J., Kangnung-Wonju National University
Some numerical and experimental investigations of stratified shear flows

14：25—15:00 Coffee Break

15：00—15:25 Kouchi, Y., Chugoku Electric Power Co.
URANS and LES computations of channel flows with triangular roughness on side walls

15：25—15:50 Fujita, I., Kobe University
Efficient method for river surface flow measurements

15：50—16:25 Lee, S. O., Hongik University
3D CFD simulation in Reverse Electrodialysis for Electrical Power Generation from Sea and River

16：25—16:50 Yokojima, S., Mashiko, T., Matsuzaka, T. and Miyahara, T., Shizuoka University
Collision statistics of Lagrangian particles in isotropic turbulence

# Numerical Prediction of Sediment Load in a River using Lateral Distribution Method

March 16, 2012

Sung-Uk Choi

Department of Civil & Environmental Engineering
Yonsei University

## Background

- We're in the process of developing 3D numerical model that is capable of simulating sediment transport in the river and resulting morphological change.
- Assessment of the morphological change requires prior knowledge on sediment transport

## Research Needs

- Sediment run off will increase due to development thoughtless for the environment
- Sediment load in the river will increase
- A model to predict total sediment load is necessary

- The model can be utilized to predict morphological change of the river and reservoir sedimentation
- It can also provide information to compliment for measurement data.

## Increase of Sediment Run Off due to Residential Land Development

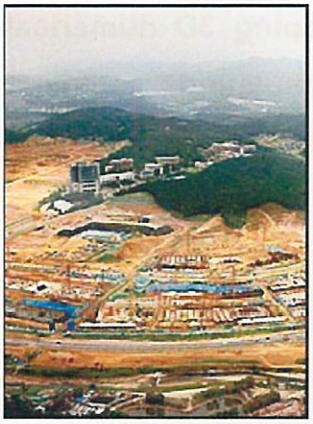

- In July 2000, the Taancheon stream was buried due to sediment over supply from the residential land development site.
- Many construction companies were building about 200 high story apartments at 100 m form MSL.
- Run off increased by land development was not reflected in the drainage system for the site.

# Current Status of Reservoir Sedimentation (류태상 등, 2010)

## For dams more than 20 yrs old in Korea

| 구 분 | 총저수량 (백만㎥) | 유효저수량 (백만㎥) | 담 수 년 도 | 퇴사량 | | 저수용량감소율 | | 비퇴사량 | | |
|---|---|---|---|---|---|---|---|---|---|---|
| | | | | 조사년도 | (백만㎥) | 총저수량대비 | 유효저수대비 | 설계 | 실측 | 대비 |
| 소양강 | 2,900 | 1,900 | '72년 | '06년 | 82 | 2.83% | 4.32% | 500 | 914 | 183% |
| 충 주 | 2,750 | 1,789 | '84년 | '08년 | 130 | 4.73% | 7.27% | 1,000 | 853 | 85% |
| 안 동 | 1,248 | 1,000 | '75년 | '08년 | 6 | 0.48% | 0.60% | 133 | 109 | 82% |
| 합 천 | 790 | 560 | '88년 | '02년 | 8 | 1.01% | 1.43% | 695 | 639 | 92% |
| 남 강 | 309 | 300 | '98년 | '04년 | 13 | 4.21% | 4.33% | 450 | 350 | 78% |
| 대 천 | 1,490 | 790 | '80년 | '06년 | 81 | 5.44% | 10.25% | 300 | 616 | 205% |
| 섬진강 | 466 | 370 | '65년 | '83년 | 19 | 4.08% | 5.14% | 500 | 459 | 92% |
| 주암(본) | 457 | 352 | '90년 | '03년 | 5 | 1.09% | 1.42% | 400 | 469 | 117% |
| 주암(조) | 250 | 210 | '90년 | '03년 | 2 | 0.80% | 0.95% | 400 | 1,089 | 272% |
| 계 | 10,660 | 7,271 | | | 346 | 3.25% | 4.76% | | | |

- Total sediment yield from 9 dams during last 10 yrs is 346 million $m^3$, which is 6-7 times larger than the total storage Boohang dam and Whabook dam currently under construction.
- Sediment yield from Daecheong dam changes from 114 $m^3/km^2/yr$ in 1991 to 616 $m^3/km^2/yr$ in 2006 (5.4 times increases)

# Mississippi River, USA



- Sedimentation due to flood threatens navigation
- Flood on June, 2011 narrowed the width of southwest path from 228 m to 60 m, which makes it difficult to keep the navigable depth of 13.7 m

# Research Objective

- To propose a numerical algorithm of predicting total sediment load (bedload and suspended load) based on the lateral distribution method, which may replace 1D approach that cannot account for geometric distribution of discharge

# 1D Approach for Total Load

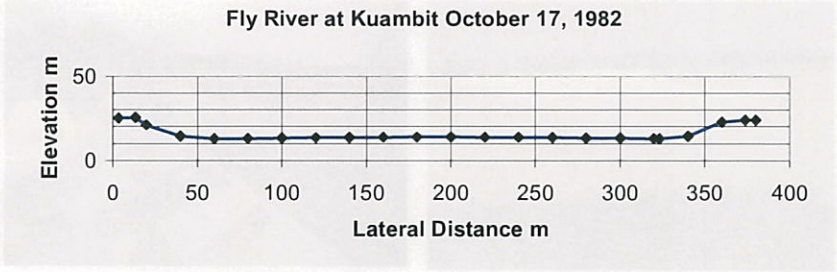


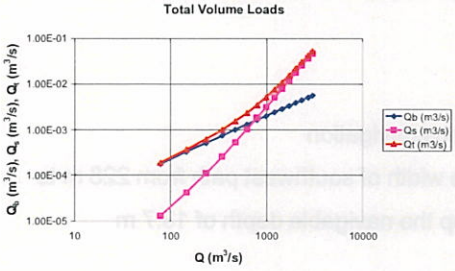


- 1D uniform flow in a rectangular channel is assumed.
- Flow concentration due to channel geometry cannot be taken into account.

## Research Method

- Lateral Distribution Method is used to obtain depth-averaged velocity over the width
- Various bedload formulas are tested and used
- Rousean distribution is assumed for suspended sediment with entrainment function
- Total sediment load is predicted

- Predicted total sediment load is compared with measured data

## Assumptions

- Uniform flow without backwater effect

- 1D bedload transport:
- no sediment transport in the lateral direction:
- a wide channel with a negligible slope in the lateral direction

# Lateral Distribution Method

$$ghS = \frac{1}{\rho}\tau_b - \frac{\partial}{\partial y}\left(\nu_t \frac{\partial q}{\partial y}\right) + \frac{1}{\rho}F_{vD}$$

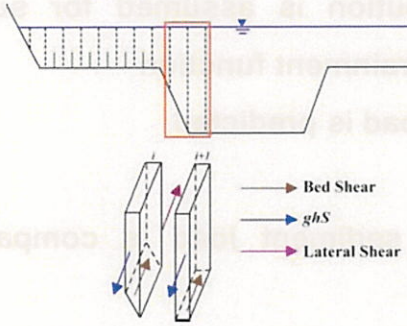


$$\tau_b = \frac{\rho g n^2}{h^{7/3}} q^2$$

$$n = \frac{D_{50}^{\frac{1}{6}}}{21.0}$$

$$\nu_t = \alpha U^* h$$

# Shear Stress Partition

- Bed shear stress is composed of form drag and skin friction
- Only skin friction contributes to sediment transport
- Einstein partition is used

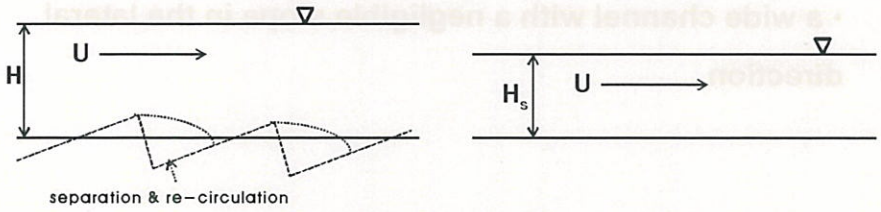


$$\tau_{bs} = \rho g H_s S = \rho C_{fs} U^2$$

# Bedload Formula

- DuBoys type: no bedload if $\tau < \tau_{cr}$

  modified Meyer-Peter and Muller formula

$$q_b^* = 3.97\left(\tau^* - \tau_c^*\right)^{1.5}, \quad \tau_c^* = 0.0495$$

  Ashida and Michiue formula

$$q_b^* = 17\left(\tau^* - \tau_c^*\right)\left(\sqrt{\tau^*} - \sqrt{\tau_c^*}\right), \quad \tau_c^* = 0.05$$

- Exponential function type: exponential decay if $\tau < \tau_{cr}$ from Einstein's approach

$$q_b^* = 12\left(\tau^*\right)^{3/2} \exp\left(-4.5\frac{\tau^*}{\tau_c^*}\right), \quad \tau_c^* = 0.055$$

# Modified Meyer-Peter Muller Formula

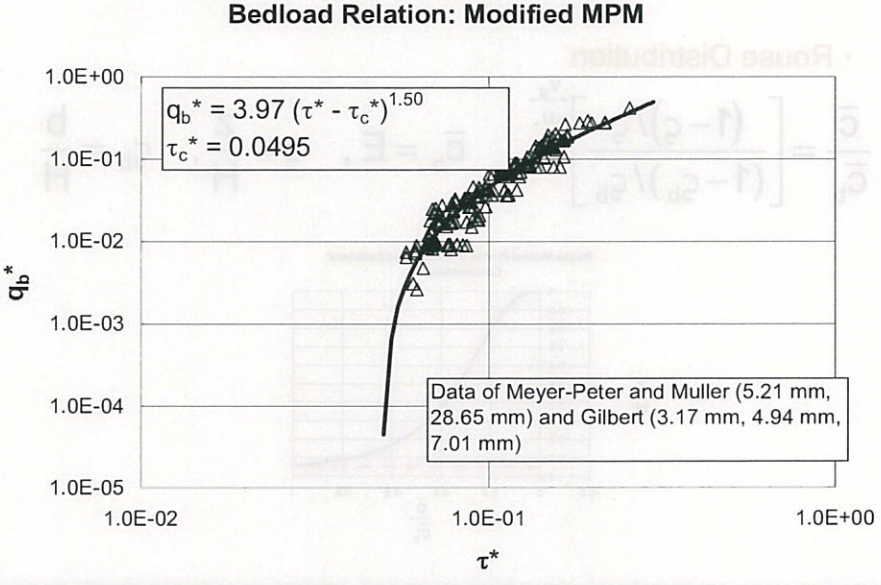

# The Paper by Wong & Parker

## Reanalysis and Correction of Bed-Load Relation of Meyer-Peter and Müller Using Their Own Database

Miguel Wong[1] and Gary Parker[2]

**Abstract:** The pioneering predictor of fluvial bed-load transport rate proposed by Meyer-Peter and Müller in 1948 is still extensively used in basic research and engineering applications. A review of the basis for its formulation reveals, however, that an unnecessary bed roughness correction was applied to cases of plane-bed morphodynamic equilibrium. Its inclusion followed a flow resistance parameterization in terms of the Nikuradse roughness height, which has been shown (well after the publication of their work) to be inappropriate for the characterization of mobile bed rough conditions in rivers. Removing the unnecessary correction and incorporating an improved correction of the boundary shear stress due to sidewall effects allow elucidation of the most parsimonious form of the bed-load relation of Meyer-Peter and Müller that is dictated by their own data set. The new predictor is presented in terms of two alternative power law forms. These amended forms show that, in the case of lower-regime plane-bed equilibrium transport of uniform bed sediment, the new estimates of volume bed-load transport rates are less than or equal to half the values that would be obtained with the original relation of Meyer-Peter and Müller in the absence of the unnecessary bed roughness correction. The meticulous database and clear analysis of the original work of Meyer-Peter and Müller greatly aided the present writers in their reanalysis, which liberally uses the hindsight offered by 58 years of subsequent research.

**DOI:** 10.1061/(ASCE)0733-9429(2006)132:11(1159)

**CE Database subject headings:** Bed load; Boundary shear; Flow resistance; Friction; Bedforms; Flumes.



# Suspended Load (1)

- Rouse Distribution

$$\frac{\bar{c}}{\bar{c}_b} = \left[\frac{(1-\varsigma)/\varsigma}{(1-\varsigma_b)/\varsigma_b}\right]^{\frac{v_s}{\kappa u_*}}, \quad \bar{c}_b = E, \quad \varsigma = \frac{z}{H}, \quad \varsigma_b = \frac{b}{H}$$

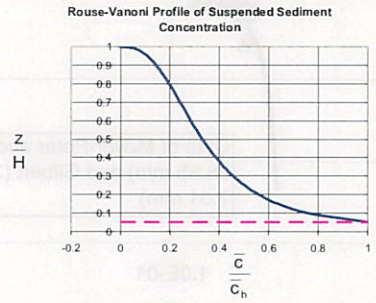

# Suspended Load (2)

- Entrainment Function (Garcia & Parker, 1991)

$$E_{ui} = \frac{E_i}{F_i} = \frac{AZ_{ui}^5}{1 + \frac{A}{0.3} Z_{ui}^5} \quad , \quad Z_{ui} = \lambda_m \frac{u_{*s}}{v_{si}} \mathbf{Re}_{pi}^{0.6} \left( \frac{D_i}{D_{50}} \right)^{0.2} \quad , \quad \mathbf{Re}_{pi} = \frac{\sqrt{RgD_i}\, D_i}{\nu}$$

$$\lambda_m = 1 - 0.298\sigma \quad , \quad A = 1.3 \times 10^{-7}$$

- Entrainment Function (Wright & Parker, 2004)

$$Z_{ui} = \lambda_m \left( \frac{u_{*s}}{v_{si}} \mathbf{Re}_{pi}^{0.6} \right) S^{0.08} \left( \frac{D_i}{D_{50}} \right)^{0.2} \qquad A = 7.8 \times 10^{-7}$$

amended for various streams including large, low slope streams

# Suspended Load (3)

- Suspended Sediment Load per Unit Width

$$q_s = \int_0^H \overline{u}\,\overline{c}\,dz \cong \int_b^H \overline{u}\,\overline{c}\,dz \qquad \overline{c} = E \left[ \frac{(1-\varsigma)/\varsigma}{(1-\varsigma_b)/\varsigma_b} \right]^{\frac{v_s}{\kappa u_*}} \quad , \quad \varsigma = \frac{z}{H} \quad , \quad \varsigma_b = \frac{b}{H}$$

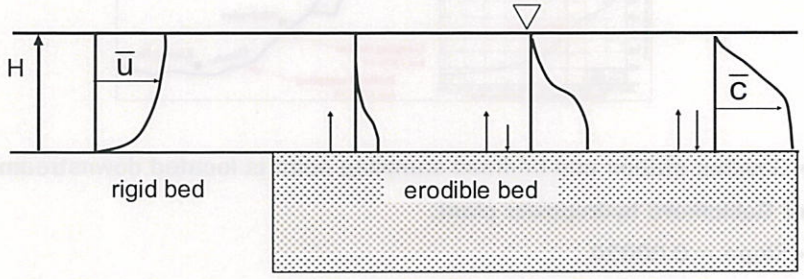

# Applications

- Bedload transport
  - The Danube River, Slovakia
- Total Sediment load transport
  - The South Han River, Korea

# Application 1: The Danube River, Slovakia


- Gauging station and bedload sampling point is located downstream of Gabicikovo hydropower plant.
- Slope = 0.00020

# Grain Size Distribution

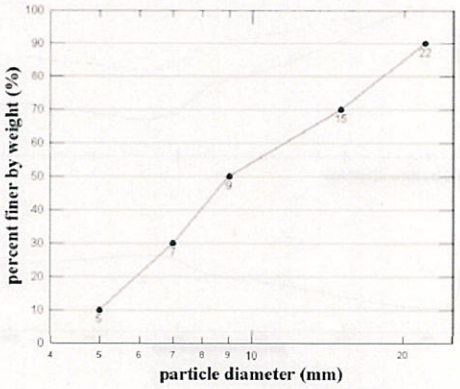


- D50: 9 mm MG (n = 0.0217 from MS) Gravel bed river
- D90: 22 mm

# Cross Section of the Sampling Station

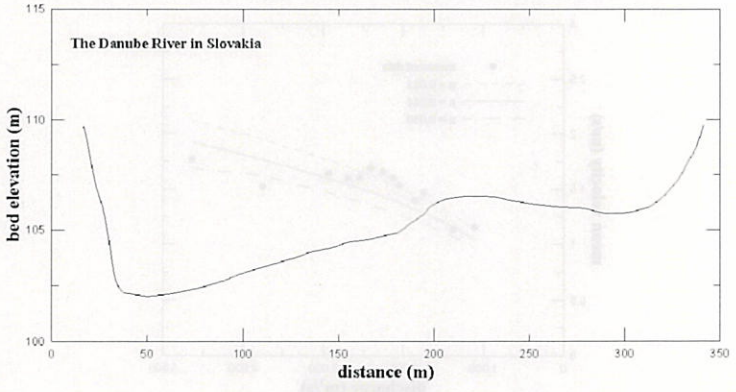


- Survey data on November, 2001
- Slight asymmetry, left side deep and right side shallow

# 유속 및 단위폭당 유량 분포

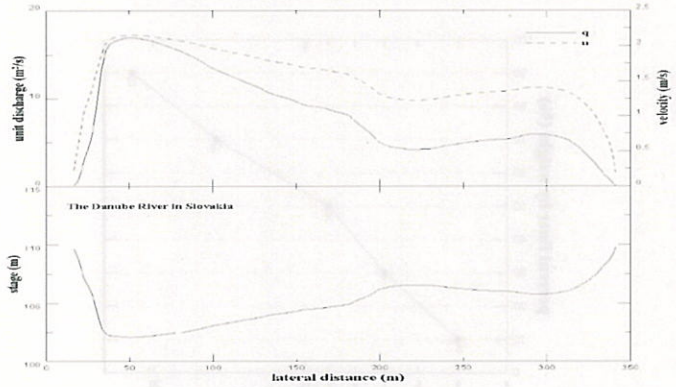


- U and q distributions for Q 4,743 cms
- U and q are not uniform across the width due to geometric distribution
- The pt. of maximum discharge does not move for different discharge because secondary currents are not taken into account.

# Roughness Coefficient

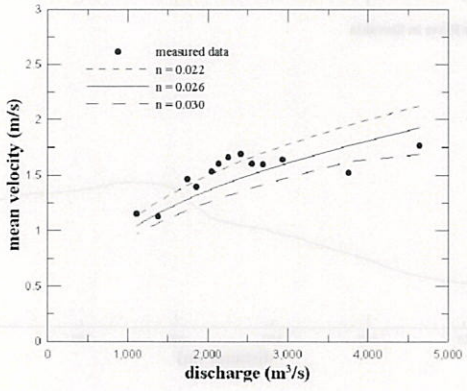


- Best matched when n = 0.026
- This is slightly larger than n from MS, which is due to bedform, change of width, and meandering.

# Distribution of Bedload

MMPM formula

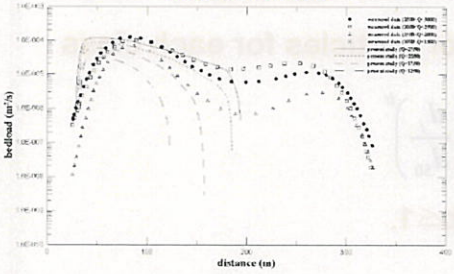


C-L formula

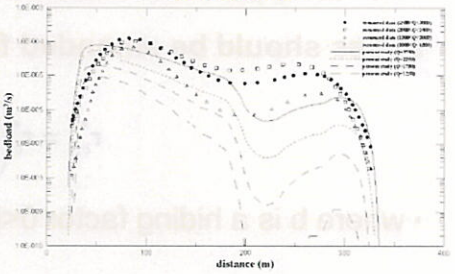


- Effective roughness height ks = 2.0D90, suggested by Camenen et al, is used.
- Limitation of using DuBoys type formula is clearly seen.
- Exponential type formula still under-predict bedload on RHS.

# Total Bedload

MMPM formula

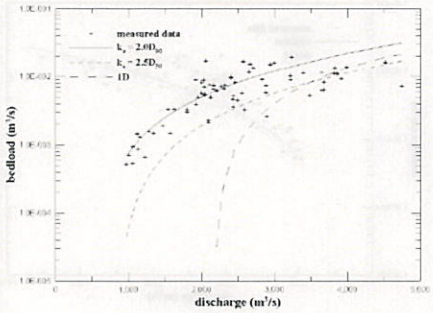


C-L formula

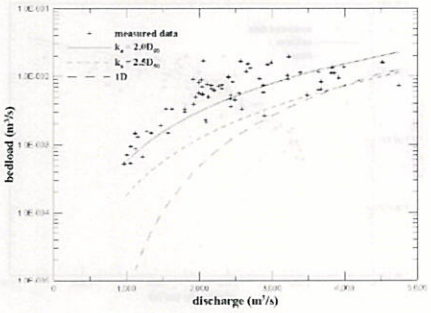


- Relative errors (MMPM: 0.571, CL: 0.418) when ks = 2.0D90 used.
- When ks = 2.5D50 used, MMPM under-predicts by the factor of 3.1 and CL 2.4.
- The 1D approach is found to under-predict total bedload is seriously, specially for low flows because….

# Mixture Effect

- To consider the mixture effect, the critical shear stress should be amended for particles for each class

$$\tau^*_{c,j} = \tau^*_c \left( \frac{d_j}{d_{50}} \right)^b$$

- where b is a hiding factor $0<b\leq 1$.

- Ferguson et al. (1989): b = 0.12
- Wilcock and Crowe (2003): $b = 0.67/[1+\exp(1.5-d_j/d_{50})]$

# Mixture Effect

MMPM formula

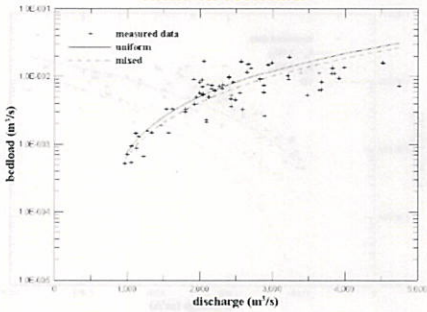


C-L formula

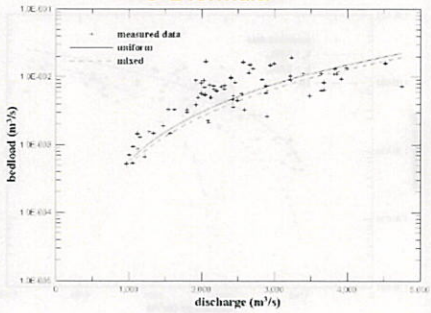


- The hiding factor by Wilcock & Crowe is used.
- MMPM predicts total bedload 20% less when mixture effect is considered, and CL 16% less.
- The trend is consistent with that in Camenen et al. (2011).

# Application 2: The South Han River

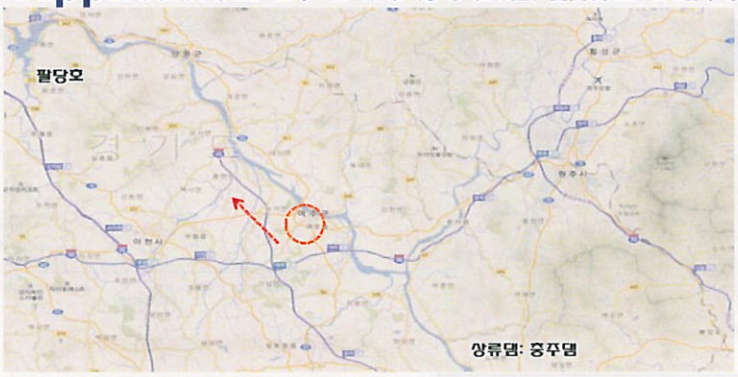


• Suspended sediment was sampled at Old Yeojoo Br. located downstream of Choongjoo Dam and upstream of Paaldang Dam.

# Sampling Suspended Sediment

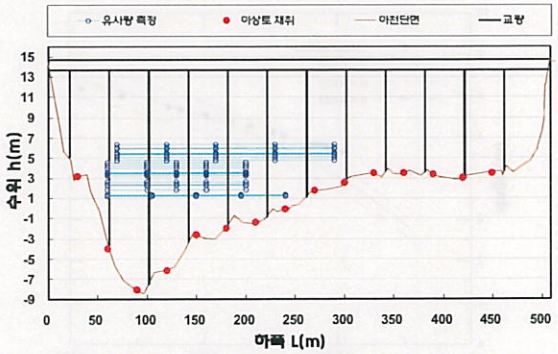


• Suspended sediment samplers such as D-74 and P-61 were used.

• Bed material sampler BM-54 were used.

• Using modified Einstein method, the total sediment load is estimated with sampled suspended sediment load.

# Grain Size Distribution of Bed Materials

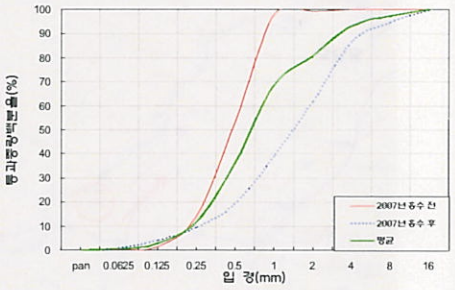


| sampling time | $D_{50}$ (mm) | $D_{65}$ (mm) | $D_{90}$ (mm) |
|---|---|---|---|
| before flood (March) | 0.48 | 0.63 | 0.87 |
| after flood (November) | 1.40 | 2.25 | 4.91 |
| average | 0.67 | 0.93 | 3.34 |

- Bed sediment particles were coarsened after the flood.
- Average of $D_{50}$ before & after the flood: 0.68 mm (CS), indicating sand bed river
- Slope of WS: 0.000175

# Calibration of Roughness Coefficient

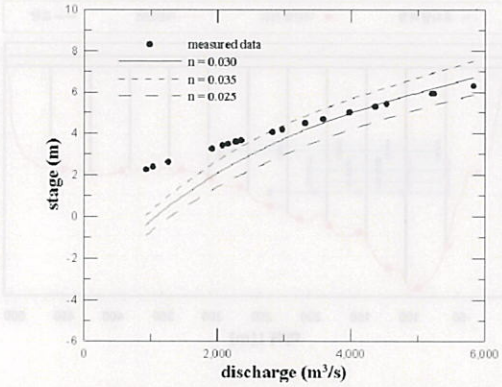


- LDM cannot reproduce the stage-discharge curve properly, specially when Q < 3,000 cms. This may be due to backwater.
- Best match when n = 0.035 (n = 0.014 from MS formula)

# Unit Discharge and Velocity

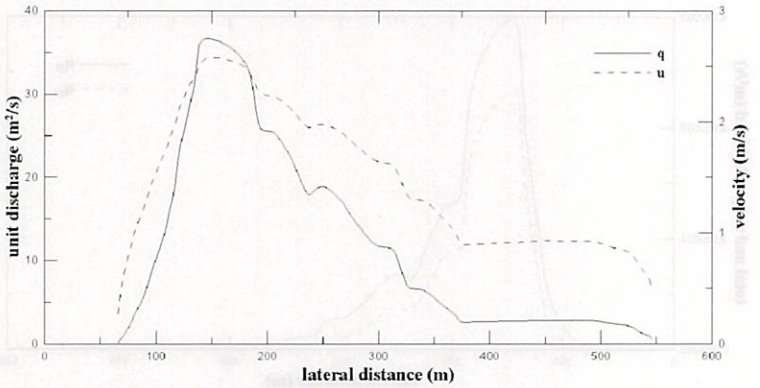


- Distribution for Q = 5,827 cms and h = 6.7 m
- Velocity at the deepest point is more than three times larger than velocity at the RHS of the channel.

# Flow Depth Partition due to Bedform

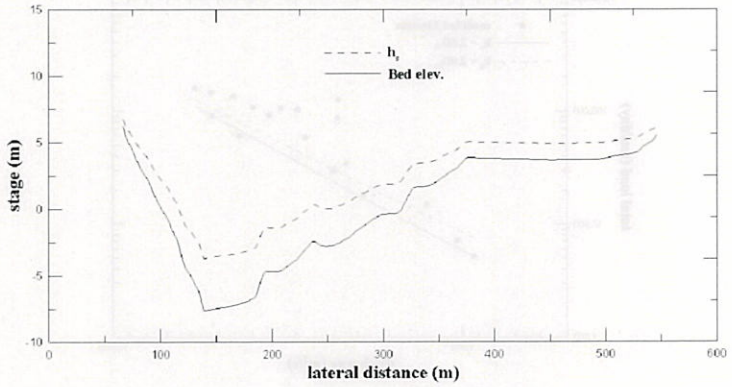


- About 30% of the total flow depth is due to skin friction.

# Distribution of Total Sediment Load

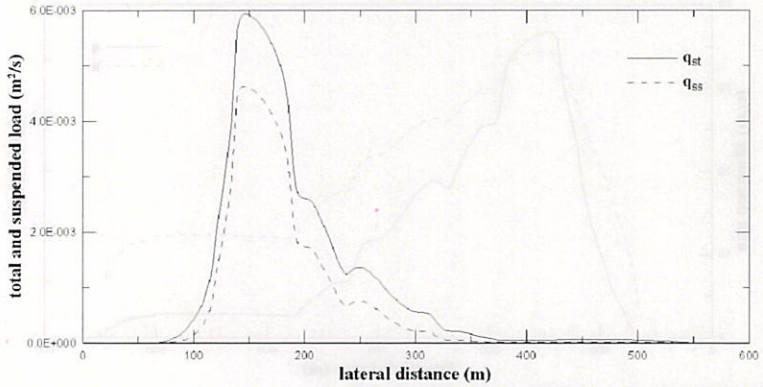


- About 33% of the total sediment load is bedload.

# Comparison with Estimated Total Load

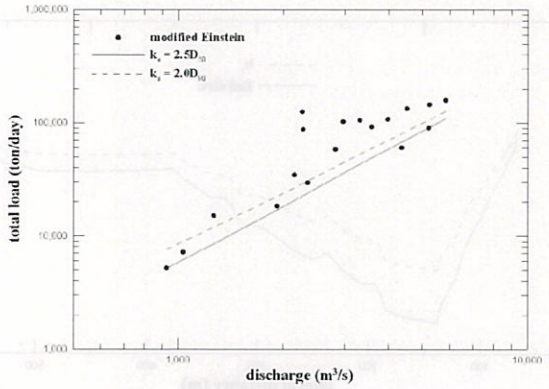


- For ks = 2.0D90, the predicted total load is about 81% of that estimated by EM.
- For ks = 2.5D50, the predicted is about 64% of estimated total load.

# MIXTURE EFFECT

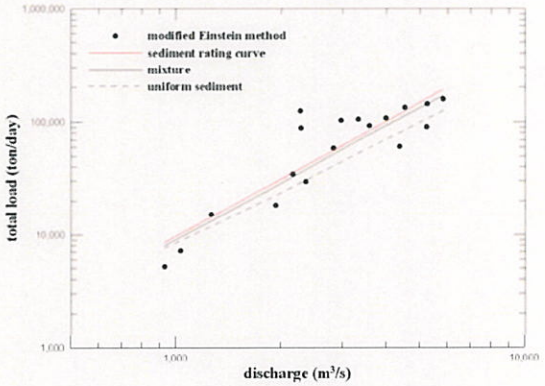


- Including the mixture effect enhances the prediction.

# Effects of vegetation over floodplain on flow resistance and velocity distribution in a compound channel

**Yoshihisa KAWAHARA**
Dept. of Civil and Environmental Engineering
**Hiroshima University**

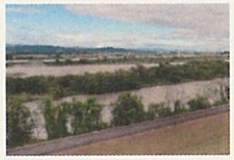

Vegetation in a river

The Ohta River flowing through Hiroshima City



# Background (1)

- Most of big rivers in Japan are designed to have a compound cross-section in their lower parts.
- Plants that can grow on bars, on floodplains and at the bank toe.
- Vegetation in rivers has been considered as a source of flow resistance, and hence, vegetation has been frequently removed to increase the flood-carrying capacity.

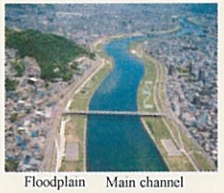

Floodplain Main channel

Cutting vegetation over floodplain

Vegetation growth in the Hii River



# Background (2)

- Vegetation is regarded as a means to preserve or create different habitats suitable for biodiversity.
- Vegetation exerts significant effects on morphological behaviors of alluvial channels by stabilizing banks and channels.

The Hikichi River

21 years later

Invasion of vegetation into floodplain



# Objectives

- To reveal the flow characteristics, such as flow resistance and velocity distributions, in a compound channel in the presence of floodplain vegetation.
- To clarify the performance of a numerical model, consisting of a nonlinear k-ε model and a vegetation model for turbulent flows in a straight compound channel with a vegetated floodplain.

- Flume experiments have been done under different vegetation layout over a floodplain.
- Unsteady RANS has been carried out for turbulent flows in vegetated compound channels.

# Experimental Setup

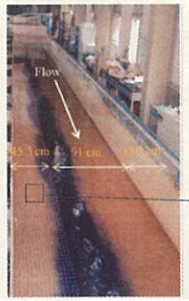


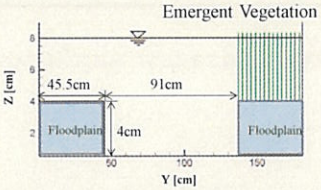


Sectional View

**Channel Specification**
- **Total length:** 2200cm
- **Total width:** 182cm
- **Floodplain width :** 45.5cm
- **Floodplain height:** 4cm
- **Bed slope:** 1/500

**Model vegetation**
- **Height:** 5cm
- **Diameter:** 3mm
- **Material:** Hard wood

**Measurement equipments**
- **Velocity components:** Electromagnetic current meter
- **Water level fluctuation:** Water level gauges (frequency 10Hz).

Hiroshima University

# Experimental Conditions (1)

| Case | Discharge (l/s) | Water Depth (cm) | Bulk Velocity (cm/s) | Vegetation Layout |
|---|---|---|---|---|
| Case 0 | 30.0 | 7.4 | 30.5 | No vegetation |
| Case 1 | | 8.0 | 27.5 | Fully covers one floodplain |
| Case 2 | | 7.9 | 27.9 | Vegetation belt (three rows) along the edge of one floodplain |
| Case 2-a | | 7.5 | 30.0 | Vegetation belt (one row) along the edge of one floodplain |
| Case 3 | | 7.3 | 31.1 | Vegetation patches (three rows) along the edge of one floodplain |

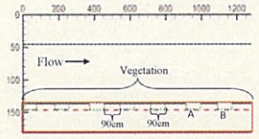


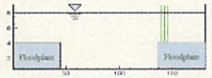


Hiroshima University

# Experimental Conditions (2)

To obtain the stage-discharge (H-Q) curve, additional experiments were carried out with different separated vegetation zones, with keeping three rows of vegetation.

| Case | Length (cm) | Distance (cm) | Comment |
|---|---|---|---|
| Case 3 | 90 | 90 | Three rows of vegetation along the edge of one floodplain |
| Case 3-a | 90 | 30 | |
| Case 3-b | 60 | 60 | |
| Case 3-c | 30 | 30 | |

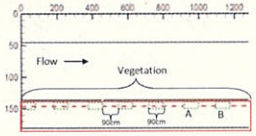


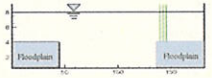


Hiroshima University

# Flow Visualization

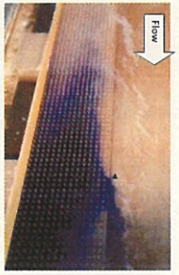




Case 1 Case 2 Case 3

A row of large horizontal vortices develop along the interface of vegetation zones.

Hiroshima University

# Velocity Fluctuation

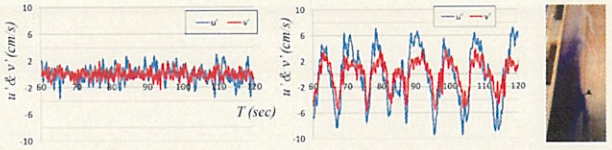


Case 0 [x=900cm, y=137cm, z=6cm]




Case 1 [x=1000cm, y=137cm, z=6cm]



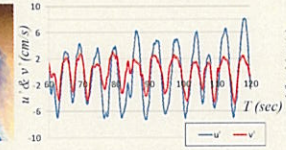


Case 2 [x=1000cm, y=137cm, z=6cm]

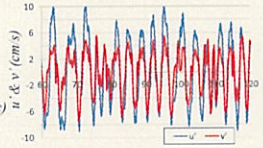


Case 3 [x=980cm, y=137cm, z=6cm]

Hiroshima University

# Energy Spectrum of *u'*

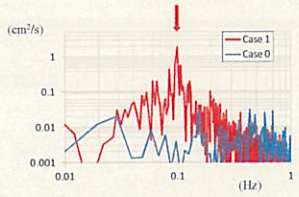


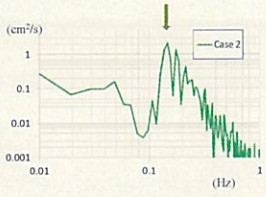


Case 0 [x=900cm], Case 1[x=1000cm]

Case 2 [x=1000cm]

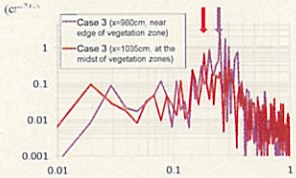


Case 3 [x=980cm, 1035cm]

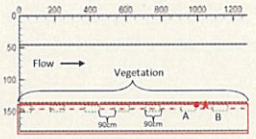


The dominant frequency increases with the decrease of width and length of vegetation zone.

# Stage-Discharge Curve (1)

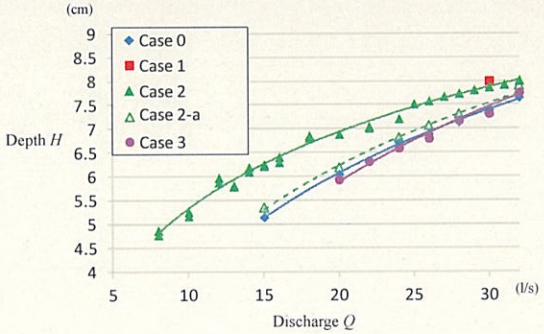


- Smaller row of vegetation along the edge of floodplain gives lower flow resistance.
- Some separated vegetation l zones may give high flood-carrying capacity.

Hiroshima University

# Stage-Discharge Curve (2)

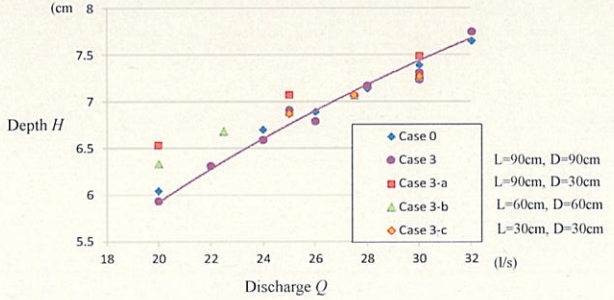


- Flow resistance increases as the distance between vegetation zones decreases with the same length.
- As far as the length and the distance have same ration, the flow resistance takes nearly the same value.

Higher resistance ~ Larger vortices ⟹ Collapse of large vortices by vegetation

# Primary Velocity *U*/*U*m

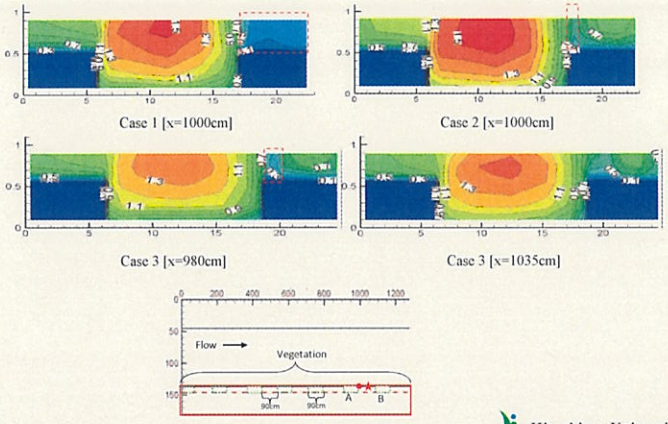


Hiroshima University

# Basic Equations for Double-Averaged Flow

Continuity equation:

$$\frac{\partial U_i}{\partial x_i} = 0$$

Momentum equations:

$$\frac{\partial U_i}{\partial t} + \frac{\partial U_j U_i}{\partial x_j} = g_i - \frac{1}{\rho}\frac{\partial P}{\partial x_i} - \frac{\partial \overline{u_i u_j}}{\partial x_j} + \nu \frac{\partial^2 U_i}{\partial x_j \partial x_j} - \frac{F_i}{\rho}$$

$$F_i = \frac{1}{2} C_D \lambda U_i \left|\vec{U}\right|$$

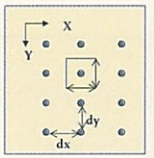


λ= D/dx*dy
D: Diameter of stem

Stresses due to double averaging : Nonlinear ***k*-ε** Model

$$-\overline{u_i u_j} = -\frac{2}{3}k\delta_{ij} + \nu_t S_{ij} - \frac{k}{\varepsilon}\nu_t \sum_{\beta=1}^{3} C_\beta \left( S_{\beta ij} - \frac{1}{3} S_{\beta \alpha \alpha} \delta_{ij} \right), \quad \nu_t = C_\mu \frac{k^2}{\varepsilon}$$

Necessity of the non-linear terms

- Secondary currents of the second kind
- Large horizontal vortices at the interface between main channel and vegetated floodplain

Hiroshima University

# Basic Equations for Turbulence

Transport equations for ***k*** and **ε** :

$$\frac{\partial k}{\partial t} + \frac{\partial U_j k}{\partial x_j} = \frac{\partial}{\partial x_m}\left[\left(\frac{\nu_t}{\sigma_k} + \nu\right)\frac{\partial k}{\partial x_m}\right] + P_{rod} - \varepsilon + F_i U_i - 2C_D \lambda \left|\vec{U}\right| k$$

$$\frac{\partial \varepsilon}{\partial t} + \frac{\partial U_j \varepsilon}{\partial x_j} = \frac{\partial}{\partial x_m}\left[\left(\frac{\nu_t}{\sigma_\varepsilon} + \nu\right)\frac{\partial \varepsilon}{\partial x_m}\right] + C_{\varepsilon 1}\frac{\varepsilon}{k} P_{rod} - C_{\varepsilon 2}\varepsilon + \frac{3}{2}\frac{\varepsilon}{k} F_i U_i - 1.4 C_D \lambda \left|\vec{U}\right| \varepsilon$$

Numerical methods

- The basic equations are discretized by Finite volume method (FVM).
- A fully implicit scheme is used for unsteady terms together with SIMPLE algorithm.
- QUICK scheme is used for the convection terms in the momentum equations, while the Power-law scheme is used for the convection terms in the *k* and *ε* equations.
- Non-equidistant grid system is used with Δt=0.01sec.

Hiroshima University

# Comparison (1) : Case 1

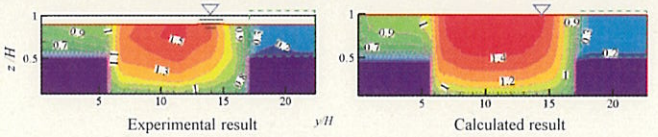


*U*/*U*$_m$-velocity contours at *x*=1000 cm

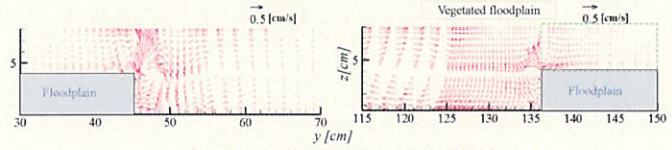


*VW*-velocity vector at *x*=1000cm

- Velocity dip is not captured due to underestimation of secondary currents near free surface.
- The secondary currents near the edge of the floodplain are reasonably reproduced.

Hiroshima University

# Comparison (2) : Case 1

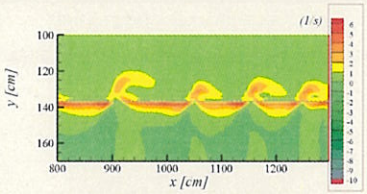


Vorticity in the vertical direction

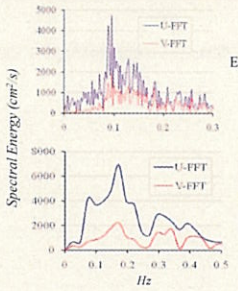


Experimental result

Numerical result

The frequency at the peak is calculated with a slight difference.

Hiroshima University

# Comparison (3): Case 2

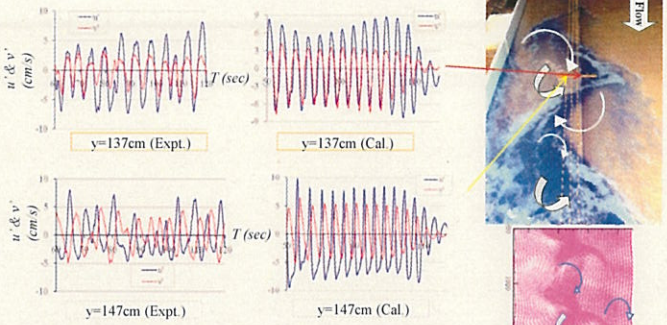





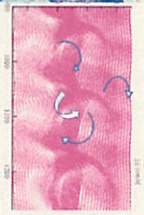

Calculated result

- Fluctuating velocity is reasonably captured by the simulation.
- Phase lag is 0° at y=137cm and 180° at y=147cm, indicating that the fluid parcel with low velocity is supplied from the vegetation zone to the main channel and the floodplain.

# Numerical Study: Stage vs. Vegetation Layout

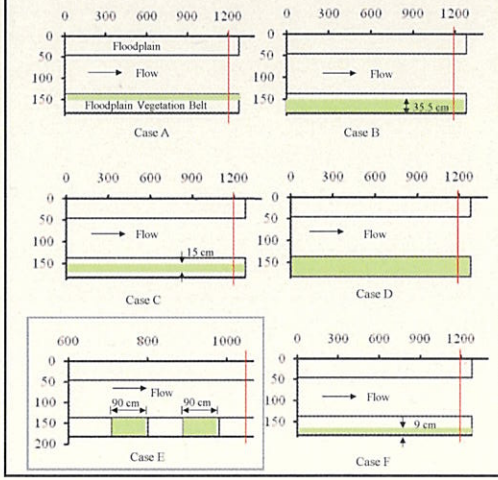


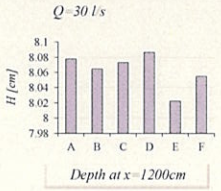


Case E gives the lowest water level across the section.

Numerical results qualitatively agree with the measurements. More detailed analysis is necessary to understand the role of large vortices in flood carrying capacity.

# Summary & Future Research

Experiments

1. Horizontal large vortices develop along the interface between the vegetated floodplain and the main channel. Their scales depend on the size, length and distance of vegetation zones.
2. Some layout of vegetation over a floodplain gives larger flood carrying capacity than the channel without vegetation. This may be related to the change in large vortices.

Numerical Simulations

1. Primary as well as secondary flows and large vortices are reasonably predicted by the present nonlinear k-ε model coupled with a vegetation model.
2. Refined flow models are necessary for the secondary flows near free surface and the large vortices in the presence of vegetation.

# Nearshore dispersion of the radioactive cesium 137 leaked from the Fukushima I Power Plant

Yusuke Uchiyama & Tomomi Ishii
(Kobe University)

*The Third Korea-Japan Mini Symposium on Modeling and Measurements of Hydraulic Flows*,
Kobe, Japan. March 16, 2012

Acknowledgements: Y. Miyazawa (JAMSTEC), D. Tsunume (CRIEPI)

## A tragedy...

The 2011 Tohuku earthquake
14:46 JST, March 11, 2011

- Eplicenter: 70 km off Oshika Penn. (undersea mega-thrust quake), 373 km from Tokyo
- Magnitude 9.0 (recorded most powerful in Japan, 7th in the world)

The quake and aftershocks (3/11-14)

## 26 minutes later...

The *tsunamis* followed the quake.

- 5-8 m upthrust on 180 km wide sea floor, at 60 km offshore
- Inundation and runup height reached 40 m.
- 15,850 deaths (92.5 % drown), 3279 still missing as of now

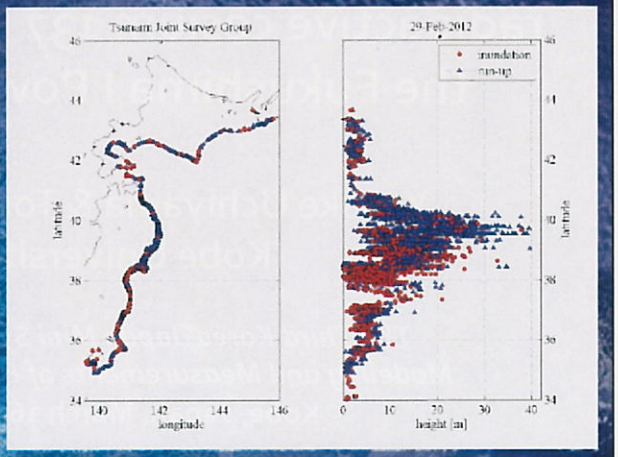


A compiled inundation record (JSCE, CEC)

## The earthquake and the tsunami

## The tragedy continues…

- It survived from the quake, but the tsunamis (13-15 m high)
- The cooling system for the reactors were severely dameged
- Reactors 1, 2 and 3 experienced *full meltdown*
- *Hydrogen explosions* at Reactors 1, 2 and 4


## Global and local impact through atmospheric transport/fallout of cesium 137

Simulated trans-Pacific transport (CEREA, France)

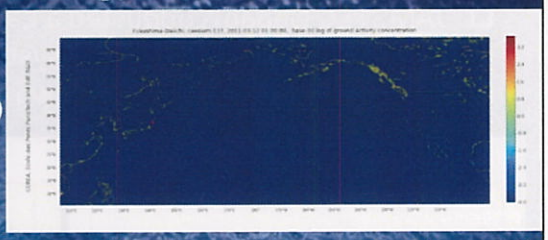

Monitored soil contamination (Ministry of Education, Japan)

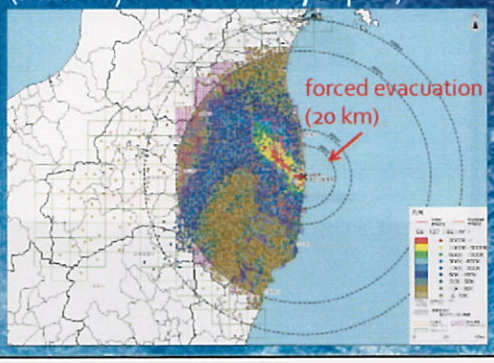


Simulated (Yasunari et al., 2011)

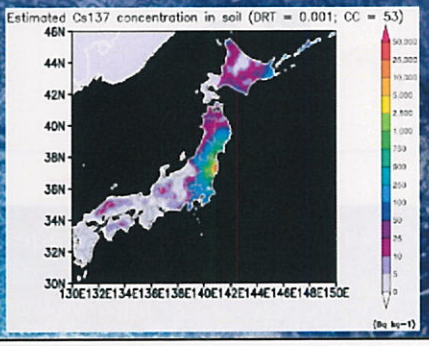

## Oceanic leakage of radioactive substances

- The blasted cooling system was compensated by pouring sea water as coolant
- leaked 3 times in a month and ½ to the ocean
- Visually observed leakage :

4/1~4/6 (Reactor 2)
**4.7 x $10^{15}$ Bq** (4.7 PBq)

?

4/4~4/10 (N & S outfalls)
1.5 x $10^{11}$ Bq (150 GBq)

5/10~11 (Reactor 3)
2.0 x $10^{13}$ Bq (20 TBq)

n.b., aerial release was 3.7 x $10^{17}$ Bq (NISA, Japan)

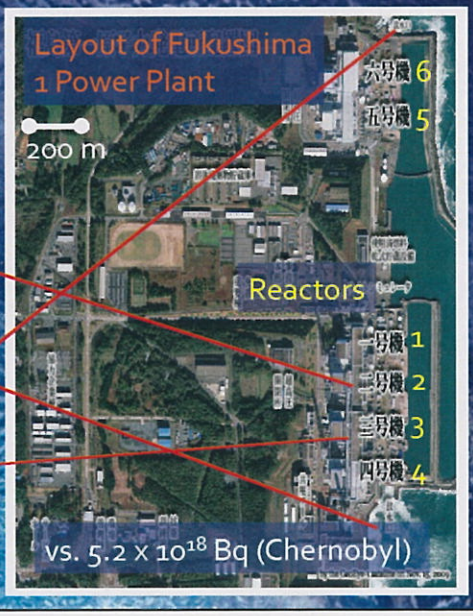


## Oceanic dispersal of cesium 137 (1)

- JAMSTEC (Japan) conducted a Lagrangian float tracking driven by the assimilative "JCOPE2" system at 1/10 deg. resolution.
- Cesium travels *2-3,000 km* in two months --- TRUE?

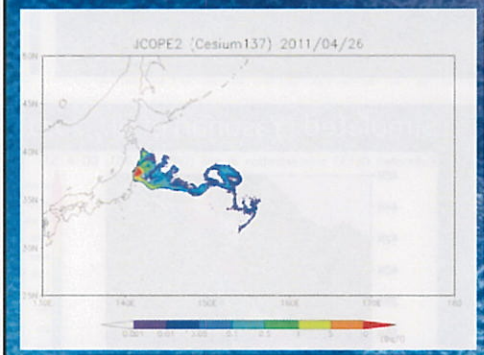


1 month after the leakage

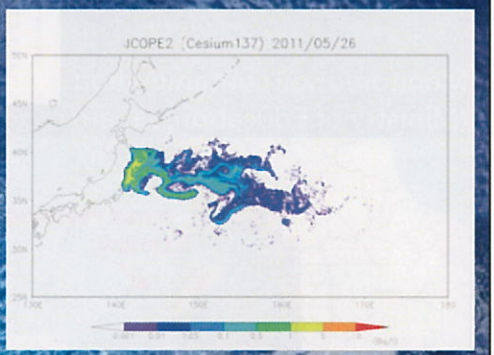


2 month later

http://www.jamstec.go.jp/frcgc/jcope/htdocs/e/fukushima.html

## Oceanic dispersal of cesium 137 (2)

- SIRROCCO/Toulouse Univ. (France) conducted more nearshore-oriented simulation at 0.6 – 5 km stretched horizontal resolution,
- Stayed nearshore by 150 km in the first 1 month, by 400 km in 2 mo.,
- Suggests $^{137}Cs$ may remain near the source,
- Mostly northward transport,
- Argue only surface $^{137}Cs$,
- A crude leakage submodel

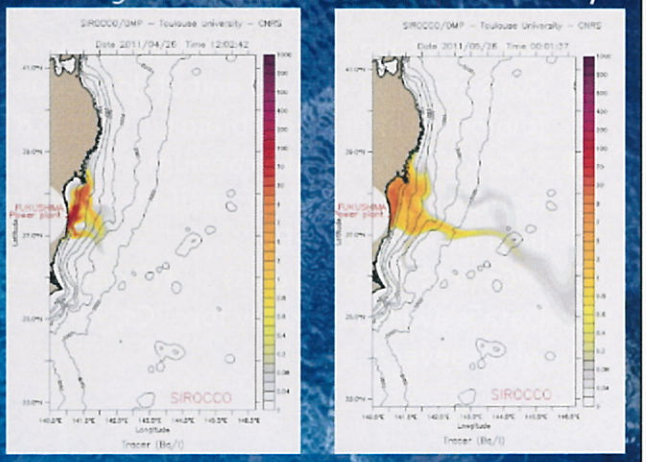


1 month after the leakage — 2 month later

http://sirocco.omp.obs-mip.fr/outils/Symphonie/Produits/Japan/SymphoniePreviJapan.htm

## Oceanic dispersal of cesium 137 (3)

- CREIPI (Japan, in Tsumune *et al.*, 2011) conducted another nearshore simulation at 1 km horizontal resolution
- Sits in nearshore by 150 km in the first 1 month, more than 200 km in 2 moths.
- Estimated total $^{137}Cs$ leakage is **$3.5 \times 10^{15}$ Bq**.
- Mostly southward transport (controversial)
- A very crude topography

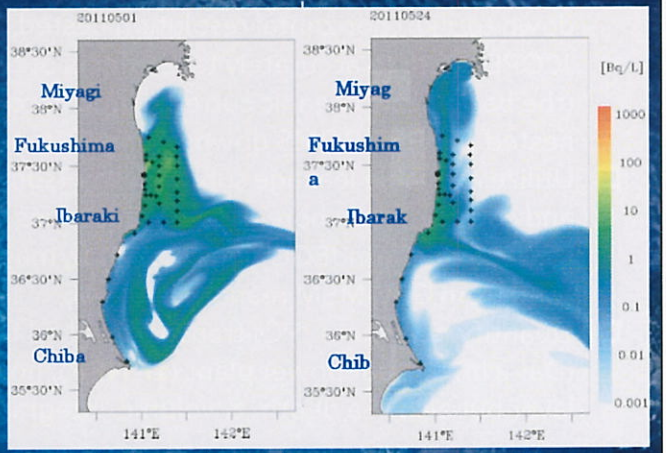


1 month after the leakage — 2 month later

http://criepi.denken.or.jp/jp/kenkikaku/report/detail/V11002.html

## Some terminologies

- Bq (Becquerel): SI-derived unit of radioactivity to measure one nucleus decaying per second. The mean soil contamination in Germany following the Chelnobyl was 2,000 – 4,000 Bq/m$^2$.
- Sv (Sievelt): SI-derived unit of dose equivalent radiation (biological effect). ex) brain CT scan: 0.8 – 5 mSv
- $^{137}$Cs (cesium-137, aka caesium-137): anthropogenic radioactive isotope of cesium with a half-life of 30.17 years, decaying by beta emission to $^{137}$Ba.
- $^{134}$Cs (a ½-life of 2 years) , $^{131}$I (8 days), $^{90}$St (28.79 years)
- Data is available mostly for $^{137}$Cs, while no direct measurement whatsoever.

## Objectives

- Properly account for $^{137}$Cs dispersal in the nearshore,
- Conduct a retrospective high-resolution oceanic modeling at down to 1 km horizontal resolution nested in the assimilative JCOPE2 data to accurately take effects of the Kurohio/Oyashio (the basin-scale oceanic currents) into account using a triply-nested JCOPE2-ROMS downscaling system,
- Utilize a reliable leakage submodel by Tsunume et al. (2011), and consider nearshore oceanic properties such as detailed topography from JEGG-500 (JODC), 14 major rivers, realistic wind from GPV-MSM reanalysis (JMA),
- Quantify nearshore $^{137}$Cs transport leaked from the Fukushima 1 (Dai-ichi) nuclear power plant (**1F NPP**), not only in the surface layer but also in a depth- & volume-integrated sense.

# A triply-nested oceanic downscaling system

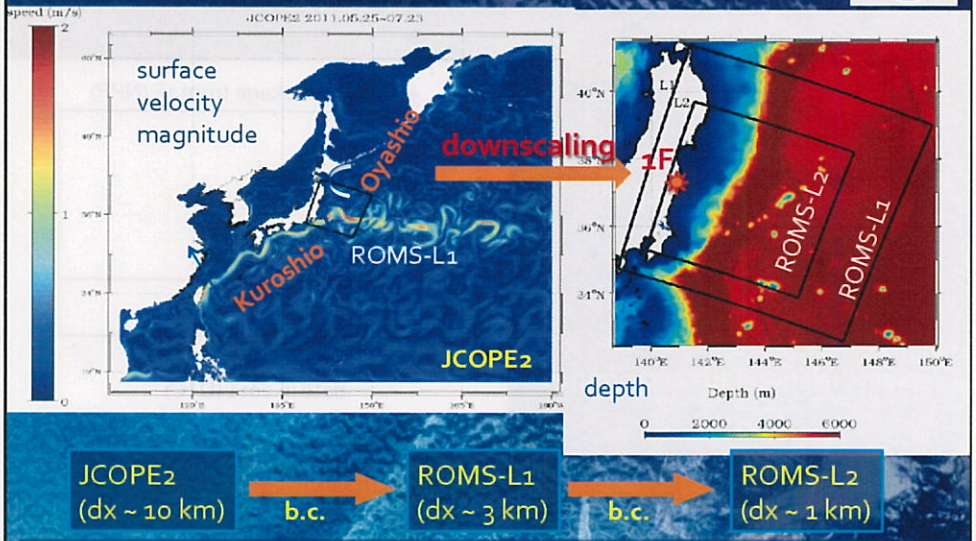


JCOPE2 (dx ~ 10 km) → b.c. → ROMS-L1 (dx ~ 3 km) → b.c. → ROMS-L2 (dx ~ 1 km)

**JCOPE2**: Japan Coastal Ocean Predictability Experiment (POM-based 3D-VAR oceanic database maintained by JAMSTEC; cf, Miyazawa *et al.*, 2009)

# Numerical configuration for ROMS-L2

**ROMS** (Regional Oceanic Modeling System; Shchepetkin & McWilliams, 2005): a state-of-the-art Primitive eq., free-surface, split-explicit, terrain-following, hydrostatic 3-D ocean model.

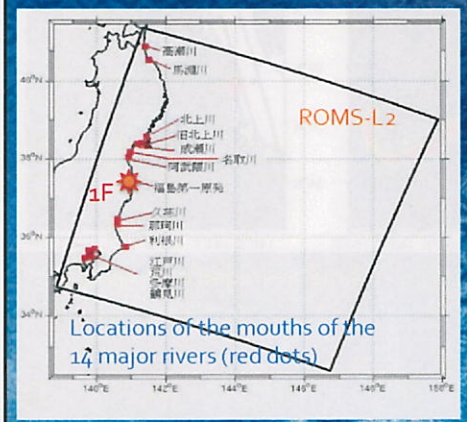


Locations of the mouths of the 14 major rivers (red dots)

| | |
|---|---|
| computational period | Jan. 1, 2011 – Oct. 31, 2011, UTC |
| horizontal grids | 512 × 512 (x 32 vertical) |
| horizontal resolution | 1.0 km |
| vertical gridding (sigma coordinate) | 32 layers (refined near the surface) |
| surface wind stress | **JMA GPV-MSM** (dx ~ 5km, hourly) |
| rad./heat fluxes<br>sea surface temp.<br>river runoff<br>(14 major rivers) | COADS05<br>Pathfinder AVHRR<br>**Precipitation/run-off database** |
| boundary conditions | ROMS-L1 (3km, 12-hourly update) |
| baroclinic time step | 60 sec. |
| topography | JEGG500+SRTM30 |

## $^{137}$Cs leakage submodel (Tsunume *et al.*, 2011)

$^{137}$Cs leakage and its period are *UNKNOWN* (to be specified)

↓

Determine the leakage period based on iodine-131 vs. cesium-137 ratio → **Mar. 26 – Apr. 6, 2011**

↓

Release hypothetical **1.0 Bq/s** $^{137}$Cs outflux at **1F** (Fukushima 1 NPP) to compute relative $^{137}$Cs concentration

↓

Compare the computed relative concentration with the measured one nearest to 1F to evaluate **magnification factor *M***

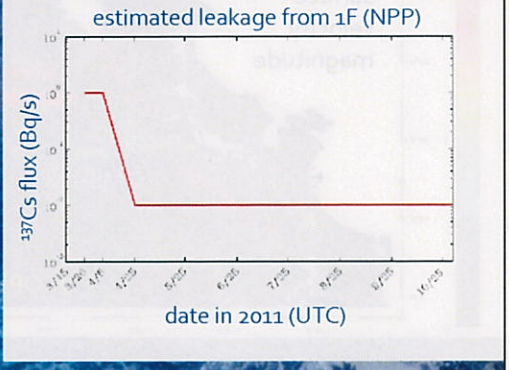


→ $^{137}$Cs concentration = relative concentration x ***M***
(indirect leakage estimation)

## Validation (1): reproduction of *Kuroshio* path

**ROMS-L2 (1 km)**

assimilative JCOPE2 (10 km)

altimeter-derived geostrophic velocity (30 km, AVISO)

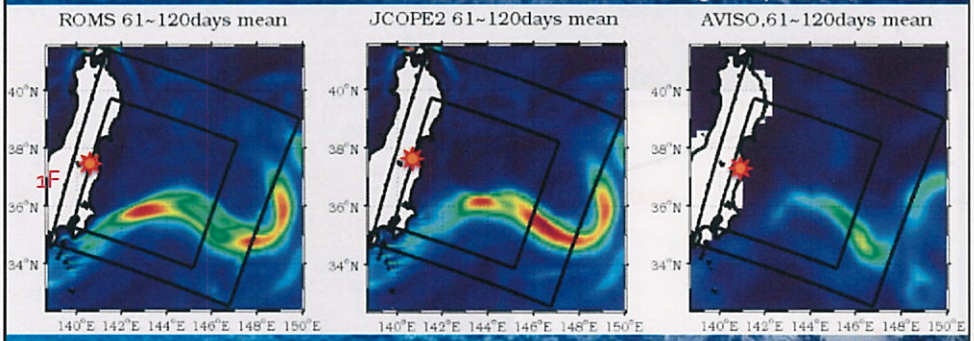


time-averaged over 5/25~7/23

## Validation (2): $^{137}$Cs concentration at 1F

magnification rate
$M = 1.01 \times 10^{10}$

total leakage of $^{137}$Cs: **$1.35 \times 10^{16}$ (Bq)**
cf, $3.5 \times 10^{15}$ (Bq) by Tsunume

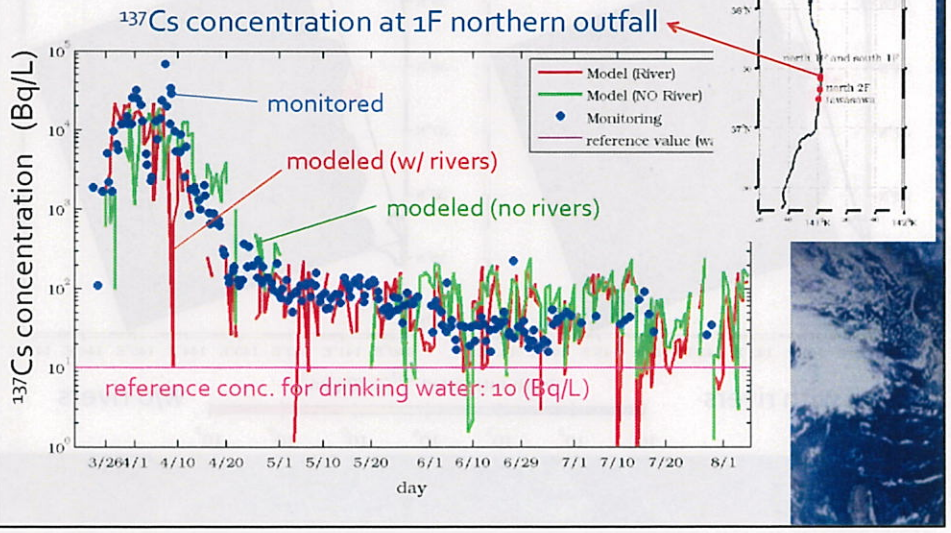


## Validation (3): $^{137}$Cs conc. at Natsuigawa

- substantial improvement with the rivers

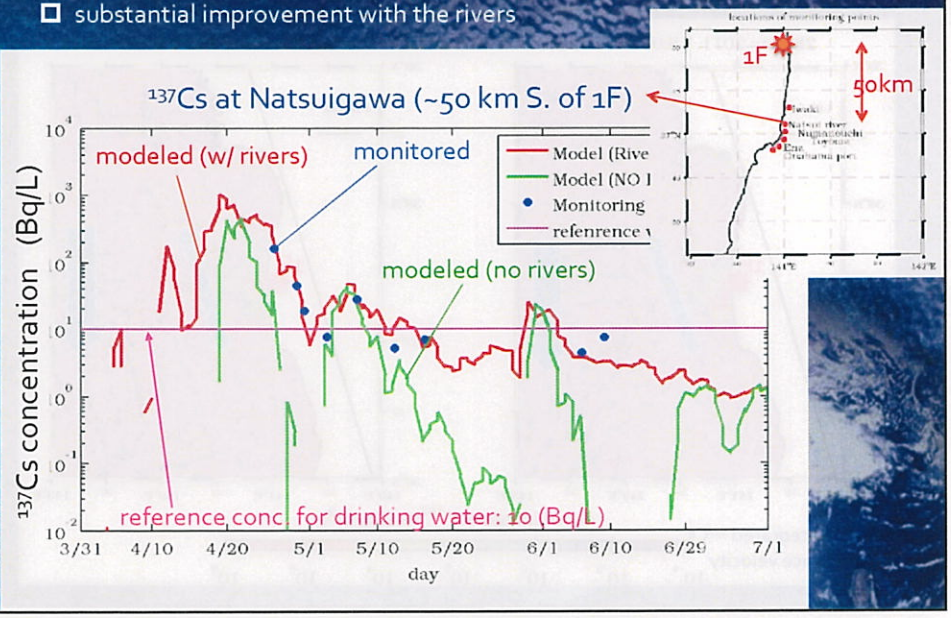

## Depth-integrated $^{137}$Cs concentrations

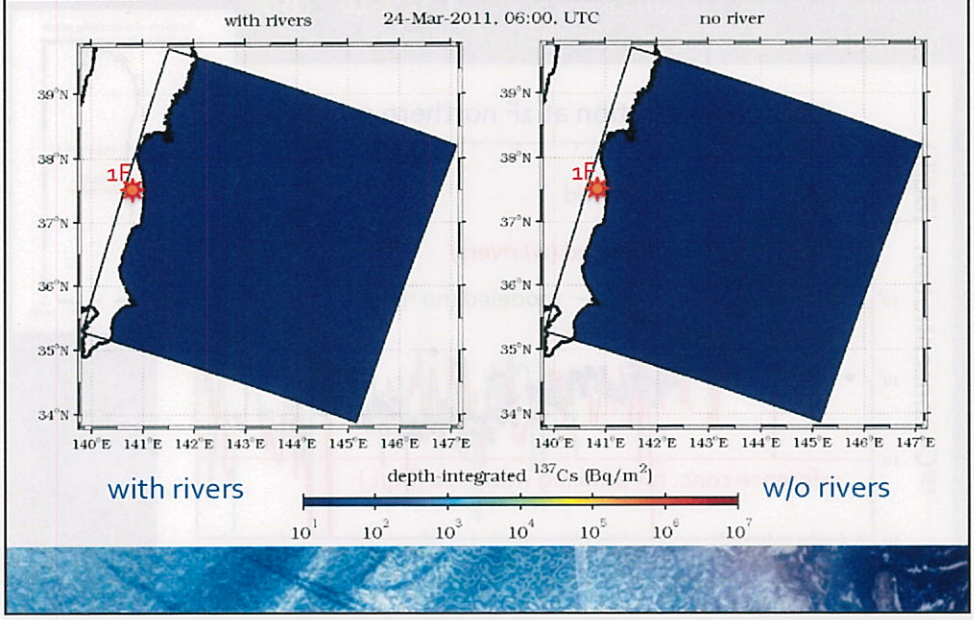


## Oceanic dispersal of $^{137}$Cs on 3/28 (2 days later)

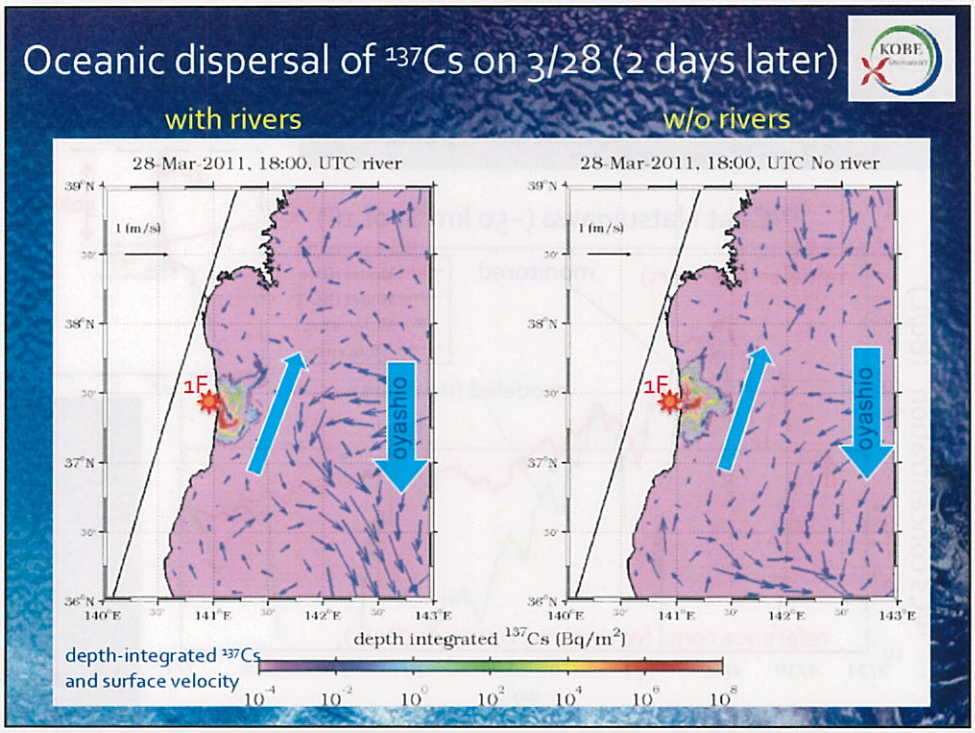

## Oceanic dispersal of $^{137}$Cs on 3/31 (5 days later)

with rivers

w/o rivers

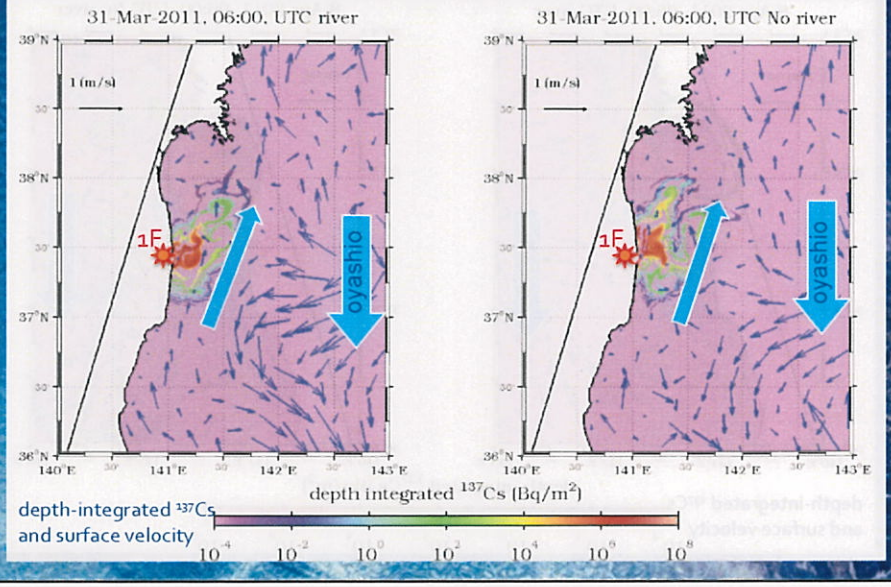


## Oceanic dispersal of $^{137}$Cs on 4/2 (7 days later)

with rivers

w/o rivers

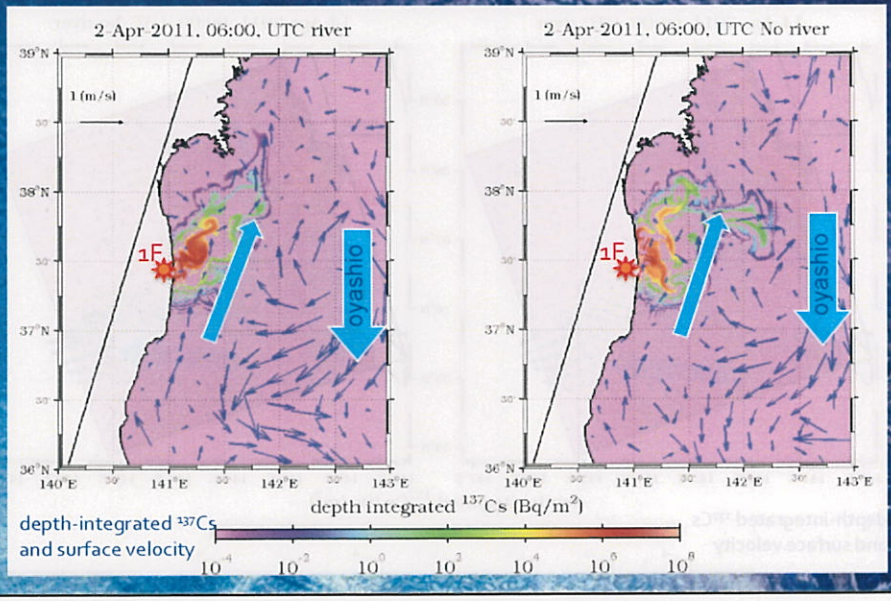

# Oceanic dispersal of $^{137}$Cs on 4/8 (13 days later)

with rivers w/o rivers

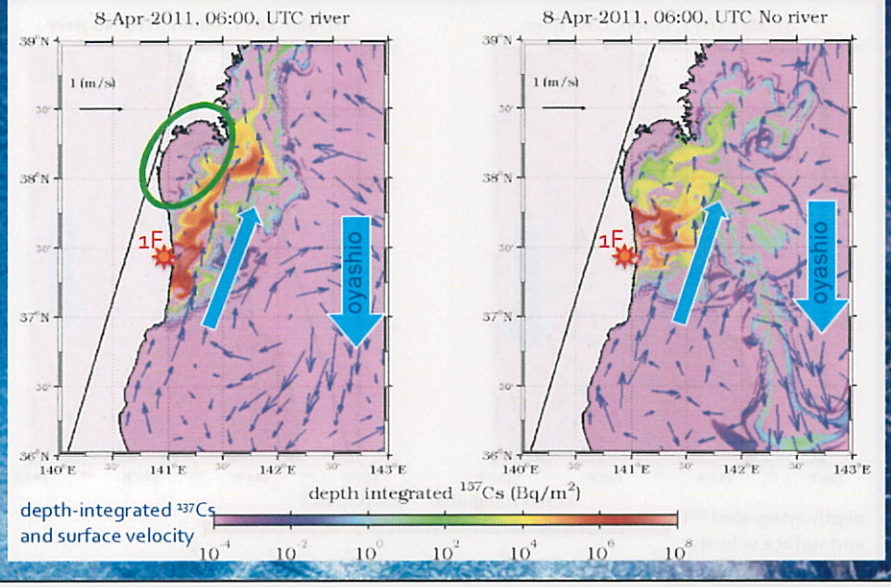


# Oceanic dispersal of $^{137}$Cs on 4/14 (19 days later)

with rivers w/o rivers

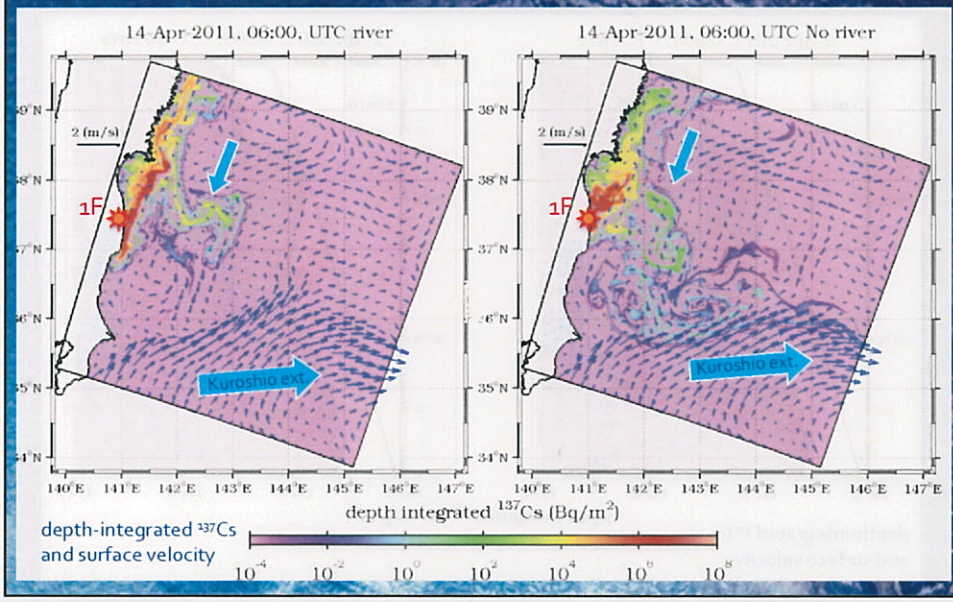

## Oceanic dispersal of $^{137}$Cs on 4/20 (25 days later)

with rivers

w/o rivers

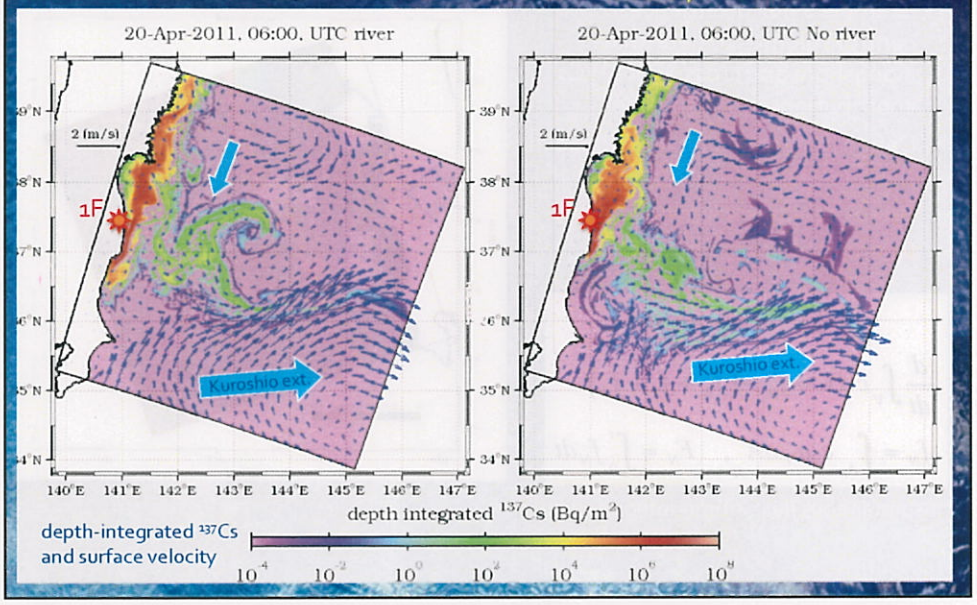


## Point-wise PDF as a function of $^{137}$Cs and $y_r$

PDF w/o rivers

PDF with rivers

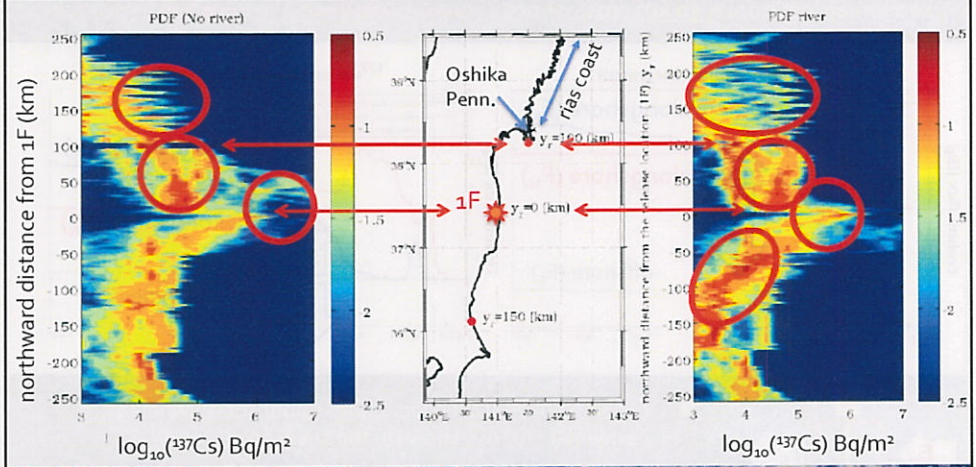


- South of 1F: lower $^{137}$Cs PDF spread as going away from 1F (rivers act to enhance higher PDF)
- North of 1F: nearshore northward current brought the high $^{137}$Cs to Oshika Penn. to be uniform PDF
- Heterogeneous PDF appears associated with a rias coastline north of Oshika Penn. to form "*hotspots*"

# $^{137}$Cs budget in nearshore control volumes

- Examine a flux divergence in two control volumes to determine alongshore and cross-shore $^{137}$Cs contributions in $^{137}$Cs budget
- Define rectangular boxes aligned in the mean coastline centered at 1F
- **Box 1**: 100km × 50km (YELLOW)
- **Box 2**: 100km × 100km (RED)

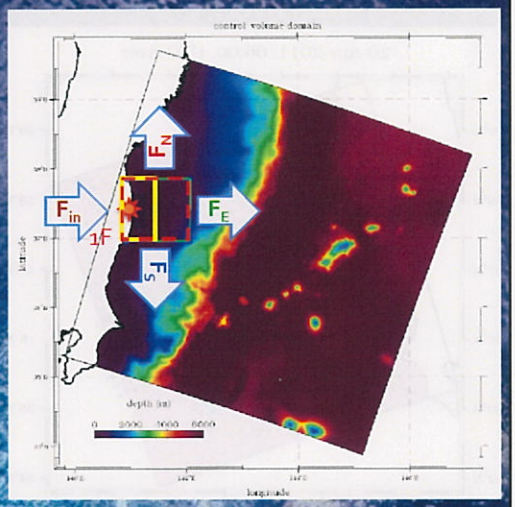


$^{137}$Cs flux budget:

$$\frac{d}{dt}\int_V c\,dV = f_{in} - (f_N + f_S + f_E)$$

$$f_N = \int_{A_N} c_n u_N \, dA_N, \quad F_N = \int_0^t f_N dt$$

instantaneous flux | time-integrated flux (cumulative flux)

# Cumulative $^{137}$Cs outfluxes *F* at 3 boundaries

**Box 1 (small)**
100 km alongshore x ***50 km*** cross-shore

**Box 2 (large)**
100 km alongshore x ***100 km*** cross-shore

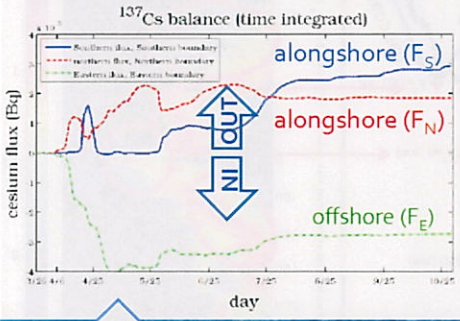


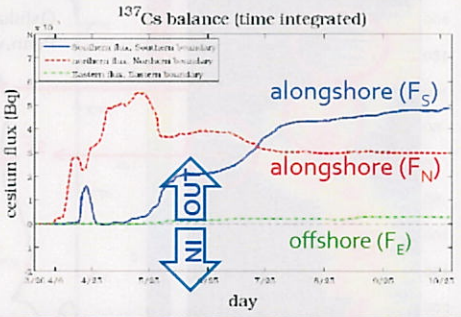


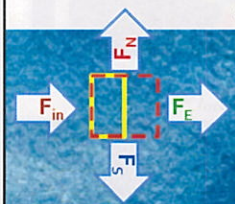


- Outgoing fluxes at S/N boundaries (alongshore) whereas incoming at E (cross-shore) in the small box (1) and approximately *nil* in the large box (2)
- Dominance of the alongshore (particularly southward) transport over the offshore dilution

## Alongshore $^{137}$Cs transport at N/S boundaries (1) Reynolds decomposition

- To investigate a role played by mesoscale eddies in the prevailing alongshore $^{137}$Cs transport,
- The cut-off period for the linear low-pass Butterworth filter is chosen to be 120 days (based on the mean $^{137}$Cs variability).

instantaneous flux

$$f_\alpha \cong \int_{A_\alpha} \bar{u}\,\bar{c}\,dA_\alpha + \int_{A_\alpha} u'c'\,dA_\alpha \quad (\alpha = N, S, E)$$

$$\equiv f_\alpha^{mean} + f_\alpha^{eddy} \qquad \text{(mean + eddy)}$$

cumulative flux

$$F_\alpha \cong \int_0^t f_\alpha^{mean}\,dt + \int_0^t f_\alpha^{eddy}\,dt$$

$$\equiv F_\alpha^{mean} + F_\alpha^{eddy} \qquad \text{(mean + eddy)}$$

## Alongshore $^{137}$Cs transport at N/S boundaries (2) mean vs. eddy contributions

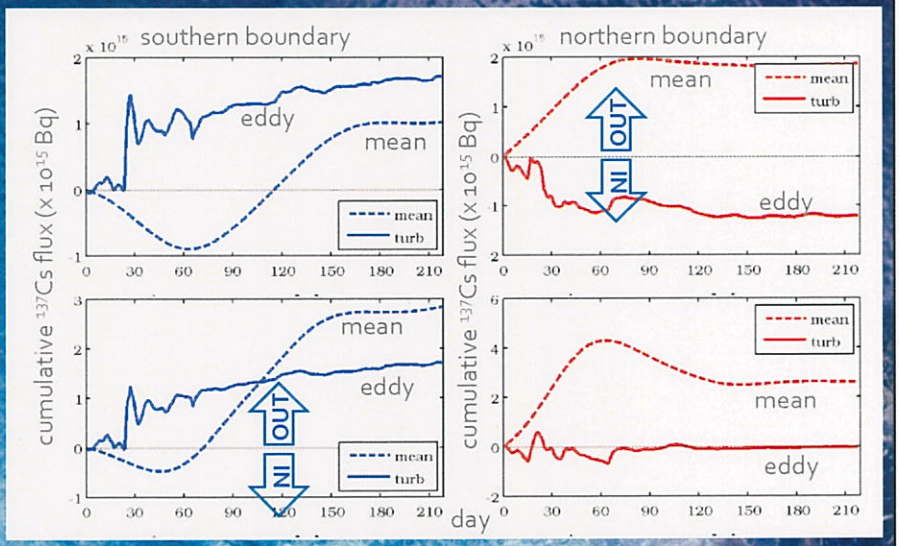

## Summary and outlook

- The model successfully reproduces the overall oceanic currents and associated $^{137}Cs$ concentration off Fukushima (1F),
- The total amount of the leaked $^{137}Cs$ is estimated **$1.35 \times 10^{16}$ Bq** while the previous work suggested **$3.5 \times 10^{15}$ Bq**, as 3.85 times as much (n.b., TEPCO official reported **$9.4 \times 10^{14}$ Bq** $^{137}Cs$),
- The PDF analysis indicates possible "*hotspots*" with high $^{137}Cs$ concentrations along the rias coast (Sanriku), north of 38.2°N,
- Cumulative alongshore transport predominantly occurred particularly to the south where the PDF/concentration are rather small. In turn, offshore transport merely plays a minor role in the $^{137}Cs$ budget (resembles the French simulation),
- Eddy transport is suggested to be a key player to enhance the southward transport,
- Nearshore recirculation of dissolved $^{137}Cs$ and sediment-attached component are to be further investigated.

Dongguk University

# Energy growth and anisotropic characteristics in a buoyancy activating turbulence (Microstructure turbulence mixing)

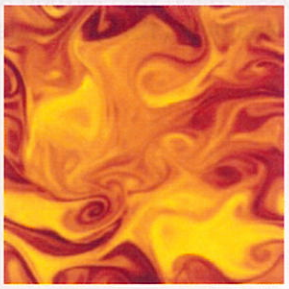

Ph.D. Jin Hwan Hwang,
2012. 03.15. Kobe university, Japan

Dongguk University

## Micro mixing process

- Small scale turbulence is critical in understanding mixing in the ocean, lake, reservoir, etc.
- In many physical process, fossilized turbulence is discussed in this presentation
  - Fossilization of heat or salt and potential energy fluctuation

Dongguk University

## Residual potential energy

- Excessive or remnant potential energy : Gerz *et al* (1989), Ramdsen and Holloway (1992).
- Fossilization was termed and reported in some of previous works (e. g. Nasmyth (1970), Woods *et al* (1969), Gibson (1993)).

Dongguk University

## Fossil turbulence

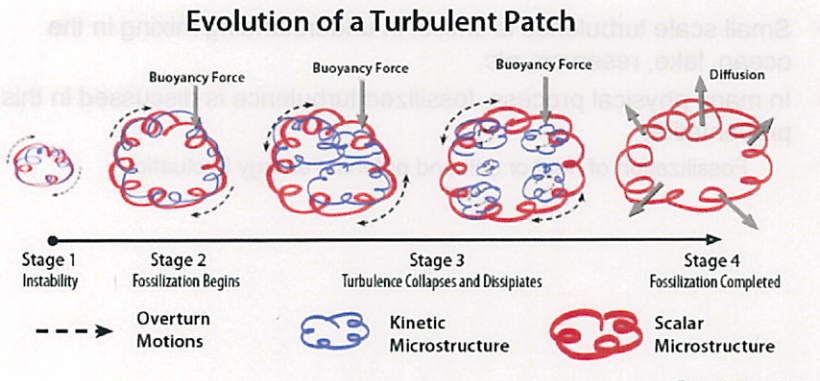


From Leung, 2011

Dongguk University

## Introduction

- Fossilization of turbulence : due to the difference diffusivities of momentum and scalars. In the water, after momentum diffuses away, but still heat fluctuates.
- Gerz and Yamazkai 1993:
  - After turbulence disappears, potential energy is left behind

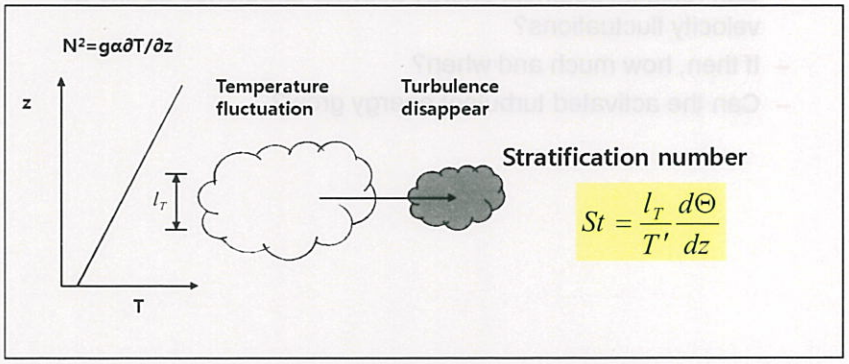


Dongguk University

## Introduction

- If shear forces on residual potential energy, can this energy grow and activate turbulence kinetic energy to develop?

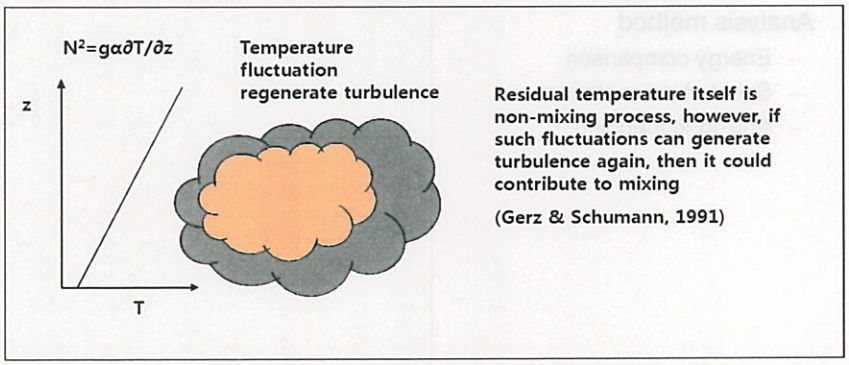

Dongguk University

## Goal of research

- Main question:
  - Can residual potential energy activate turbulence as like as velocity fluctuations?
  - If then, how much and when?
  - Can the activated turbulent energy grow?

Dongguk University

## Method general

- Simulation method
  - Direct Numerical Simulation
  - Rapid distortion theory for the strongly stratified cases
- Analysis method
  - Energy comparison
  - Spectral presentation
  - Anisorpic mapping

Dongguk University

## Methodology

- Solving Navier-Stokes and thermodynamically linearized energy equations
- Solving in a cubical domain
  - Grid : $64^3$ generally, highly sheared case $128^3$
- Temporal domain is integrated with a second order finite difference method
- Pressure field:
  - Solving a Poisson equation by inverting the Laplace operator
  - For periodic and shear-periodic boundaries in the horizontal and vertical direction, respectively.
- Initial perturbation condition
  - Initializing the anisotropic fields using random numbers that obey preset correlation coefficients and an input energy spectrum (Ozarg, 1982)

9

Dongguk University

## Governing equations

- Background velocity and temperature
  - $U(x_3)$: the mean horizontal background velocity
  - $\Theta(x_3)$ : the mean temperature profile.
  - Those are linear with height.
- Characteristic time scale : Buoyancy frequency

$$\tau^* = 2\pi / N \qquad \text{where} \qquad N^2 = \alpha g \frac{d\Theta}{dz}$$

- Characteristic length scale : the initial temperature distribution

$$\ell_T^* = \frac{1}{2}\pi \int \frac{1}{\kappa} S(\kappa) d\kappa, \qquad \text{where } \kappa = \left(\kappa_1^2 + \kappa_2^2 + \kappa_3^2\right)^{1/2}$$

  - $S(\kappa)$ defines the shape of the temperature perturbation spectrum

$$S(\kappa) = \frac{16}{2\pi}\left(\frac{2}{\pi}\right)^{1/2} \frac{\kappa^4}{\kappa_5^5} \exp\left[-2\left(\kappa / \kappa_p\right)^2\right]$$

$$\kappa_p = (8\pi)^{1/2} \quad \text{(peak integer wavenumber)}$$

10

Dongguk University

## Governing equations (2)

- Non-dimensional momentum equations become

$$\frac{\partial u_i}{\partial t} + Ri^{-1/2} x_3 \frac{\partial u_i}{\partial x_1} + Ri^{-1/2} u_3 \delta_{il} + \frac{\partial}{\partial x_j}(u_i u_j) = -\frac{\partial p}{\partial x_j} - St^{-1} T \delta_{i3} + \mathrm{Re}^{-1} \frac{\partial^2 u_i}{\partial x_j^2}$$

$$\frac{\partial T}{\partial t} + Ri^{-1/2} x_3 \frac{\partial T}{\partial x_1} + \frac{\partial}{\partial_j}(u_j T) = -St u_3 + \mathrm{Re}^{-1} \mathrm{Pr}^{-1} \frac{\partial^2 T}{\partial x_j^2}$$

$$\frac{\partial u_i}{\partial x_i} = 0$$

- Where $Ri = \dfrac{N^2}{(\partial U / \partial z)^2} = \dfrac{N^2}{S^2}$ $\mathrm{Re} = \dfrac{N \ell_T^2}{\nu}$, $\mathrm{Pr} = \dfrac{\nu}{D}$
- The stratification number $St = \dfrac{\ell_T}{T'} \dfrac{\partial \Theta}{\partial z}$, $(T' = \overline{TT}^{1/2})$

  Which represents the strength of the initial perturbations relative to the mean background gradient of temperature.

11

Dongguk University

## Summary of simulation conditions

| Case | St | Ri | Re | Grid number |
|---|---|---|---|---|
| As1 | 0.1 | 0.04 | 11.6 | 64 |
| As2 | 0.1 | 0.25 | 11.6 | 64 |
| Bs1 | 0.25 | 0.08 | 57.4 | 128 |
| Bs2 | 0.25 | 0.16 | 57.4 | 128 |
| Bs3 | 0.25 | 0.25 | 57.4 | 64 |
| Bs4 | 0.25 | 0.5 | 57.4 | 64 |
| Bs5 | 0.25 | 1 | 57.4 | 64 |
| Cs1 | 0.5 | 0.16 | 57.4 | 64 |
| Cs2 | 0.5 | 0.25 | 57.4 | 64 |
| Cs3 | 0.5 | 0.5 | 57.4 | 64 |
| Cs4 | 0.5 | 1 | 57.4 | 64 |
| Ds1 | 0.75 | 0.16 | 57.4 | 64 |
| Ds2 | 0.75 | 0.25 | 57.4 | 64 |
| Ds3 | 0.75 | 1 | 57.4 | 64 |
| Fs1 | 4 | 0.08 | 57.4 | 64 |
| Fs2 | 4 | 0.16 | 57.4 | 64 |
| Fs3 | 4 | 1 | 57.4 | 64 |
| fs4 | 4 | 10 | 57.4 | 64 |

12

Dongguk University

# RESULTS OF SIMULATION



Dongguk University

## Initial residual potential distributions

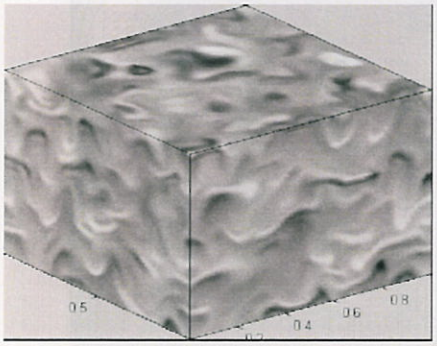

St = 0.25

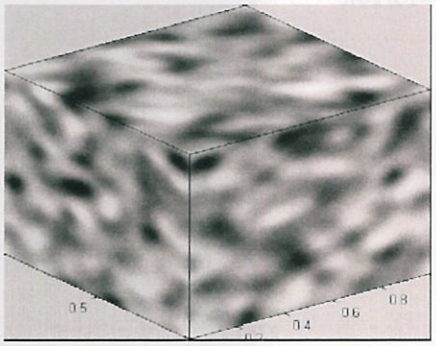

St = 4

Dongguk University

## Temperature and velocity contour from top (St = 4)

Nt/2π
=1/4π

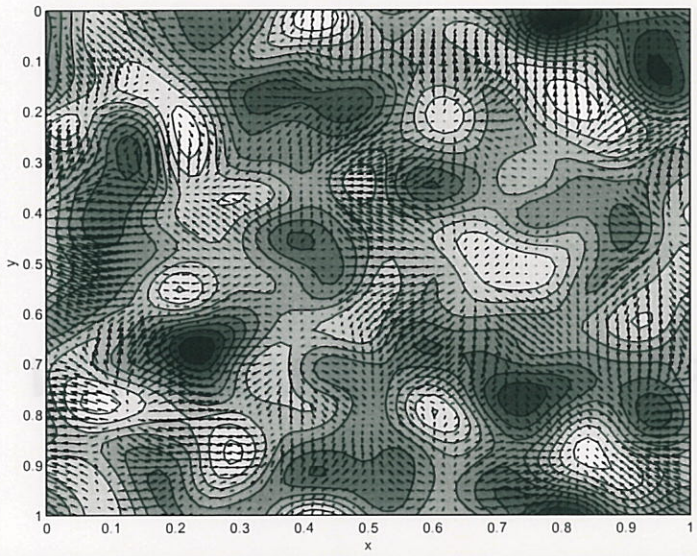


Dongguk University

Nt/2π
=19/20π

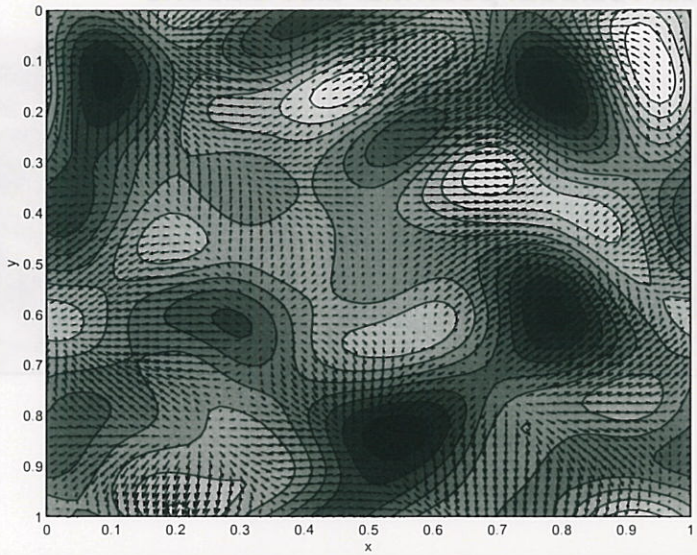

Dongguk University

## Temperature and velocity contour from top (St = 0.25)

Nt/2π
=1/4π

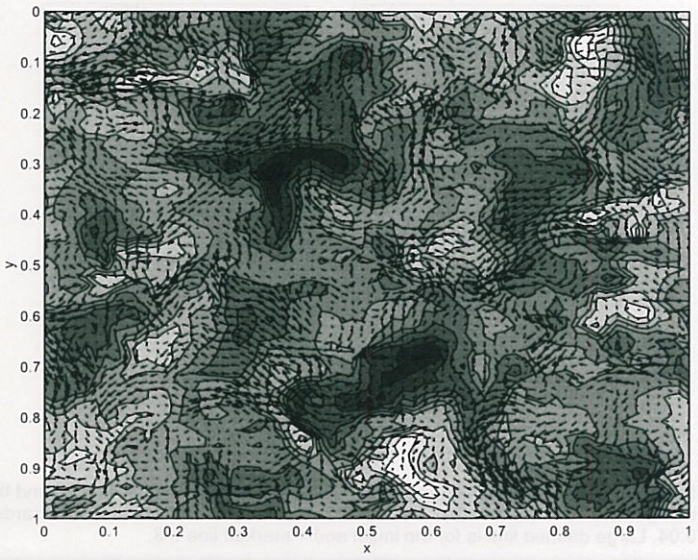


Dongguk University

Nt/2π
=19/20π

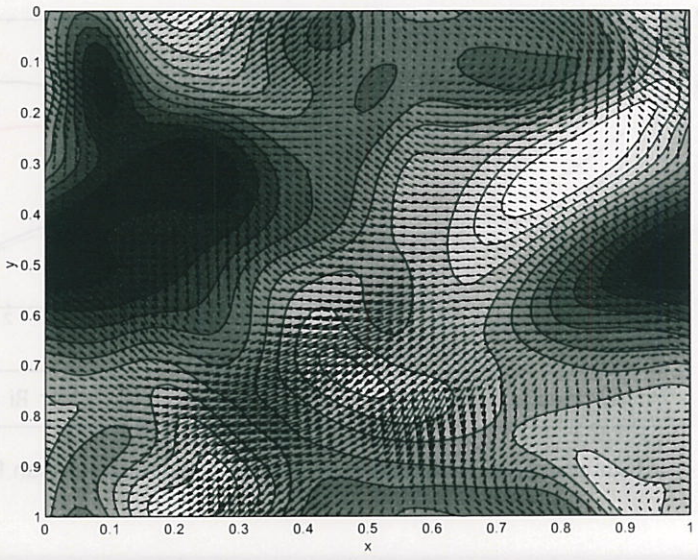

Dongguk University

## Energy and dissipation spectra

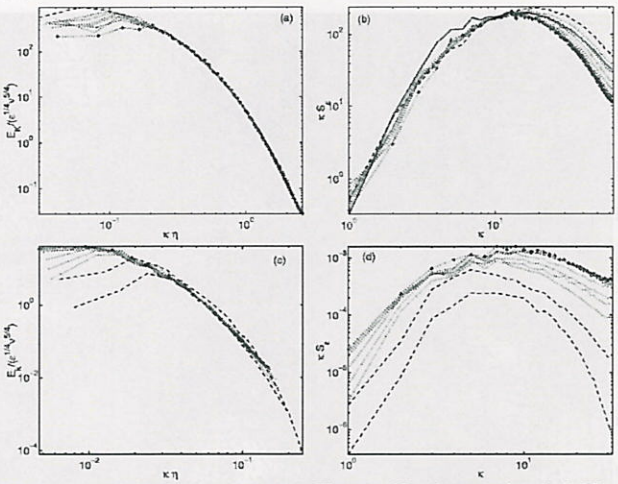


- Kinetic energy and dissipation spectra. The stratification number is 0.25 and the Richardson number is 0.16 in (a) and (b). The stratification number is 0.1 and the Richardson number is 0.04. Large dashed line is for the initial and + marked line t=3.

Dongguk University

## Energy evolution (St = 0.25)

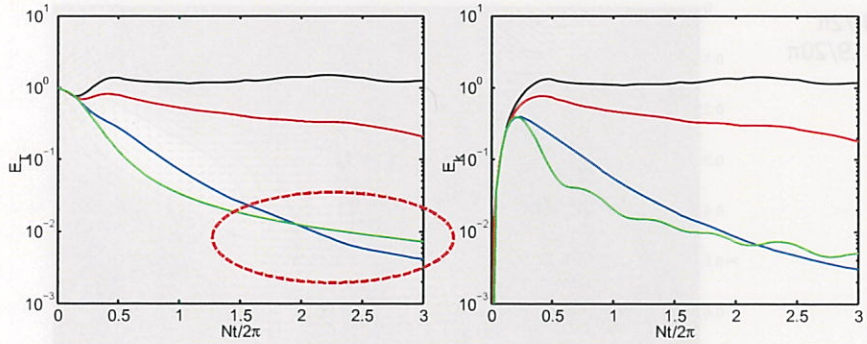


- Total and kinetic energies of unsheared flow are larger than Ri = 1

Dongguk University

## Energy evolution (St = 4)

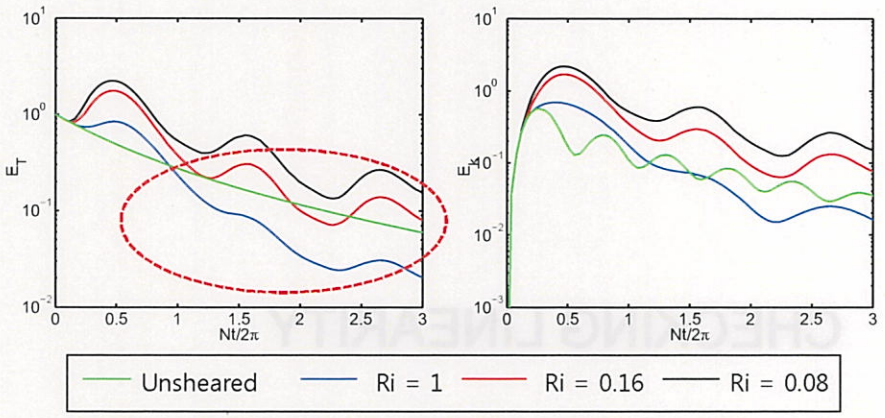


- Total and kinetic energies of unsheared flow are larger than Ri = 1

Dongguk University

## Turbulence intensity ($\varepsilon/\nu N^2$)

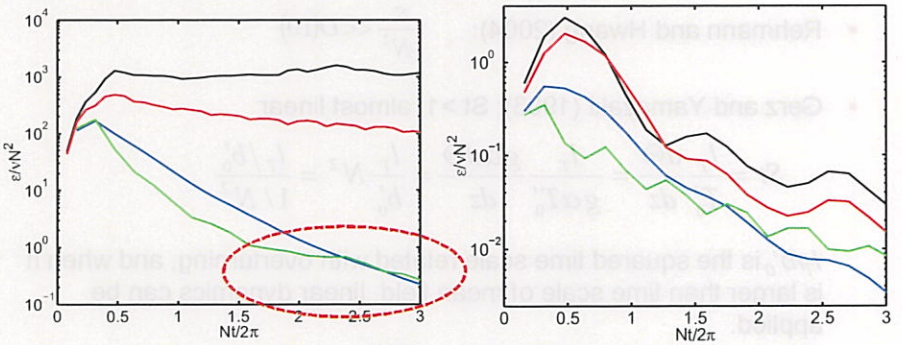


St < 1 : $\varepsilon/\nu N^2$ is much larger than O(10)

St > 1 : $\varepsilon/\nu N^2$ is smaller than O(10)

Dongguk University

# CHECKING LINEARITY

Dongguk University

## Rapid Distortion Theory

- Rehmann and Hwang (2004): $\frac{\varepsilon}{\nu N^2} << O(10)$
- Gerz and Yamazaki (1993): St >1, almost linear

$$St = \frac{l_T}{T_0'}\frac{d\Theta}{dz} = \frac{l_T}{g\alpha T_0'}\frac{g\alpha d\Theta}{dz} = \frac{l_T}{b_0'}N^2 = \frac{l_T/b_0'}{1/N^2}$$

$l_T/b'_0$ is the squared time scale related with overturning, and when it is larger than time scale of mean field, linear dynamics can be applied.

- Hanazaki and Hunt (1996): $Fr_\lambda = \frac{u_\lambda}{N\lambda} < 1$

Dongguk University

## DNS and RDT comparison in unsheared condition (St = 4)

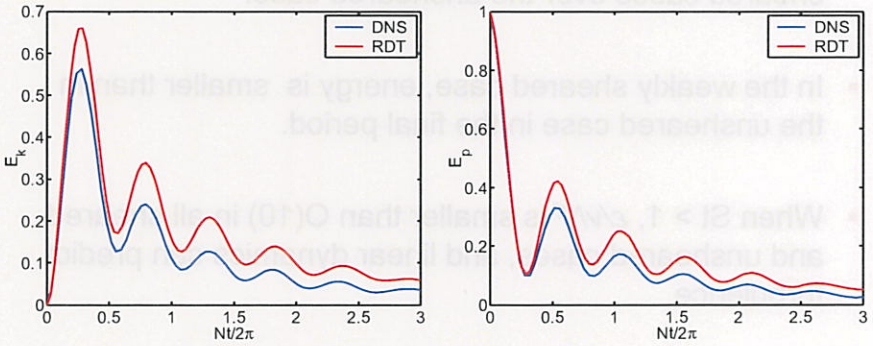


Dongguk University

## DNS and RDT comparison in strongly sheared condition (Ri = 0.01, St = 4)

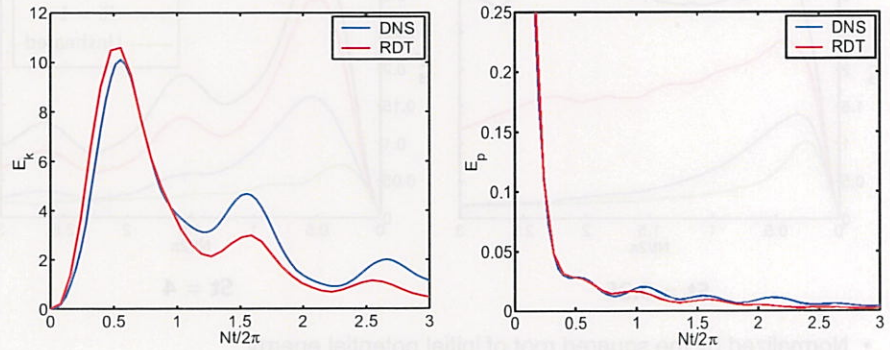

Dongguk University

## Intermediate conclusion

- In the initial period, shear can energize turbulence in all sheared cases over the unsheared case.
- In the weakly sheared case, energy is smaller than in the unsheared case in the final period.
- When St > 1, $\varepsilon/\nu N^2$ is smaller than O(10) in all sheared and unsheared cases, and linear dynamics can predict turbulence.

Dongguk University

## R.M.S. velocity in shear direction

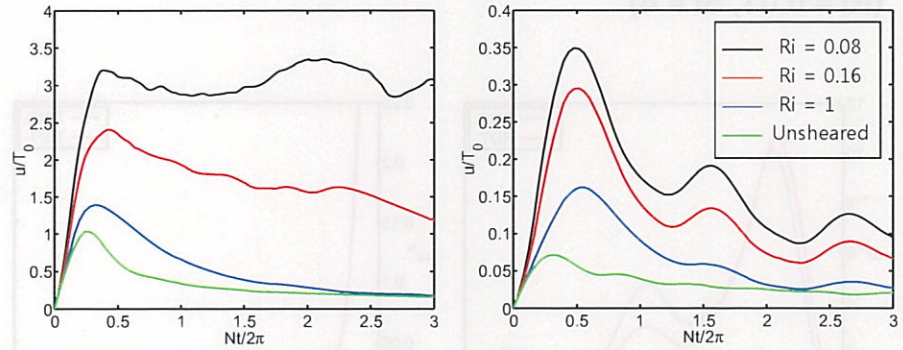


St = 0.25 St = 4

- Normalized by the squared root of initial potential energy
- $u/T_0$ increase with shear

Dongguk University

## R.M.S. velocity in vertical direction

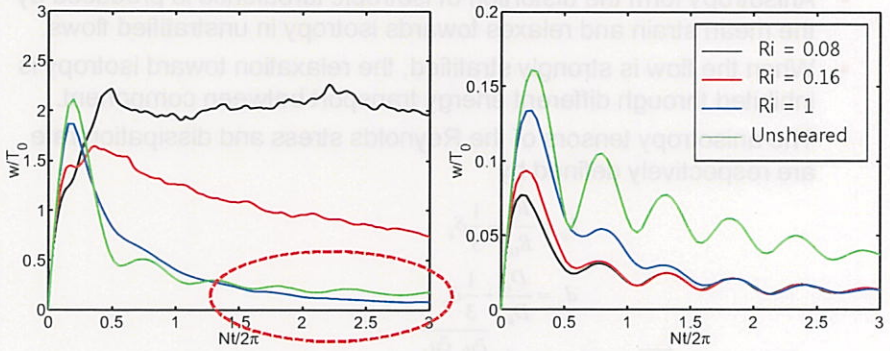


St = 0.25 St = 4

$w/T_0$ increases with shear in super-critical decreases with shear in sub-critical

Dongguk University

## ANISOTROPIC PROPERTIES

Dongguk University

## Anisotropic invariant map

- Anisotropy form the distortion of isotropic turbulence is produced by the mean strain and relaxes towards isotropy in unstratified flows.
- When the flow is strongly stratified, the relaxation toward isotropy is inhibited through different energy transport between component.
- The anisotropy tensors of the Reynolds stress and dissipation rate are respectively defined by

$$b_{ij} = \frac{R_{ij}}{R_{kk}} - \frac{1}{3}\delta_{ij}$$

$$d_{ij} = \frac{D_{ij}}{D_{kk}} - \frac{1}{3}\delta_{ij}$$

where $R_{ij} = \overline{u_i u_j}$, and $D_{ij} = 2\nu \overline{\frac{\partial u_i}{\partial x_k}\frac{\partial u_j}{\partial x_k}}$

31

Dongguk University

## Anisotropic invariant map

- The invariants are given by

$$I_b = 0, \qquad II_b = -\frac{1}{2} b_{ij} b_{ji}, \qquad III_b = \frac{1}{3} b_{ij} b_{jk} b_{ki}$$

$$I_d = 0, \qquad II_d = -\frac{1}{2} d_{ij} d_{ji}, \qquad III_b = \frac{1}{3} d_{ij} d_{jk} d_{ki}$$

where *b* denotes Reynolds stress and *d* denotes dissipation anisotropy.

- The boundaries of the anisotropy invariant map correspond to limiting cases. The upper boundaries is described by

$$G_b = \frac{1}{9} + 3III_b + II_b = 0$$

and it corresponds to two-component turbulence. The lower left boundary corresponds to the axisymmetric contraction cases with rod-like turbulence, then the axisymmetry parameter $A_b$ is -1, where

$$A_b = \frac{III_b / 2}{(-II_b / 3)^{3/2}}$$

- The lower right boundary corresponds to axisymmetric expansion. The bottom cusp corresponds to isotropy, while the right most point corresponds to one-component turbulence.

32

Dongguk University

## Turbulence structures on the boundaries of the AIM's

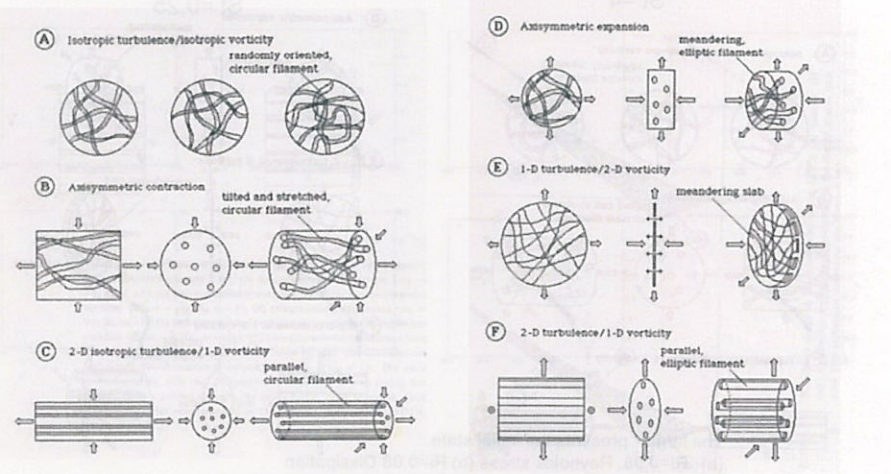


From W.C. Reynolds, 1985



Dongguk University

## Turbulence structures on the boundaries of the AIM's

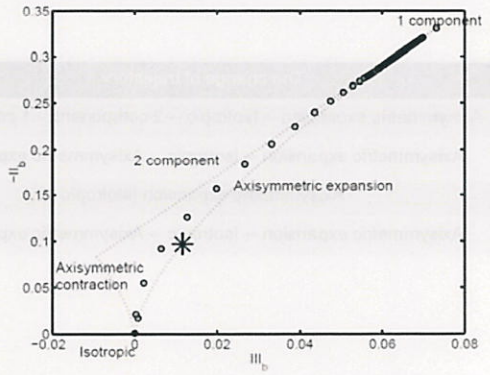


- Representative AIM

Dongguk University

## Turbulence structures on the boundaries of the AIM's

St =4 St =0.25

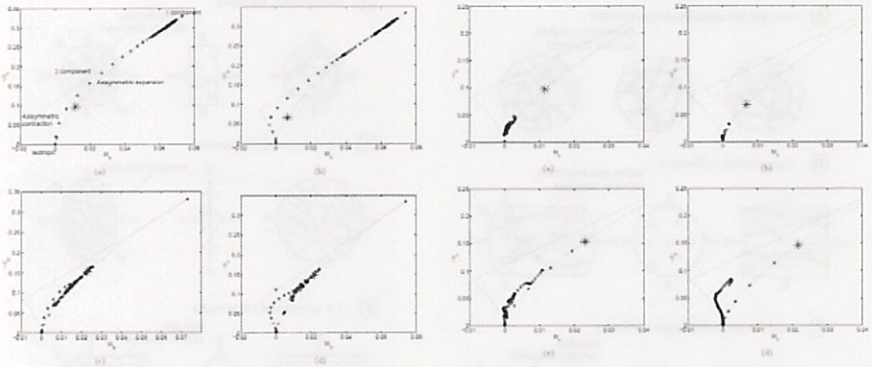

The large * presents the initial state.
(a) Ri=0.08, Reynolds stress (b) Ri=0.08 Dissipation
(c) Ri=1, Reynolds stress (d) Ri=1, Dissipation invariant

35

Dongguk University

## Turbulence structures on the boundaries of the AIM's

- Summary of the trajectories of the anisotropy invariants

| St | Ri | The change of trajectory |
|---|---|---|
| 4 | 0.08 | Axisymmetric expansion → Isotropic → 2 component → 1 component |
| 4 | 1 | Axisymmetric expansion → Isotropic → Axisymmetric expansion |
| 0.25 | 0.08 | Axisymmetric expansion Istotropic |
| 0.25 | 1 | Axisymmetric expansion → Isotropic → Axisymmetric expansion |

36

Dongguk University

# SUMMARY & CONCLUSION

Dongguk University

## Summary

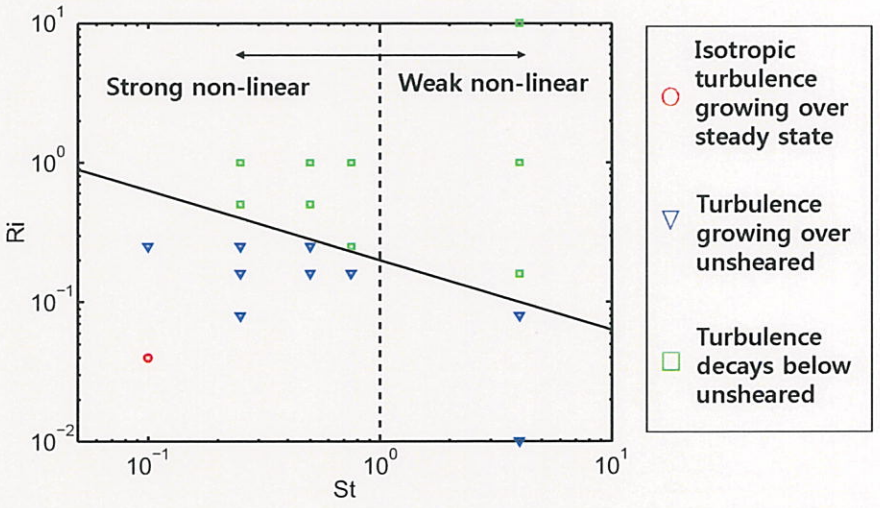

Dongguk University

## Conclusion

- In the initial period, shear can energize turbulence in all sheared cases over the unsheared case.
- In the weakly sheared case, energy is smaller than in the unsheared case in the final period.
- When St > 1, $\varepsilon/\nu N^2$ is smaller than O(10) in all sheared and unsheared cases, and linear dynamics can predict turbulence.

# Kobe University Large Eddy Simulation Code (KULES)
## - its capability and applications -

Akihiko Nakayama
Dept. Civil Engineering,
Kobe University

1

Last time (2010) Shibata showed

## Flood of Aug. 2nd, 2009

Aerial photo

Calculation

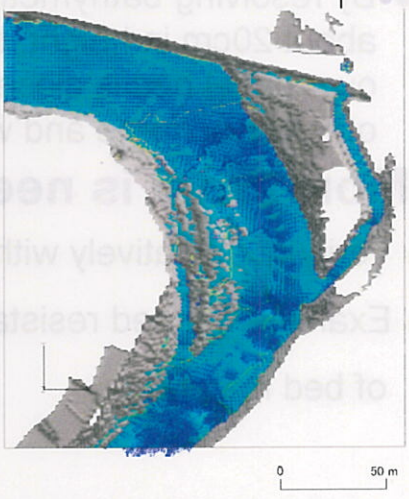


- Calculation reproduces flow, but it does not reach stationary state (flows too fast)

2

Also Ikenaga(Nakayama) presented SPH LES

## obstacle on the floor

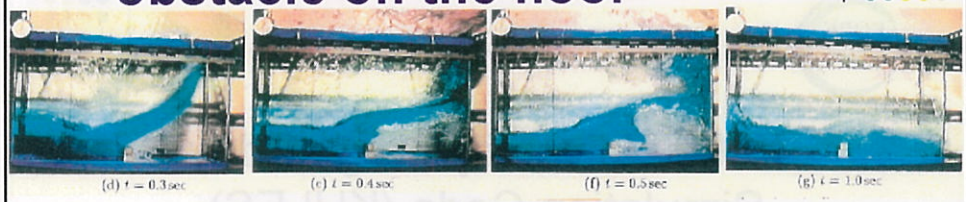


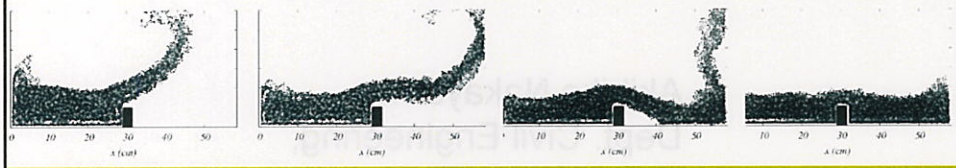

Shibata's summary

## Summary

- By resolving bathymetry and largest stones to about 20cm in height, the LES calculation of flow over gavel bed is close to observed flow in terms of flow discharge and water level.

## More work is needed

- Verify quantitatively with the field data.
- Examine the bed resistance results in terms of sizes of bed material

4

Ikenaga's conclusions

## Conclusions

- Conventional SPH method needs artificially enhanced viscosity in order to make stable calculation.
- In order to reflect the effects of turbulent fluctuations, basic equations of motion for the kernel integral representation of flow velocity is re-derived.
- The results for the motion of collapsing water column with or without obstacle compare very well with the experimental results.

## What do we want?

- **Realistic**
  **and good turbulence model**
- **Versatile**
  **more than or other than commercial or free software**
- **Affordable**
  **No expertise in computing**

6

## Does LES do it?

- **What is LES?**
  **Turbulence model that is grid-size (Δ) dependent and converges to the NS solution as Δ/l→0**
- **Other approaches of turbulent flow calculation?**
  **Reynolds averages - need calibrated model**
  **Sampling - not known yet**

7

## We have worked on

Staggered grid in Cartesian coordinates(KULES-RG)

1. without free surface, improved wall model(KULES-wind)
2. with moving free surface, improved BC's(KULES-river)
3. temperature and concentration variation with Boussinesq approx. (KULES-plume)
4. moving solid body(KULES-body)
5. movable bed (KULES-sediment)

Collocated grid in curvilinear coordinates (KULES –CG)

1. without free surface, improved ground model(KULES-wind)
2. with moving free surface(KULES-channel)
3. temperature and concentration variation with Boussinesq approx. (KULES-plume)

# Elements of KULES's

1. Basic approach and equations
   - Implicit and explicit filter
   - Sampling in stead of filtering
2. Sub grid model
   - Smagorinsky or dynamic Smagorinsky
   - Shear-improved and near wall damping
   - Mixed time scale or other model
   - sub-grid free-surface fluctuation
3. Difference Scheme
   - upwind, utopia & Quick
   - conservative central difference
4. Wall model
   - smooth and rough surface
   - dynamic wall model

9

# KULES – RG

Free-surface HSMAC algorithm

water cell
regular HSMAC iteration on pressure and velocity

surface cell
pressure from BC and velocity from m.e.
free surface is moved by kinematic cond.

wetting front
same as surface cell, except velocity front conditioned on roughness

external cell
pressure and velocity both from BC

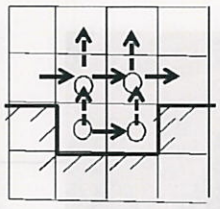

velocity

pressure

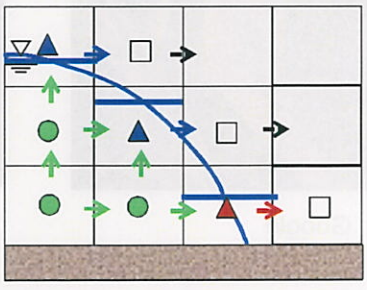

10

# Boundary conditions for rivers

**inflow**

mean flow - given discharge hydrograph

turbulence - approach section for development

**outflow**

velocity – partially-clamped radiation

surface slope – uniform flow

or

elevation – from stage -discharge relation

**bed and bank**

zero normal velocity

tangential stress – rough surface model

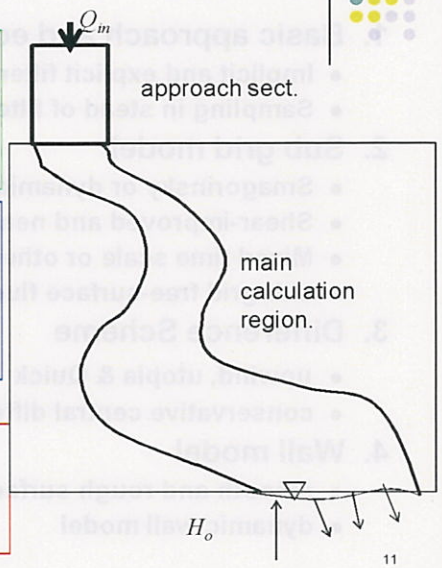


11

# Application to flow around river bend

Google

Aug. 10, 2009

# Results of surface velocity and elevation

Inflow hydrograph

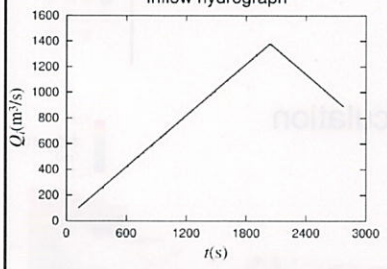


observed elevation and discharge

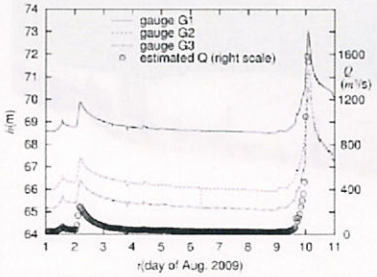


$t$=100s to 2200s

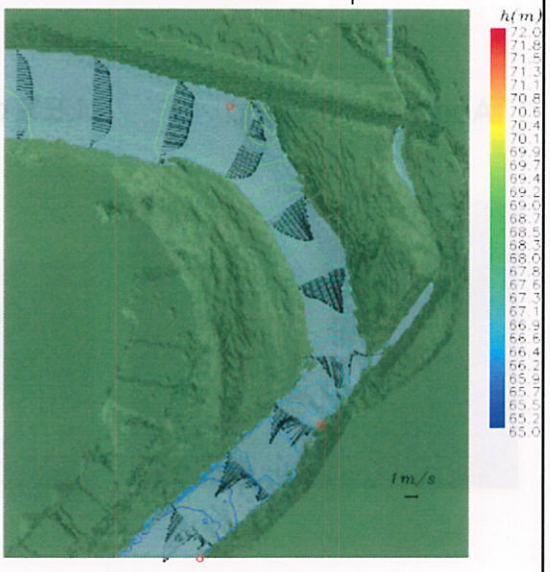


interval between contours is 20cm

# Results of surface velocity and elevation

$t$=2200s on

Inflow hydrograph

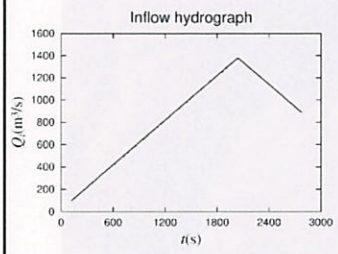


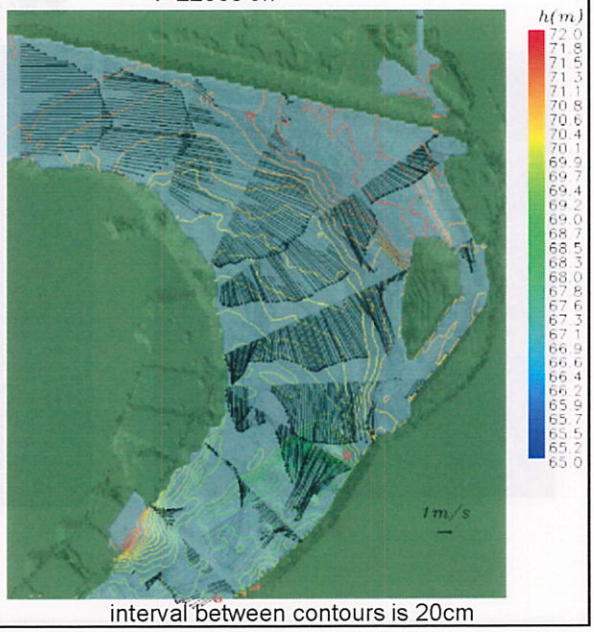


interval between contours is 20cm

# from previous results

## Surface fluctuation

Aug.2 flood video

LES calculation

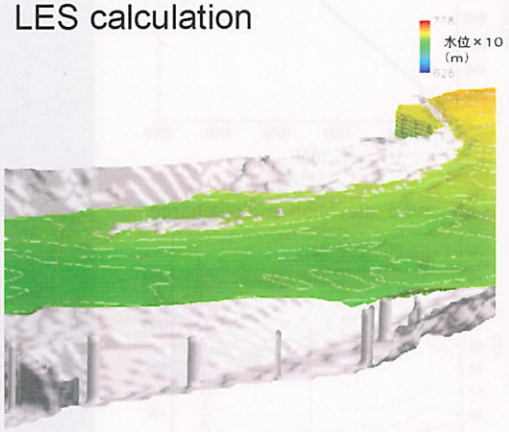


15

# Previous results

流量$Q_{in}$=200m3/s より 低下

● 水位計

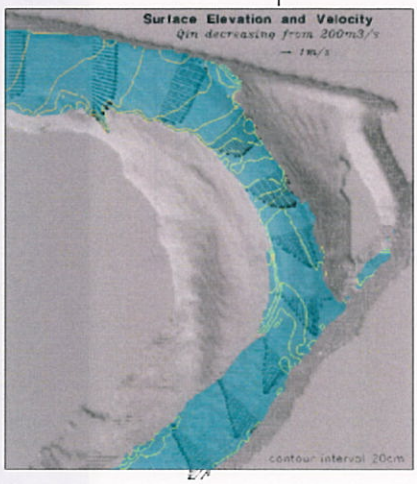

## Comparison with depth-averaged 2d calculation

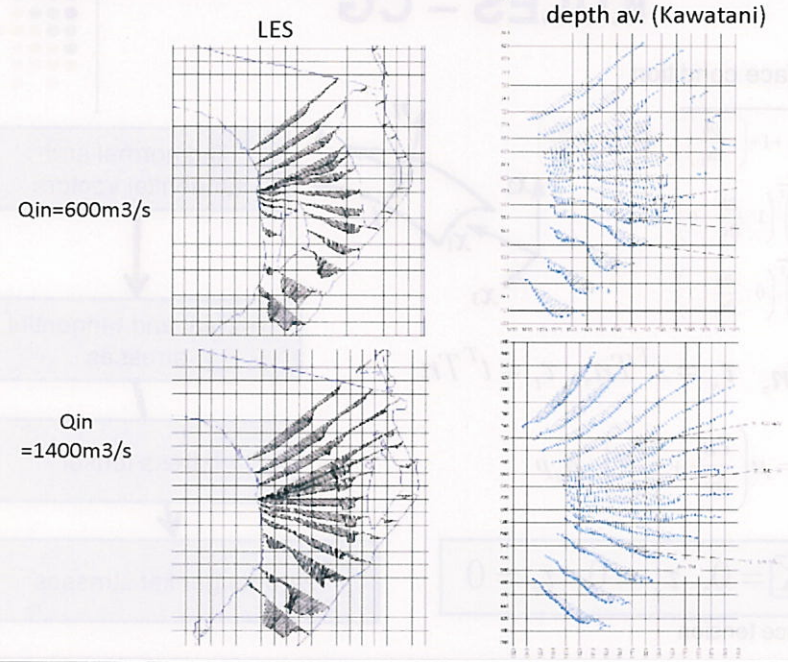


17

## KULES - CG

- Straight vertical - sigma
- Bathymetry-fitted and free surface-following

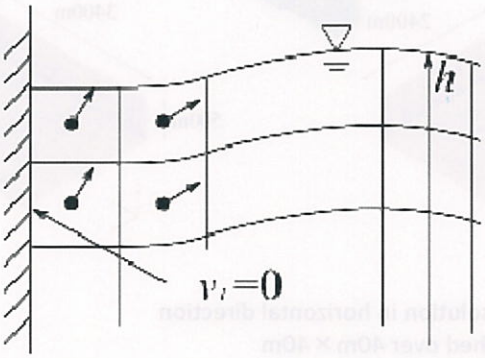


18

# KULES – CG

Free surface condition

$$n = 1/\sqrt{\left(-\frac{\partial h}{\partial x_1}\right)^2 + 1 + \left(-\frac{\partial h}{\partial x_3}\right)^2}\left(-\frac{\partial h}{\partial x_1} \quad 1 \quad -\frac{\partial h}{\partial x_3}\right)^T$$

$$s = 1/\sqrt{1+\left(\frac{\partial h}{\partial x_1}\right)^2}\left(1 \quad \frac{\partial h}{\partial x_1} \quad 0\right)^T$$

$$t = 1/\sqrt{1+\left(\frac{\partial h}{\partial x_3}\right)^2}\left(0 \quad \frac{\partial h}{\partial x_3} \quad 1\right)^T$$

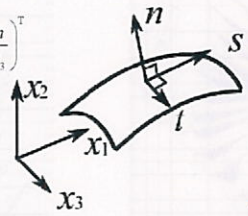


$$\tau_n = n^T T n, \quad \tau_s = s^T T n, \quad \tau_t = t^T T n$$

$$T_{ij} = \mu\left(\frac{\partial u_i}{\partial x_j} + \frac{\partial u_j}{\partial x_i}\right) - \delta_{ij} p$$

$$\tau_n + \sigma K = 0, \quad \tau_s = 0, \quad \tau_t = 0$$

Surface tension

find normal and tangential vectors

normal and tangential stresses

stress tensor

zero tangential stresses

19

# KULES - CG

## Application to atmospheric flow over natural terrain

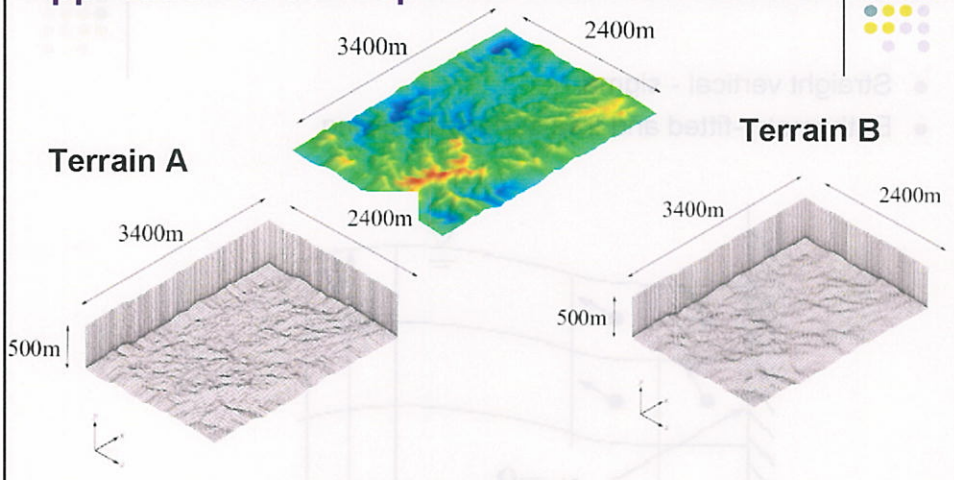


Terrain A: 5m resolution in horizontal direction

Terrain B : smoothed over 40m × 40m

20

**1-4m protrusions are smoothed in Terrain B compared with Terrain A**

# Application to curved channel

Bathymetry and free-surface following sigma

| | No. grids |
|---|---|
| streamwise | 460 |
| cross flow | 80 |
| Vertical | 30 |
| $y+$ | 1927 |
| Bed slope | 1/1000 |
| $Re$ | 950000 |
| $Fr$ | 0.38 |

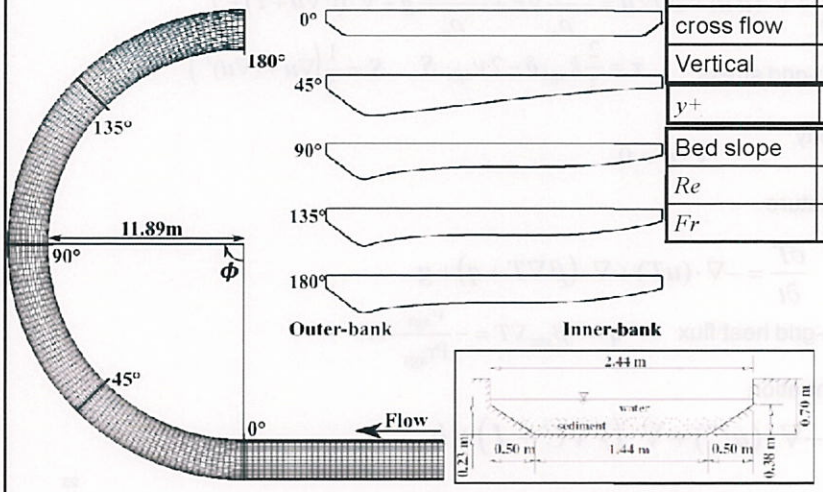


21

# Example results

instantaneous velocity magnitude

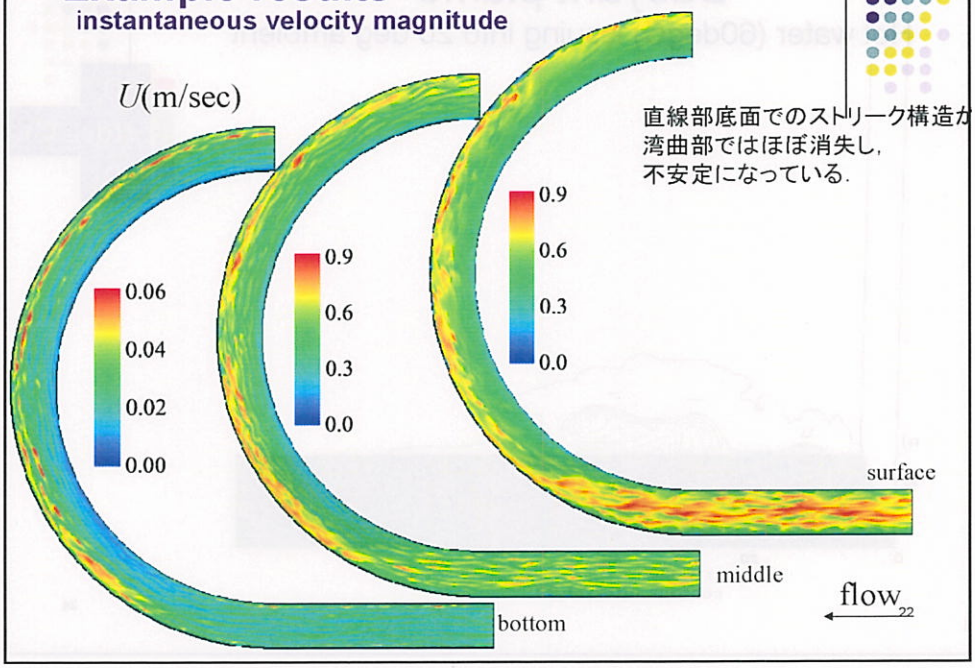


直線部底面でのストリーク構造が
湾曲部ではほぼ消失し，
不安定になっている．

22

# KULES – RG plume

## Basic equations

- Momentum

$$\frac{\partial \boldsymbol{u}}{\partial t} + \nabla \cdot (\boldsymbol{u}\,\boldsymbol{u}) + 2\Omega \times \boldsymbol{u} = -\frac{1}{\rho_a}\nabla P + \frac{\rho - \rho_a}{\rho_a}\boldsymbol{g} + \nabla \cdot \left(\nu \nabla \boldsymbol{u} + \boldsymbol{\tau}\right) + \boldsymbol{f}$$

Sub-grid stress $\quad \boldsymbol{\tau} = \frac{2}{3}k_{sgs}\boldsymbol{\delta} - 2\nu_{sgs}\,\boldsymbol{S} \qquad \boldsymbol{S} = \frac{1}{2}\left(\nabla \boldsymbol{u} + (\nabla \boldsymbol{u})^T\right)$

- Continuity

$$\nabla \cdot \boldsymbol{u} = 0$$

- Temperature

$$\frac{\partial T}{\partial t} = -\nabla \cdot (\boldsymbol{u}T) + \nabla \cdot \left(\beta \nabla T + \boldsymbol{q}\right) + g$$

Sub-grid heat flux $\quad \boldsymbol{q} = -\beta_{sgs}\nabla T = -\frac{\nu_{sgs}}{\mathrm{Pr}_{sgs}}\nabla T$

- concentration

$$\frac{\partial C}{\partial t} = -\nabla \cdot (\boldsymbol{u}C) + \nabla \cdot \left(\gamma \nabla C + \boldsymbol{J}\right) + h$$

Sub-grid scalar flux $\quad \boldsymbol{J} = -\gamma_{sgs}\nabla C = -\frac{\nu_{sgs}}{\mathrm{Pr}}\nabla C$

23

# Buoyant plume

Hot water (60degC) issuing into 20 deg ambient

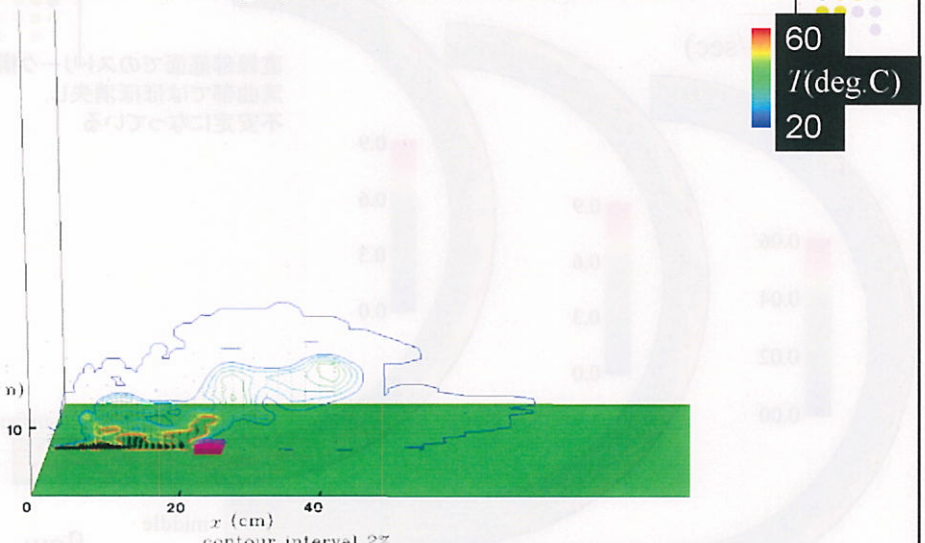


24

## Application to waste water outfall

velocity, concentration and temperature in vertical plane passing through one of 6 operating ports

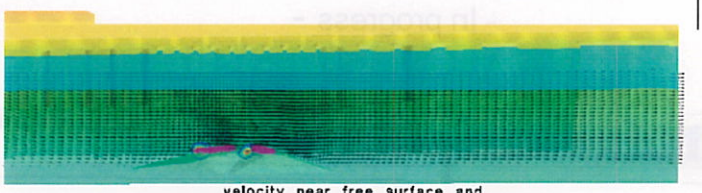


velocity near free surface and surface of constant concentration 5%

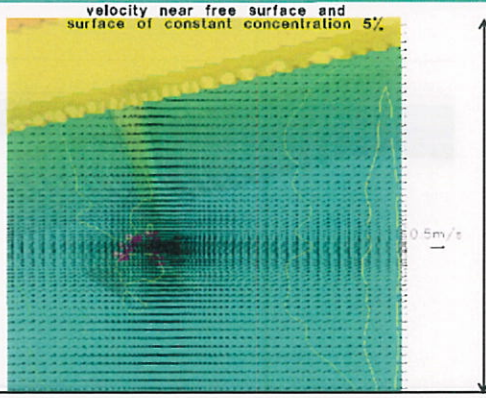


fresh water into sea water

80m

25

## KULES - body

Application to tsunami washing a bridge deck

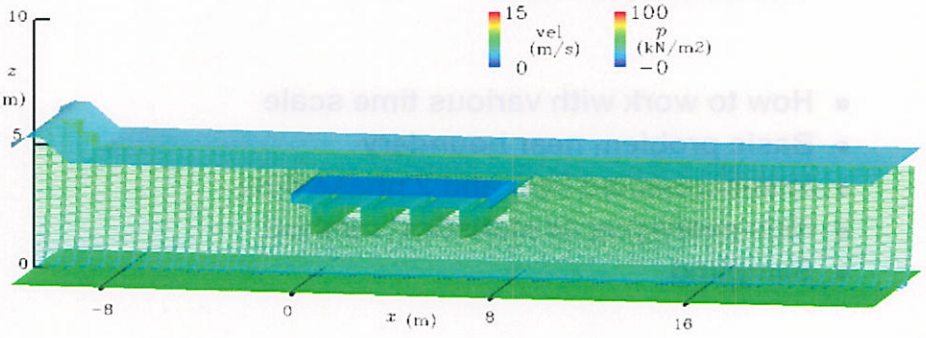


26

## KULES - sediment

Application to scour by tsunami

- In progress -

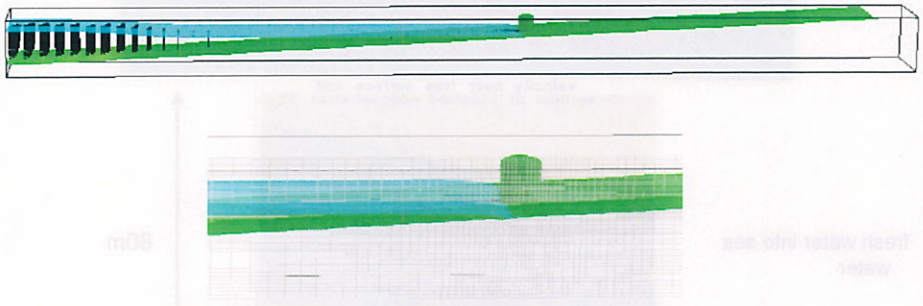

27

## Summary and future work

- **LES methods being used to simulate various simple flows**

- **How to work with various time scale**
- **Basic problem near boundary**
- **Non-connected flow and 2 phase flow**
- **New averaging or statistical method**
- **Sampling**

28

## Difficulty of spatial averaging approach

- spatial filtering

$$\overline{u_i(\boldsymbol{x},t)} = \iiint_D u_i(\boldsymbol{\xi},t)G(\boldsymbol{\xi},\boldsymbol{x})d\boldsymbol{\xi} \qquad (1)$$

$G(\xi, x)$: filter kernel,
$D$ : flow region

$\iiint_D G(\boldsymbol{\xi},\boldsymbol{x})d\boldsymbol{\xi} = 1$ smoothing

- commutes with spatial differentiation
  - only away from boundary

$$\overline{\frac{\partial u_i}{\partial x_j}} = \frac{\partial \overline{u_i}}{\partial x_j} \qquad (2)$$

  - does not commute near boundary if $G(\boldsymbol{\xi},\boldsymbol{x}) \neq G(\boldsymbol{x},\boldsymbol{\xi})$
  - does not commute with product, hence sub-grid stress

$$\overline{u_i u_j} \neq \overline{u_i}\,\overline{u_j} \qquad R_{ij} = \overline{u_i u_j} - \overline{u_i}\,\overline{u_j} \neq 0 \qquad (3)$$

29

## Idea of sampling

- sample of $u_i$ at position $x$, and time $t$

$$S(u_i) = S_{\boldsymbol{x},t}(u_i) = u_i(\boldsymbol{x},t) \qquad (4)$$

- commutes with nonlinear operation

$$S(u_i u_j) = S(u_i)S(u_j) \qquad (5)$$

- does not commute with spatial differentiation

$$S\left(\frac{\partial u_i}{\partial x_j}\right) = \frac{\delta S(u_i)}{\delta x_j} + E_{xj}(u_i) \qquad (6)$$

$\frac{\delta S(u_i)}{\delta x_j}$ : differencing of samples

$E_{xj}(u_i)$ : sub-sampling error in diffrentiation with respect to $x_j$

30

## Equations for sampled values

- momentum equation for samples values

$$\frac{\partial S(u_i)}{\partial t}+\frac{\delta}{\delta x_j}\left(S(u_i)S(u_j)\right)=-\frac{1}{\rho}\frac{\delta S(p)}{\delta x_i}+g_i+\nu\frac{\delta^2}{\delta x_j \delta x_j}S(u_i) \tag{7}$$
$$-E_{xj}\left(u_i u_j\right)-\frac{1}{\rho}E_{xi}(p)+\nu E_{xj,xj}(u_i)$$

- continuity of sampled values

$$\frac{\delta S(u_i)}{\delta x_i}+E_{xi}(u_i)=0 \tag{8}$$

Sub-sampling term $E_{xj}(u_i)$ will depend on the estimate or definition of $\frac{\delta S(u_i)}{\delta x_j}$

31

# Some Numerical and Experimental Investigations of Stratified Shear Flows

Joongcheol Paik
Department of Civil Engineering
Gangneung-Wonju National University

Third Korea-Japan Mimi-Symposium on
Modeling and Measurement of Hydraulic Flows
March 16, 2012

Kobe University

# Outlines

- Motivation
- Numerical Works
  - Negatively Buoyant Wall Jet
  - Stratified Shear Flow
- Experimental Work
  - Intrusive gravity current in a stratified fluid
- Summary

*Previous Works*

## A Staged Modeling Approach: from EFDC to 3D high-resolution simulations

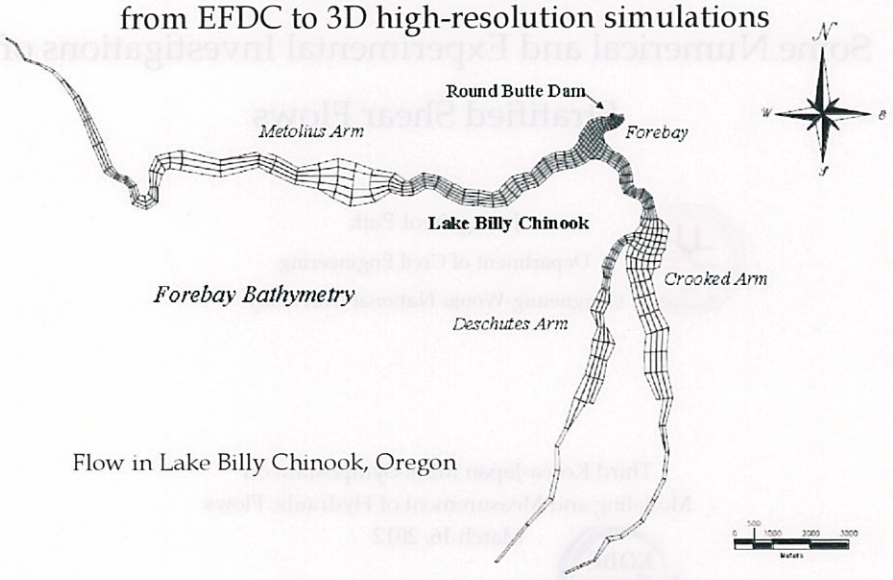


Flow in Lake Billy Chinook, Oregon

[Khangaonkar, Yang, Paik, Sotiropoulos, *JCR*, 2008]

*Previous Works*

## Selected withdrawal

Numerical simulation of selected withdrawal

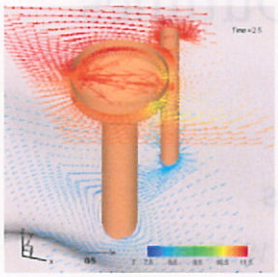

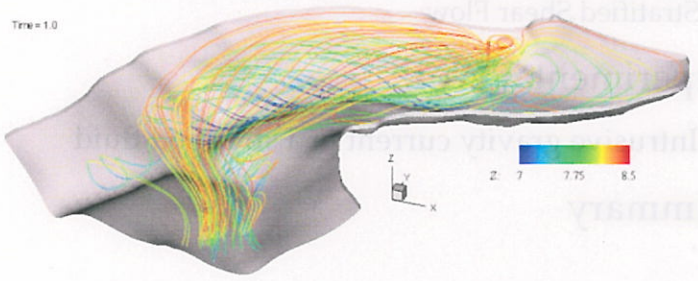


[Khangaonkar, Yang, Paik, Sotiropoulos, *JCR*, 2008]

# Governing equations

Large-scale momentum equations

$$\frac{\Gamma}{J}\frac{\partial u_i}{\partial t}+\frac{\partial}{\partial \xi^j}\left(\frac{1}{J}u_i U^j\right)=-\frac{\partial}{\partial \xi^j}\left(\frac{1}{J}p\xi^j_{x_i}\right)$$
$$+\frac{\partial}{\partial \xi^j}\left[\frac{1}{J}\left(\frac{1}{\mathrm{Re}}+\nu_t\right)\left(g^{mj}\frac{\partial u_i}{\partial \xi^m}+R_{mi}\xi^j_{x_m}\right)\right]-e_i^g\frac{1}{J}\frac{T}{Fr^2}$$

Temperature transport equation

$$\frac{1}{J}\frac{\partial T}{\partial t}+\frac{\partial}{\partial \xi^m}\left[\frac{1}{J}\left(UT-\left(\frac{1}{\mathrm{Pr}\,\mathrm{Re}}+\frac{\nu_t}{\mathrm{Pr}_t}\right)g^{mj}\frac{\partial T}{\partial \xi^m}\right)\right]=0$$

$$\mathrm{Re}=\frac{u_{ref}L_{ref}}{\nu}\qquad \mathrm{Fr}=\frac{U_{ref}}{\sqrt{\beta g L_{ref}\left(T_h-T_c\right)}}$$

# SGS models

Mason & Derbyshire (BLM, 1990)

$$\nu_t=\frac{\lambda^2}{\phi^2}S$$

where

$$S=\left(2S_{ij}S_{ij}\right)^{1/2}$$

$$\frac{1}{\phi}=1-\eta R_f,\ \text{with}\ \eta=3$$

$$\frac{1}{\lambda}=\frac{1}{\lambda_0}+\frac{1}{\left[\left(\kappa\left(z+z_o\right)\right)\right]}$$

$$\lambda_0=C_s\Delta\ \left[\Delta=\left(\Delta x\Delta y\Delta z\right)^{1/3}\right]$$

$z_0$ = wall roughness height

Turbulent Frandtl number
(Venayagamoorthy & Stretch, *JFM*, 2010)

$$\frac{\mathrm{Pr}_t}{\mathrm{Pr}_{t0}}=\exp\left(-\frac{Ri}{\mathrm{Pr}_{t0}\Gamma_\infty}\right)+\frac{Ri}{R_{f\infty}\mathrm{Pr}_{t0}}$$

# Test Case: Negatively buoyant wall jet

[Experiments by He et al. 2002]

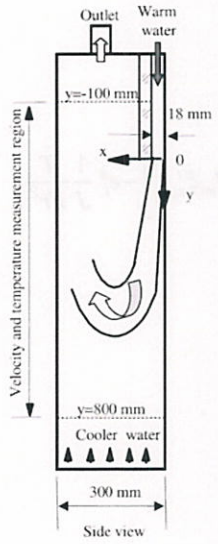


Experimental conditions

| Test | *Re* | *Gr* | *Ri* |
|---|---|---|---|
| 1 | 4754 | 0 | 0 |
| 2 | 4754 | 234000 | 0.01 |
| 3 | 6000 | 468000 | 0.013 |
| 4 | 4754 | 468000 | 0.02 |
| 5 | 3000 | 234000 | 0.026 |
| 6 | 4000 | 468000 | 0.029 |
| 7 | 3000 | 468000 | 0.052 |

$$Ri = \frac{g\beta(T_{hot} - T_{ref})L}{V^2} = \frac{gL(\rho_c - \rho_j)/\rho_j}{V_j^2}$$

$$Gr = \frac{gD^3(\rho_c - \overline{\rho j})/\rho_j}{\nu_j^2}$$



# Computational Details

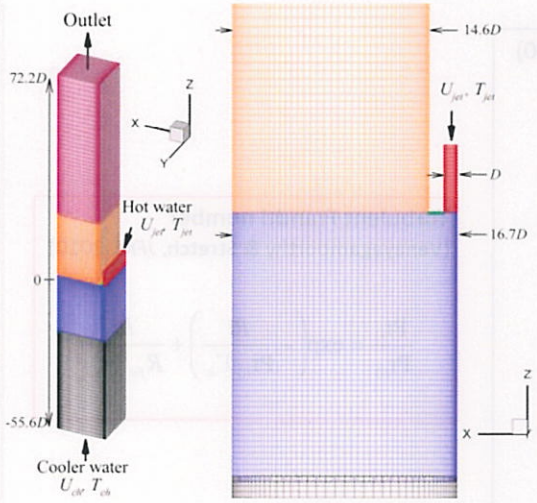


Overset grid

## Numerical approaches

- LES with two sgs models with buoyancy-correction
- Re = 4750
- $T_{jet}$ = 42° & $T_{ch}$ = 34°
- $U_{ch}/U_{jet}$ = 0.077, 0.15
- Mesh of $0.39\times10^6$ grid nodes with six sub-domains
- Non-reflecting characteristics-based outlet boundary condition

## Comparison of M-L and LES solutions

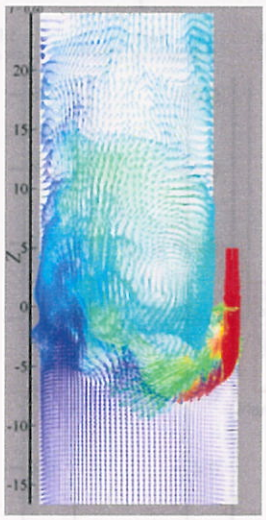

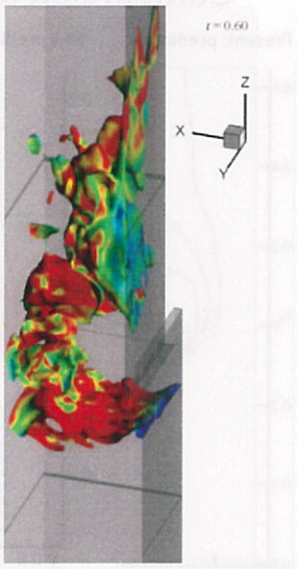


Velocity vectors colored by temperature and iso-surface of temperature at r=0.077



## Comparison of experiment and predictions

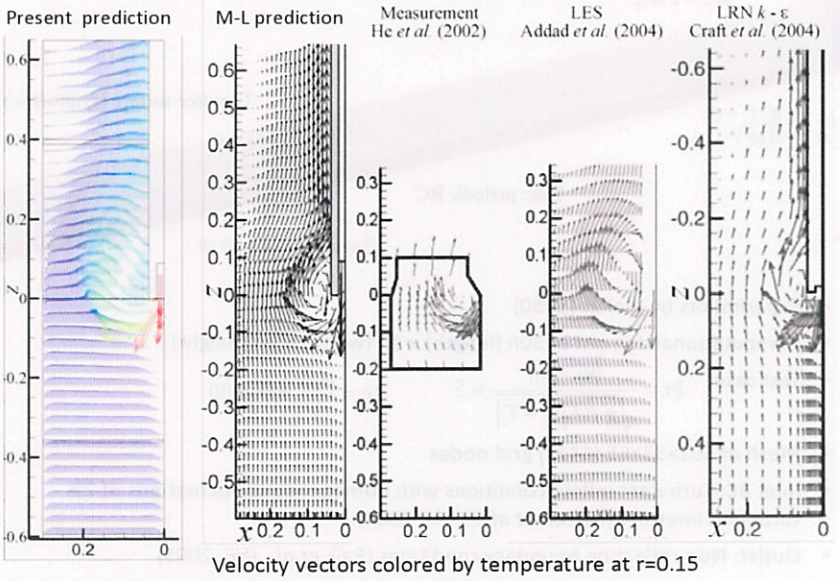


Velocity vectors colored by temperature at r=0.15

*Negatively buoyant wall jet*

# Comparison of experiment and predictions

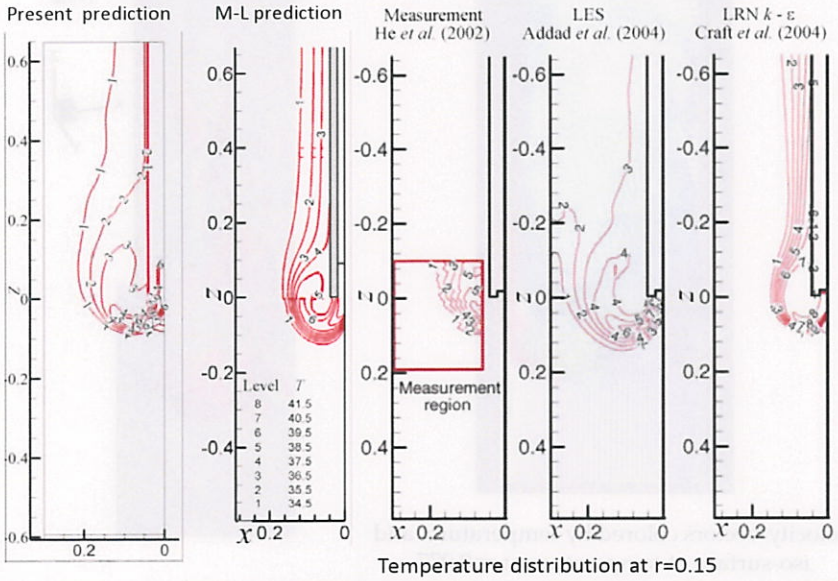


Temperature distribution at r=0.15

*Stratified shear flow*

# Computational details for a stratified shear flow

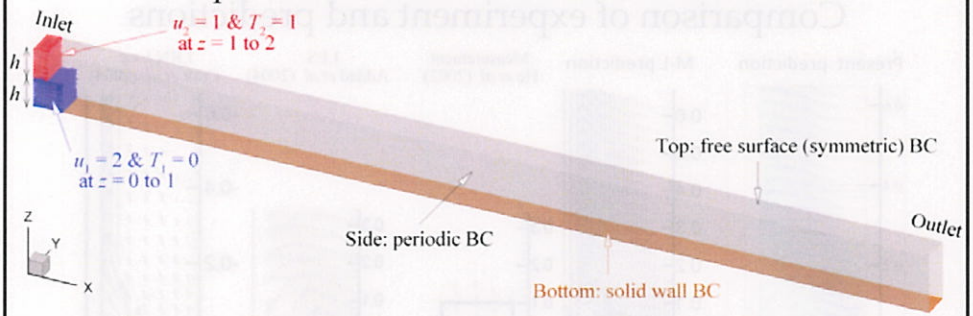


- Experiments by Viollet (1980)
- Computational domain of 30*h* (length) × 1*h* (width) × 2*h* (height)
- Test case: $\mathrm{Fr} = \dfrac{|u_2 - u_1|}{\sqrt{g\beta h|T_2 - T_1|}} = 5$ $\qquad \mathrm{Re} = \dfrac{u_2 h}{\nu} = 10{,}000$
- Mesh of 301×33×65 (646k) grid nodes
- Inlet BC: Turbulent inflow conditions with homogeneous fluctuations of 2% turbulent intensity (Batton *et al*. AIAAJ, 2004)
- Outlet: Non-reflecting boundary conditions (Paik *et al*., *JHE*, 2005)

## Numerical solutions

Temperature distribution (red $T$= 1, bule $T$ = 0)

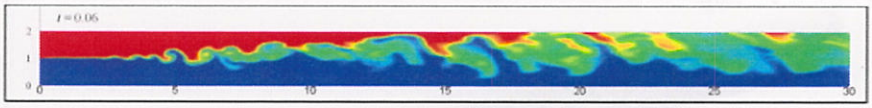


Iso-surface of temperature, $T$=0.5

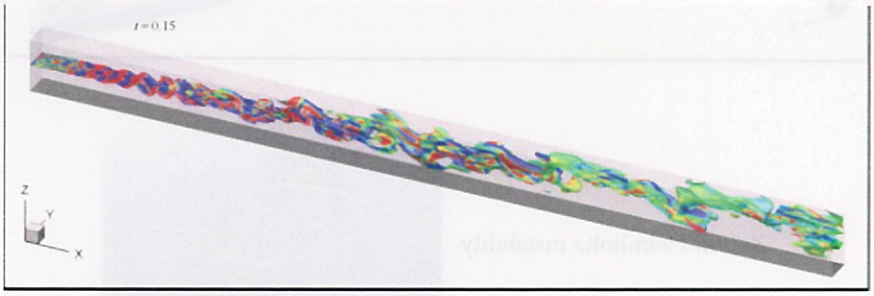


## Comparison of measurement & predictions

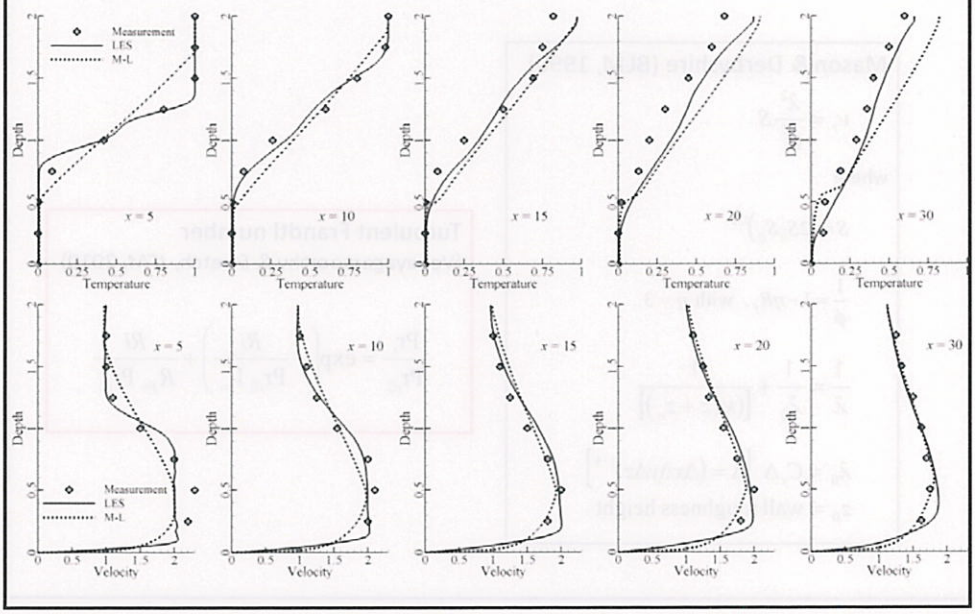

## Numerical solutions

Iso-surface of q-criteria colored by temperature

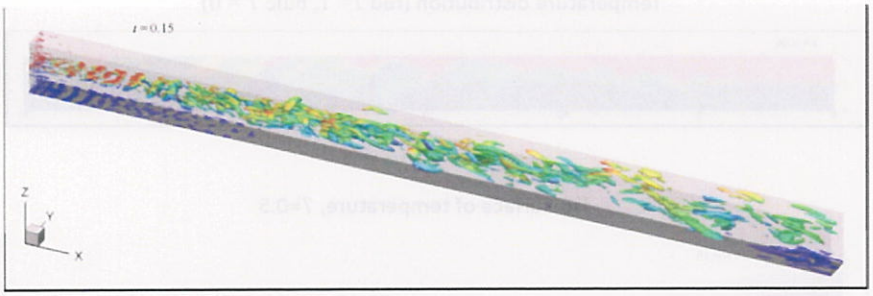


Kelvin-Helmholtz instability

## SGS models

Mason & Derbyshire (BLM, 1990)

$$\nu_t = \frac{\lambda^2}{\phi^2} S$$

where

$$S = \left(2 S_{ij} S_{ij}\right)^{1/2}$$

$$\frac{1}{\phi} = 1 - \eta R_f, \text{ with } \eta = 3$$

$$\frac{1}{\lambda} = \frac{1}{\lambda_0} + \frac{1}{\left[\left(\kappa\left(z + z_o\right)\right)\right]}$$

$$\lambda_0 = C_s \Delta \quad \left[\Delta = \left(\Delta x \Delta y \Delta z\right)^{1/3}\right]$$

$z_0$ = wall roughness height

Turbulent Frandtl number
(Venayagamoorthy & Stretch, *JFM*, 2010)

$$\frac{\mathrm{Pr}_t}{\mathrm{Pr}_{t0}} = \exp\left(-\frac{Ri}{\mathrm{Pr}_{t0}\,\Gamma_\infty}\right) + \frac{Ri}{R_{f\infty}\,\mathrm{Pr}_{t0}}$$

# Outlines

- Motivation
- Numerical Works
  - Negatively Buoyant Wall Jet
  - Stratified Shear Flow
- Experimental Work
  - Intrusive gravity current in a stratified fluid
- Summary


Turbid flow in reservoir (2003)

# Turbid Water in Imha Reservoir

Annual temperature variation (臨河Dam管理團, 2003)

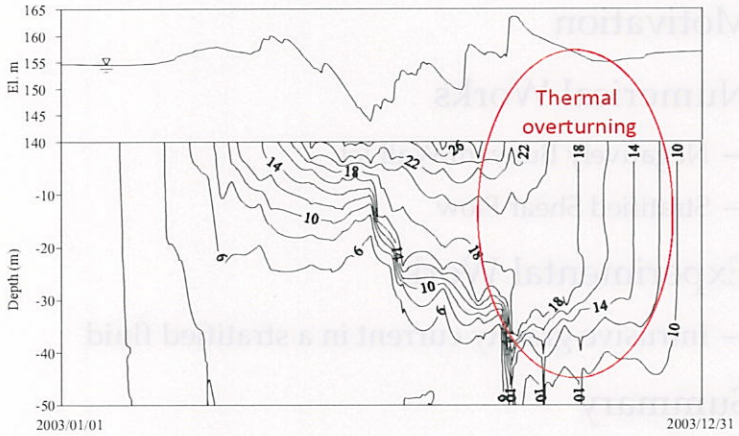


# Turbid water after overturning

(November, 2003)

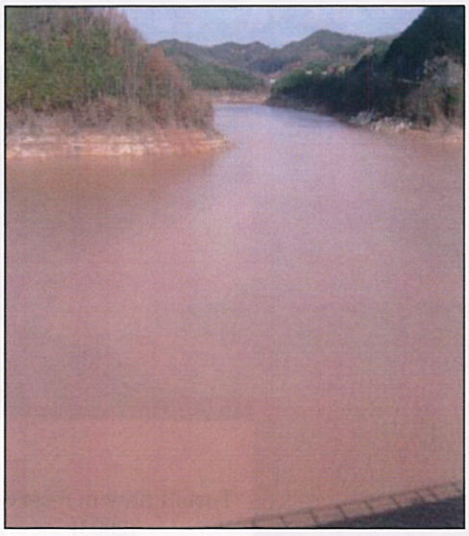

## Why turbid water?

1. Shale (頁巖 or 泥板巖) region
2. Steep arable land
3. Heavy rainfalls

# Intrusive Gravity Currents

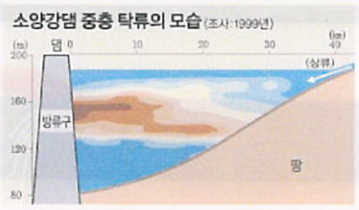


東亞日報, 2003

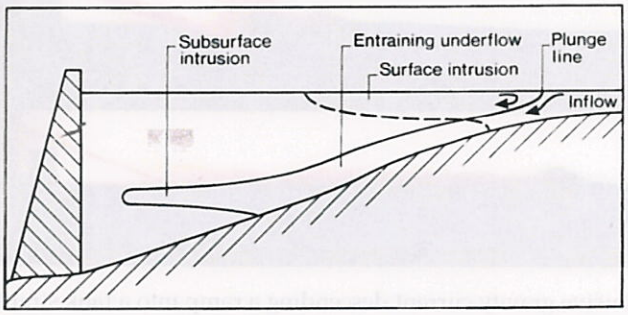


Figure 7.11 The flow of dense river water into a reservoir or lake (Simpson, 1997)

# Some experiments

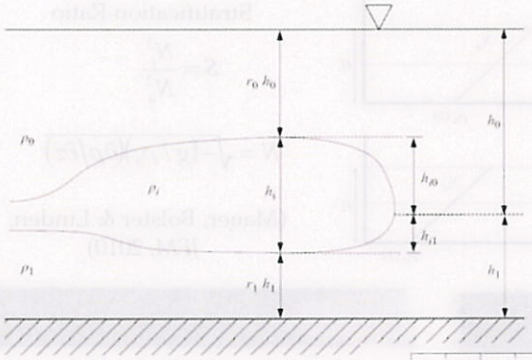

Intrusive gravity current between uniform layers of densities (Flynn & Sutherland, *JFM*, 2004)

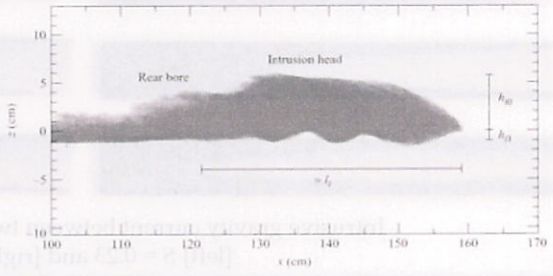

## Some experiments

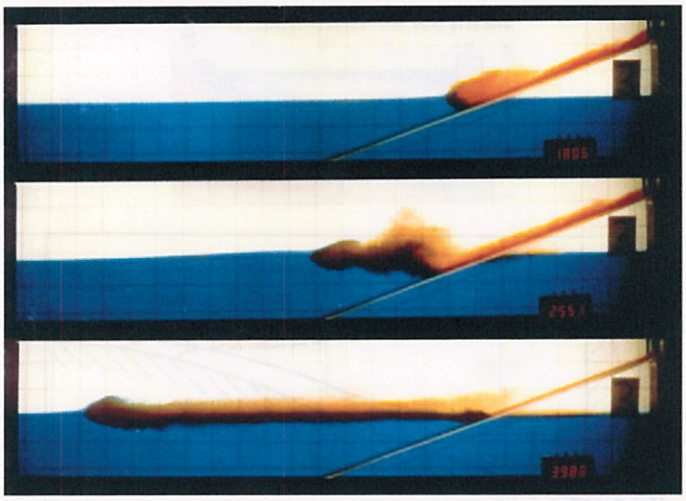

Intrusive gravity current descending a ramp into a tank stratified into two layers (Monaghan, *Annu. Rev Fluid Mech.* 2007)

## Some experiments

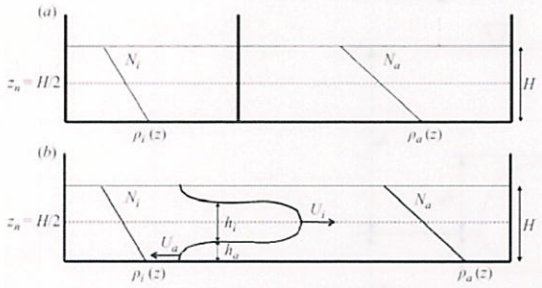


Stratification Ratio

$$S = \frac{N_i^2}{N_a^2}$$

$$N = \sqrt{-(g/\rho_0)(\partial\rho/\partial z)}$$

(Mauer, Bolster & Linden, *JFM*, 2010)

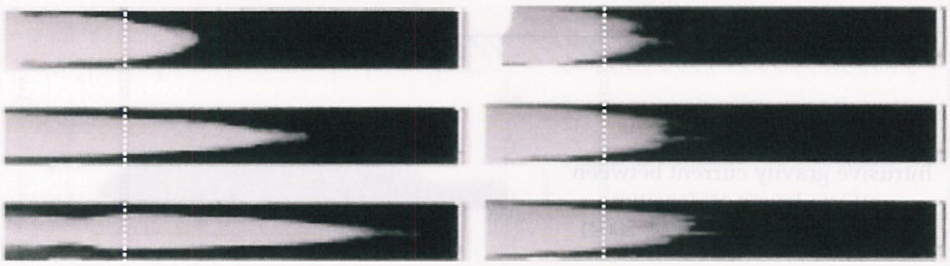

Intrusive gravity current between two stably stratified fluids: [left] $S = 0.23$ and [right] $S = 0.77$

## Experimental facility

for intrusive gravity currents in realistically stratified fluid

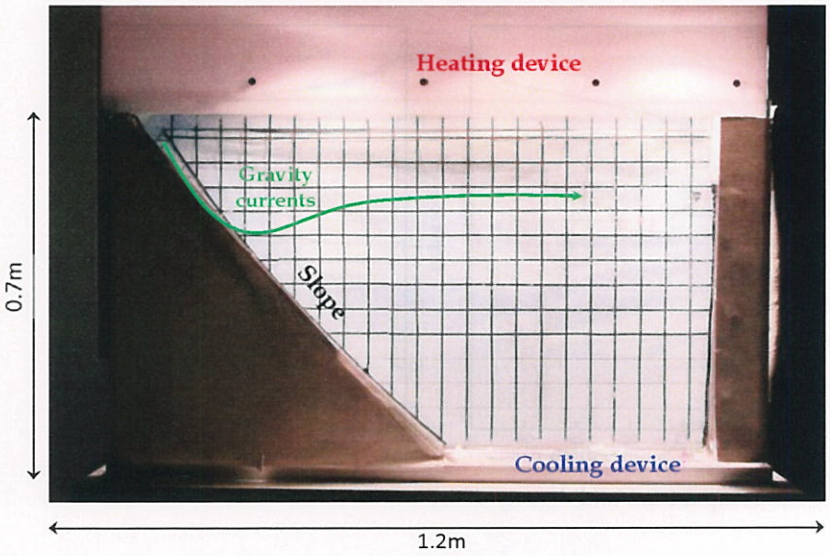


## Experimental configurations

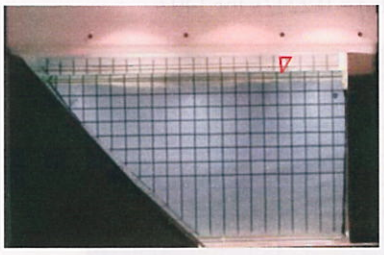

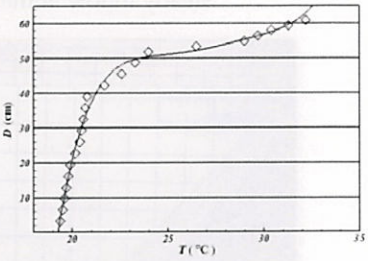


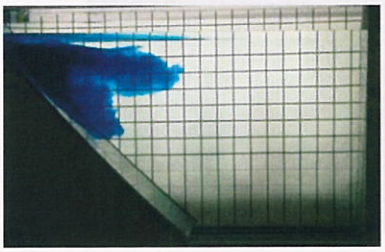

- Water tank: 120 cm X 30 cm X 70cm
- Water depth: 60 cm
- Operation of heating & cooling devices for 3 hours to reach equilibrium state of the stratification

## Experiments: Case I

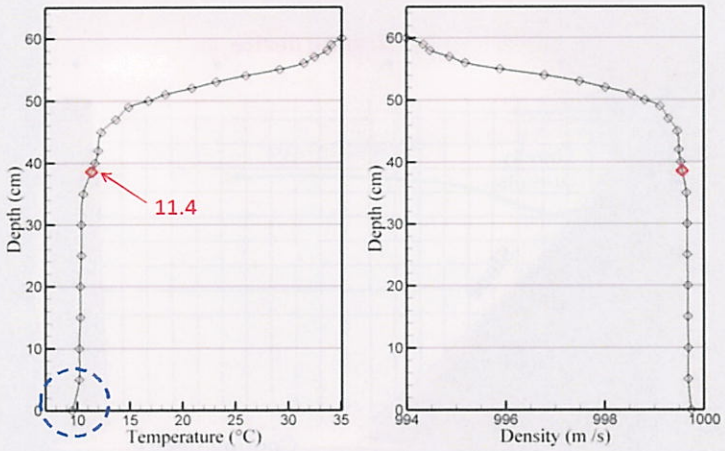


Temperature and density distributions in the vertical direction

## Experiments: Case I

Steady inflow at the inlet: $q$ = 0.22 l/s for 140 s

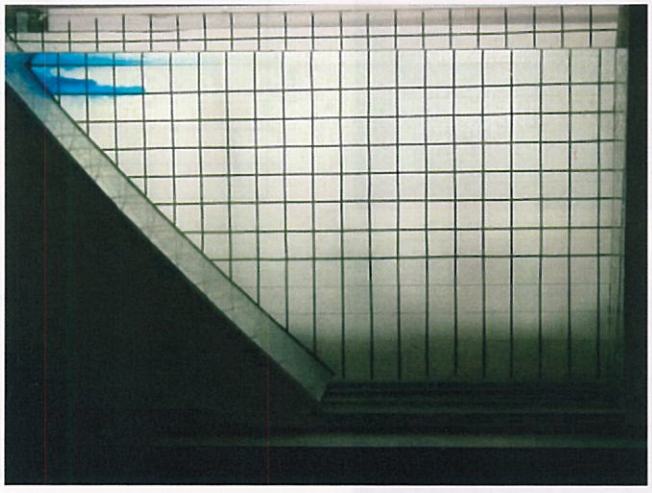

Intrusive gravity current along the slope and into thermally stratified ambient

# Experiments: Case I

Steady inflow at the inlet: $q$ = 0.22 l/s for 140 s

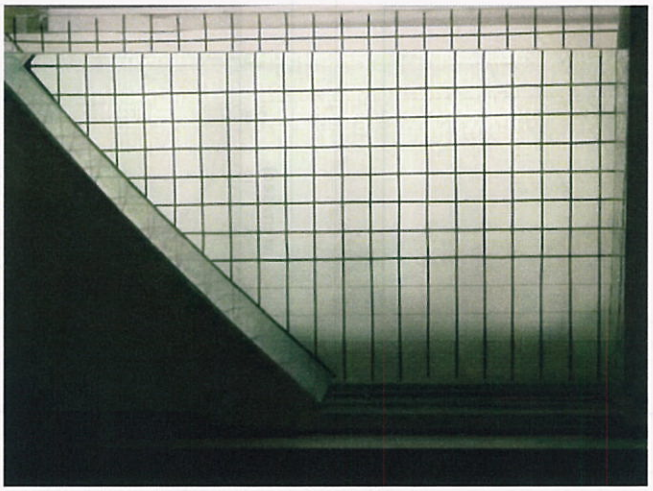

Intrusive gravity current along the slope and into thermally stratified ambient(×60)

# Experiments: Case I

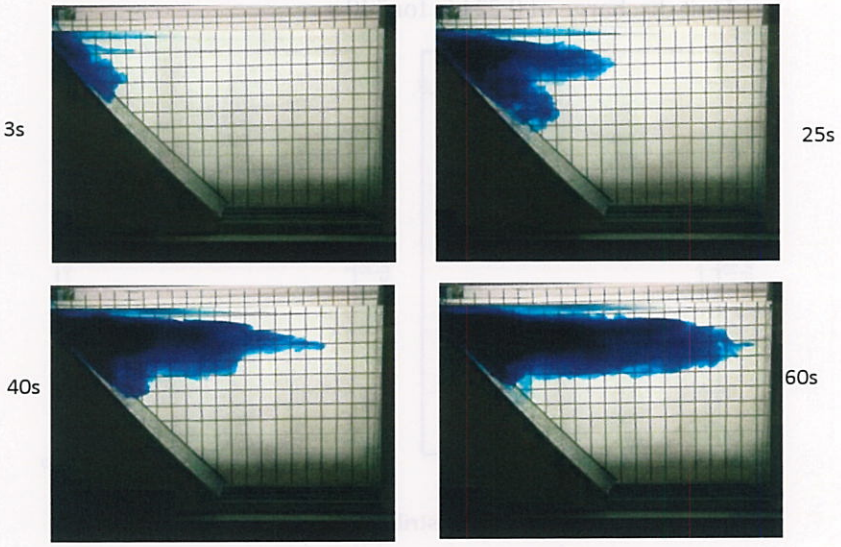


Instantaneous snapshots showing the propagation of the gravity current

# Experiments: Case I

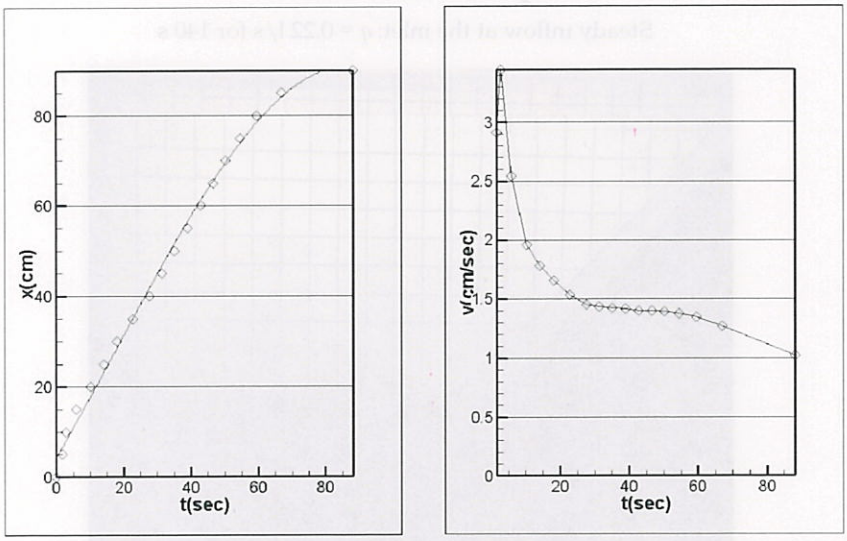


Time evolution of front location and front velocity of the intrusive gravity currents

# Experiments: Case II

- Unit discharge of 0.22 l/s for 140 s

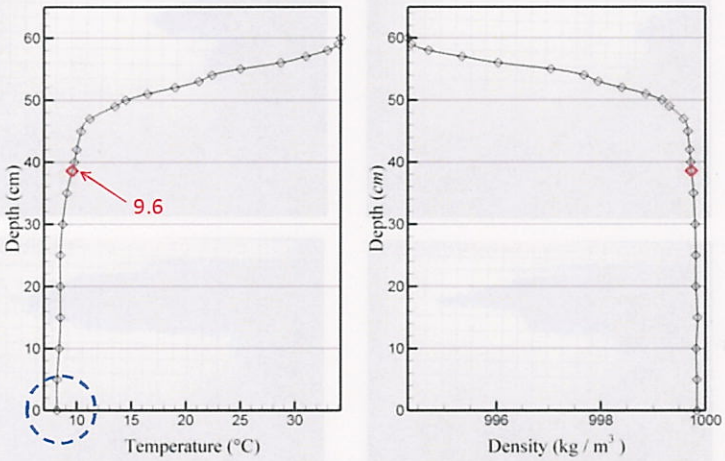


Temperature and density distributions in the vertical direction

## Experiments: Case I

Steady inflow at the inlet: $q$ = 0.22 l/s for 140 s

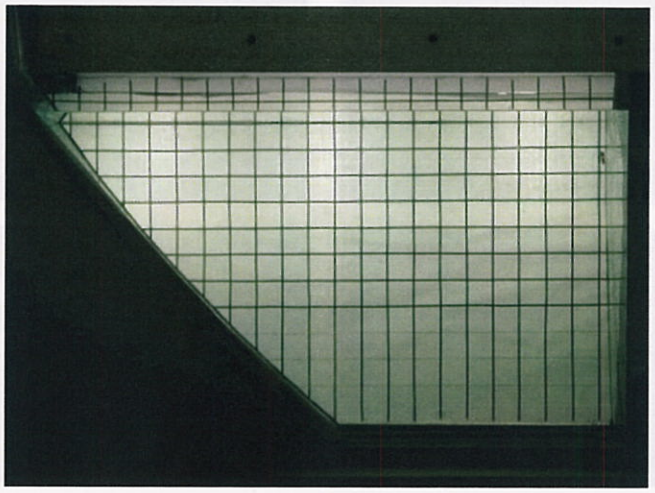

Intrusive gravity current along the slope and into thermally stratified ambient

## Experiments: Case I

Steady inflow at the inlet: $q$ = 0.22 l/s for 140 s

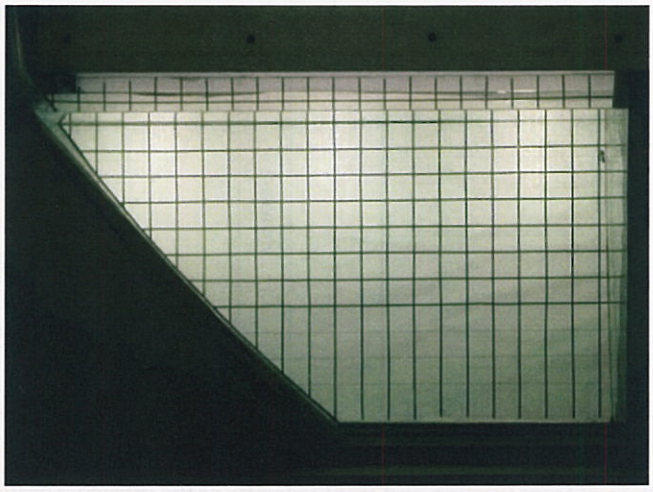

Intrusive gravity current along the slope and into thermally stratified ambient (×60)

## Experiments: Case II

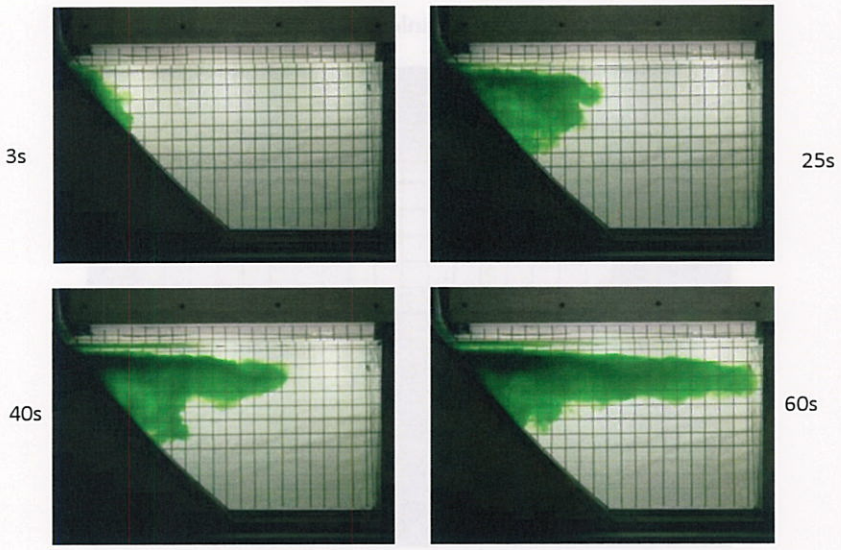


Instantaneous snapshots showing the propagation of the gravity current

## Experiments: Case II

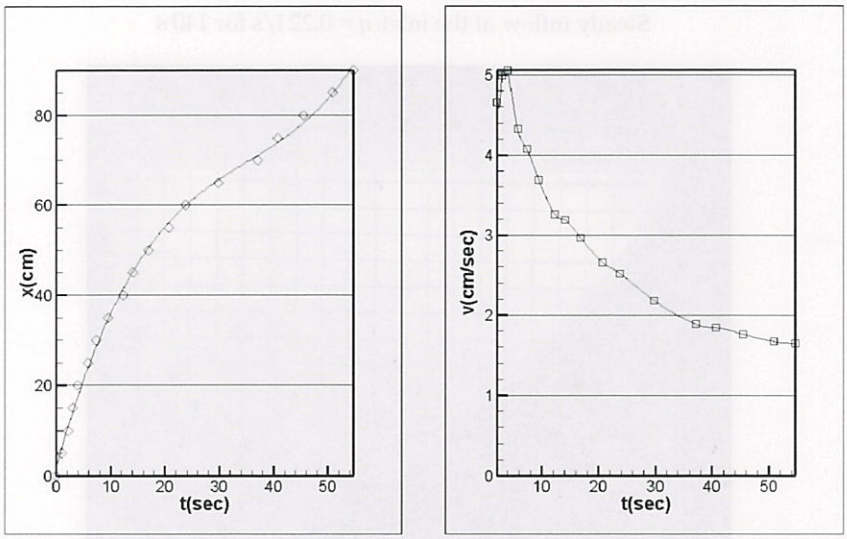


Time evolution of front location and front velocity of the intrusive gravity currents

## Experimental results

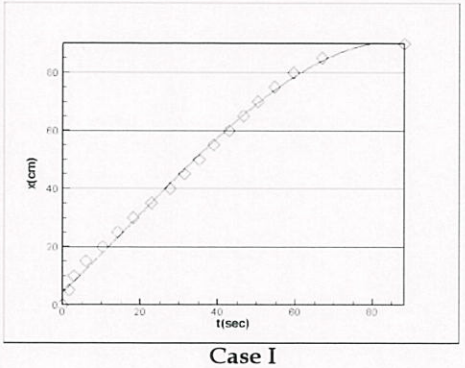


Case I

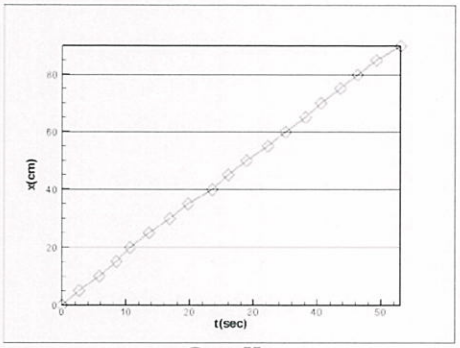


Case II

- Case 1: Front velocity decreases near the end wall
- Case 2: Front velocity keeps constant until the current reaches to the end wall
- Propagation speed of the current head is faster at Case 2 than Case 1

## Summary

- A large-eddy simulation model with the Richardson number correction for buoyancy effect has been developed and successfully applied for mixing problems of a negatively buoyant wall jet and a stratified shear flow.
- Numerical results show that the buoyancy-corrected SGS model is capable of simulating both test cases with good accuracy at affordable grid resolution, which demonstrates that the present can be a practical engineering tool.
- A experimental facility for intrusive gravity currents in realistically stratified fluid has been developed. To the best of our knowledge, it is the first time to reproduce the intrusion in realistic ambient fluid.
- Subsequent experimental investigation of intrusive gravity currents using turbid water will help us to understand the propagation and mixing dynamics of intrusive gravity currents in the real reservoirs.

*This work is supported by NRF Grant No. 2011-0003416*

# URANS and LES computations of channel flows with triangular roughness on side walls

2012/03/16

Yuichi Kouchi (The Chugoku Electric Power Co., Inc)
Takashi Hosoda (Kyoto University)
Ichiro Kimura (Hokkaido University)

## Introduction

**Background**

The importance of hydropower increases as a renewable and a domestic energy.

**Problem**

An economical development point of hydropower has decreased because a lot of hydro-power-plants have already been developed.

⇩

It is necessary to reduce greatly construction cost of hydro-power-plants to develop plants in the future.



## The porpose of this study

Reduction of the construction cost of the hydro-power-plant

⇩

Omission of concrete lining of headrace tunnels

⇩

It is necessary to evaluate the resistance law of flows in the tunnel without lining for the design.

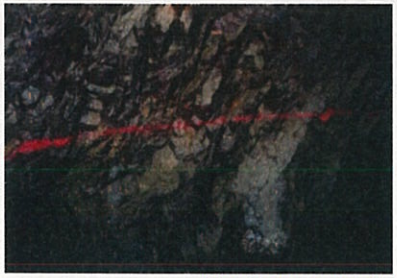

Headrace tunnel without concrete lining



## The contents of this study

**An usual method**

We have used empirically Manning's law to design headrace tunnnels. However, it is difficult to evaluate the Manning roughness coefficient of the tunnel without lining at the design stage.

⇩

**A new method**

We try to estimate the resistance law of the flow in the headrace tunnel with very large roughness by computer fluid dynamics with the grid dividing the roughness.


tunnel with concrete lining　　tunnel without concrete lining

## Calculation method

**CFD**

Recent rapid advance of computer technology has made it possible to use LES or DNS. These simulations can reproduce the turbulent flow more accurately. However, RANS type turbulence model are still valid especially for engineering purposes because they require less CPU time than LES or DNS.

In this study, we verified applicability of numerical model with URANS type turbulence models and LES for simulating the channel flows with triangular roughness on side walls.



## Outline of the experiment

- We performed a laboratory test on an open channel flow by using an experimental flume with triangular roughness on side walls .
- The height of triangular roughness is 2cm and the width is 4cm. The length of the flume is 10m. The bottom of the flume is flat.

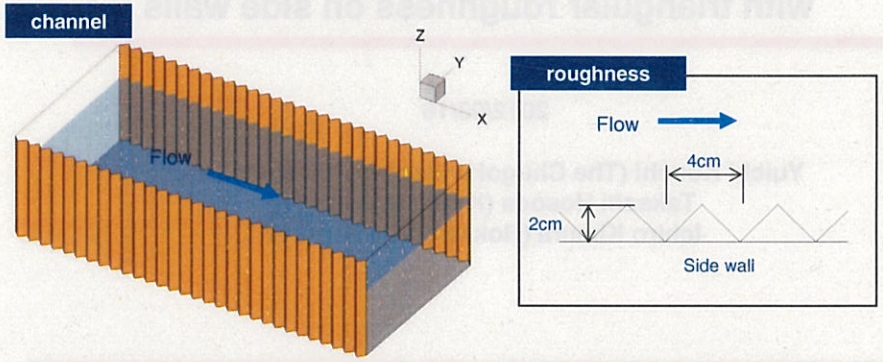




## The hydraulic conditions in the experiment

| | |
|---|---|
| Water depth(h) | 0.220m |
| Water width (B) | 0.6m |
| Discharge(Q) | 0.08m³/s |
| Average velocity (Vave) | 0.61m/s |
| Inclination(S) | 1/500 |
| Frude number (Fr) | 0.41 |
| Reynolds number (Re) | $1.3 \times 10^5$ |

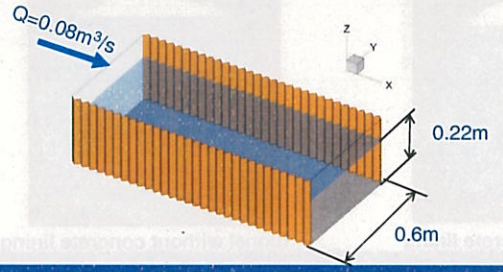




## Calculation method

- We carried out numerical analysis of three models to reproduce flow of the flume.

| Type | Model |
|---|---|
| URANS | Standard k- ε model |
| | Non-linear k- ε model |
| LES | Standard Smagorinsky model |

## Basic equation（URANS）

- The Reynolds averaged 3D flow equations with contravariant components of velocity vectors on a generalized curvilinear movable coordinate system are used as governing equations. The equations are expressed as follows.

Continuity equation

$$\frac{1}{\sqrt{g}}\frac{\partial V^{\alpha}\sqrt{g}}{\partial \xi^{\alpha}}=0$$

Momentum equation

$$\frac{\partial V^{i}}{\partial t}+\nabla_j\left[V^{i}(V^{j}-W^{j})\right]+V^{i}\nabla_j W^{j}+V^{j}\nabla_j W^{i}=F^{i}-\frac{1}{\rho}g^{ij}\nabla_j p+\nabla_j\left[-\overline{v^{i}v^{j}}\right]+2\nu\nabla_j S^{ij}$$

k equation

$$\frac{\partial k}{\partial t}+\nabla_j\left[k(V^{j}-W^{j})\right]+k\nabla_j W^{j}=-g_{ij}\overline{v^{i}v^{j}}\nabla_j V^{i}-\varepsilon+\nabla_j\left\{\left(\frac{D_t}{\sigma_k}+\nu\right)g^{ij}\nabla_i k\right\}$$

ε equation

$$\frac{\partial \varepsilon}{\partial t}+\nabla_j\left[\varepsilon(V^{j}-W^{j})\right]+\varepsilon\nabla_j W^{j}=-C_{\varepsilon 1}\frac{\varepsilon}{k}g_{ij}\overline{v^{i}v^{j}}\nabla_j V^{i}-C_{\varepsilon 2}\frac{\varepsilon^{2}}{k}+\nabla_j\left\{\left(\frac{D_t}{\sigma_k}+\nu\right)g^{ij}\nabla_i \varepsilon\right\}$$



## Non-linear k ε model

- The second order non-linear k-ε model, which can take into account the anisotropy of turbulence, is adopted as URANS model (Kimura and Hosoda 2003).

$$-\overline{v'^{i}v'^{j}}=D_t S^{ij}-\frac{2}{3}k\delta^{i}_{s}g^{sj}-\frac{k}{\varepsilon}D_t\left[\alpha_1 Q_1+\alpha_2 Q_2+\alpha_3 Q_3\right]$$

$$Q_1=S^{i\alpha}g_{\alpha\beta}\Omega^{\beta j}+S^{j\beta}g_{\beta\alpha}\Omega^{\alpha i}$$

$$Q_2=S^{i\alpha}g_{\alpha\beta}S^{\beta j}-\frac{1}{3}S^{k\alpha}g_{\alpha\alpha}S^{m\beta}g_{\beta k}\delta^{i}_{l}g^{lj}$$

$$Q_3=\Omega^{i\alpha}g_{\alpha\beta}\Omega^{\beta j}-\frac{1}{3}\Omega^{k\alpha}g_{\alpha\alpha}\Omega^{m\beta}g_{\beta k}\delta^{i}_{l}g^{lj}$$

$$S^{ij}=g^{j\alpha}\nabla_\alpha V^{i}+g^{i\alpha}\nabla_\alpha V^{j}$$

$$\Omega^{ij}=g^{j\alpha}\nabla_\alpha V^{i}-g^{i\alpha}\nabla_\alpha V^{j}$$

$$\alpha_1=-0.1325f_M$$

$$\alpha_2=0.0675f_M$$

$$\alpha_3=-0.0675f_M$$

$$f_M=\frac{1}{1+0.02M^{2}}$$

$$C_\mu=\min\left[0.09,\ \frac{0.3}{1+0.09M^{2}}\right]$$

$$M=\max[S,\Omega]$$

$$S=\frac{k}{\varepsilon}\sqrt{\frac{1}{2}S^{i\alpha}g_{\alpha\beta}S^{j\beta}g_{\beta i}}$$

$$\Omega=\frac{k}{\varepsilon}\sqrt{\frac{1}{2}\Omega^{i\alpha}g_{\alpha\beta}\Omega^{j\beta}g_{\beta i}}$$



## Basic equation（LES）

- We have adopted these equation as the governing equations of LES. The velocity in these equations is spatially filtered velocity.
- The eddy viscosity coefficient of the LES is expressed as follows.

Continuity equation

$$\frac{1}{\sqrt{g}}\frac{\partial V^{\alpha}\sqrt{g}}{\partial \xi^{\alpha}}=0$$

Momentum equation

$$\frac{\partial V^{i}}{\partial t}+\nabla_j\left[V^{i}(V^{j}-W^{j})\right]+V^{i}\nabla_j W^{j}+V^{j}\nabla_j W^{i}=F^{i}-\frac{1}{\rho}g^{ij}\nabla_j p+\nabla_j\left[-\overline{v^{i}v^{j}}\right]+2\nu\nabla_j S^{ij}$$

SGS応力

$$\nu_t=\left(C_s\Delta\right)^{2}\left(S^{ij}S^{ij}\right)^{1/2}\qquad \Delta=\left(\sqrt{g}\right)^{1/3}$$ Smagorinsky constant $C_s=0.15$



## Boundary and calculation conditions

| | |
|---|---|
| Inlet and outlet | Cyclic boundary condition |
| The centre line of channel | Symmetric condition |
| Walls | Log-low for the smooth wall |
| Free surface | The rigid-lid boundary conditions |
| Convection term(Momentum eq.) | 2nd order TVD-MUSCLE |
| Convection term(k and ε eq.) | 2nd order TVD-MUSCLE |
| Time integration | 2nd order Adams-Bashforth |
| Time step | 0.0005sec |

## Calculation grid

- We used same grid on computation of URANS and LES to examine the possibility and the limitation of URANS models. Numbers of grid points are 200 in the longitudinal direction, 70 in transverse direction and 60 in the depth-wise direction.
- In this study, the triangular roughness is divided by the small grid .The height of the roughness is 2cm and the height of first shell along the roughness is 2mm.

Grid

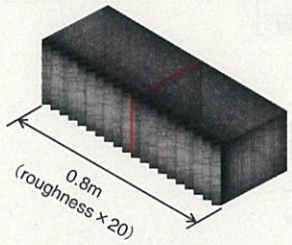


roughness

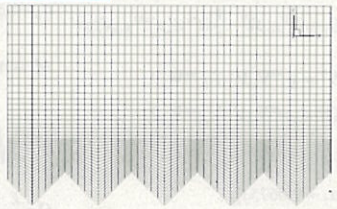

X200 × Y70 × Z60



## Experimental result

- The maximum-velocity-dip phenomenon which was measured in the experiment.

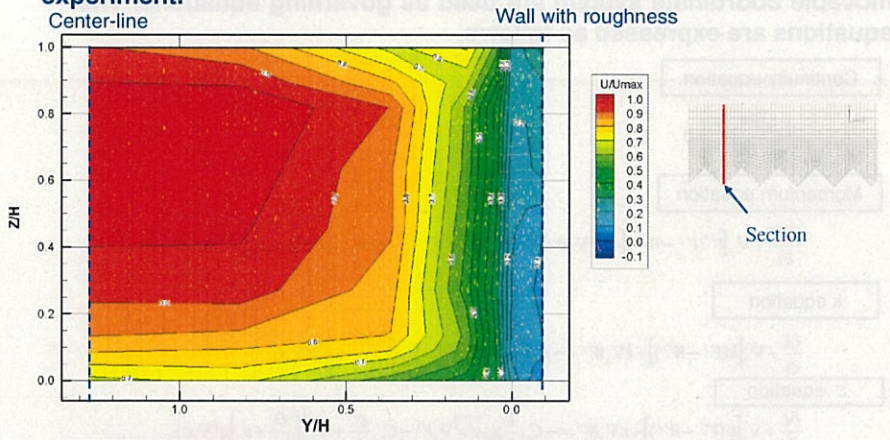


The distribution of averaged velocity in X direction



## Calculated result (URANS,non-linear k- ε model)

- The computation by URANS reproduce the maximum-velocity-dip phenomenon which was measured in experiment.

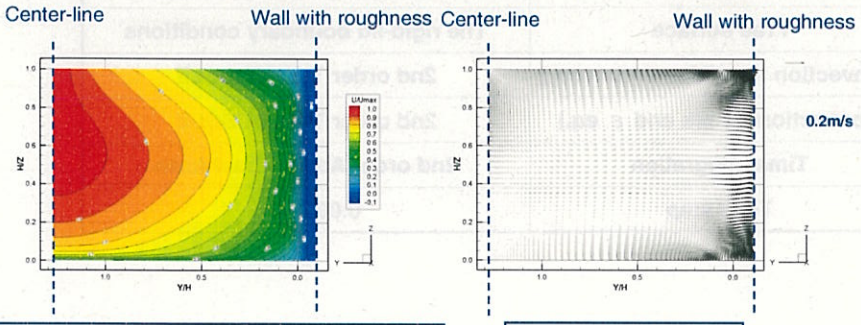


The distribution of averaged velocity in X direction

Flow pattern



## Calculated result (LES)

- The computation by LES reproduce the maximum-velocity-dip phenomenon which was measured in experiment.

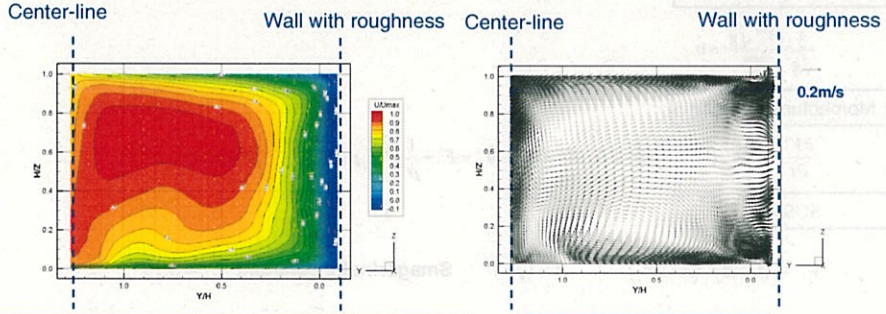


The distribution of averaged velocity in X direction

Flow pattern

## Comparison with experimental and calculated result

- The computation by URANS and LES reproduce the maximum-velocity-dip phenomenon which was measured in experiment. The computational results of LES agree with the experimental result better than the results of URANS. It is necessary to modify the URANS model and to calculate using various grids in the future work.

Experiment

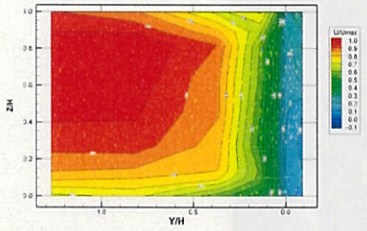

URANS(Non-linear k- ε )

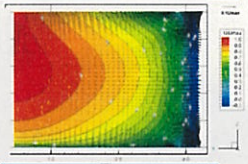

URANS(Standard k- ε )

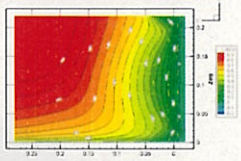

LES

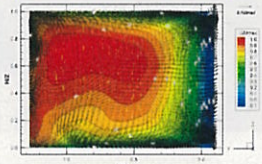



## Secondary current

- The two large vortices are shown at upside and downside in the flume at the computational results. These vortices are secondary current of second kind caused by the anisotropy of turbulence which was observed at a straight open channel flow of the previous study.

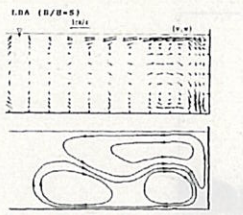

今本、石垣、塩野：開水路側壁近傍の壁面せん断力分布と流れの3次元構造について（水工学論文集1995）

URANS(Non-linear k- ε )

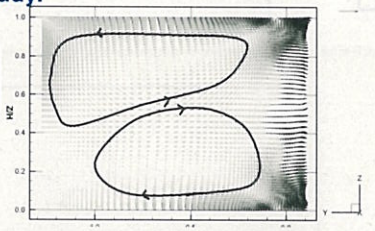

LES

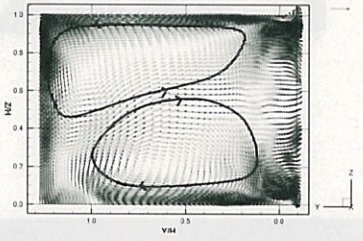



## y+

- From the calculated result, the time averaged y+ along the roughness is about 5 to 15, the maximum of momentary y+ is about 40. This value is a little small to apply log-law for URANS simulations. However most areas are the outside of the viscous sub-layer, it can be considered that we can use log-law for URANS simulations.

URANS(Non-linear k- ε )

Time averaged y+

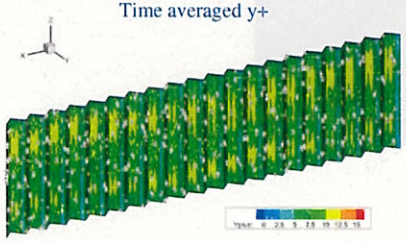

momentary y+

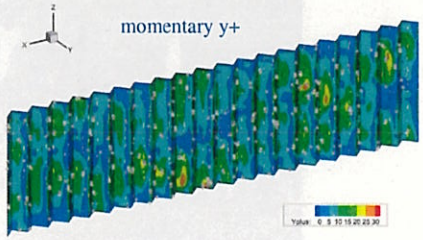



## 3D-structure of flow

- In order to examine properties of three dimensional flows near the side walls, the calculated results of URANS are visualized. This animation shows the invariants of the velocity-gradient tensor of the result of URANS.

URANS(Non-linear k- ε )

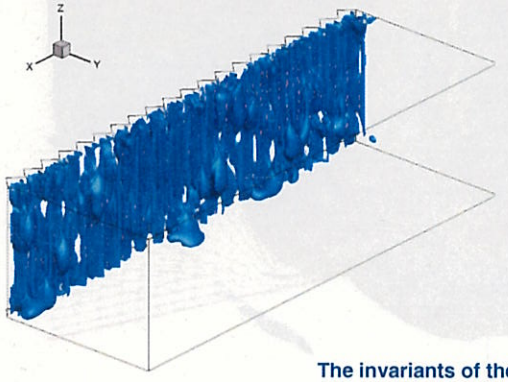

$$\lambda_2 = -\frac{1}{2}\frac{\partial u_i}{\partial x_j}\frac{\partial u_j}{\partial x_i}$$

The invariants of the velocity-gradient tensor

## 3D-structure of flow

URANS(Non-linear k-ε )

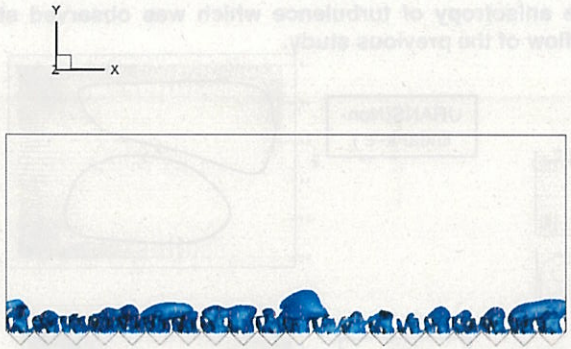




## The vortex tubes near the free surface

- There are three kinds of vortex tubes. The vortex tubes near the free surface rotate in the anti-clockwise direction.

URANS(Non-linear k-ε )

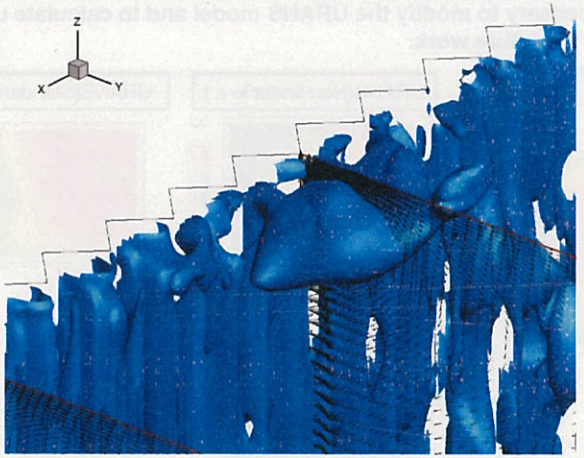




## The vortex tubes near the bottom

- On the other hand, the vortex tubes near the bottom rotate in the clockwise direction.

URANS(Non-linear k-ε )

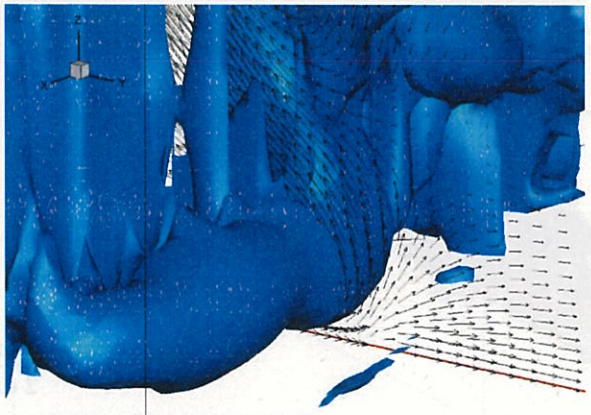



## Hairpin vortexes

- Hairpin vortexes composed of two vortex tubes are seen in half the height of depth .

URANS(Non-linear k-ε )

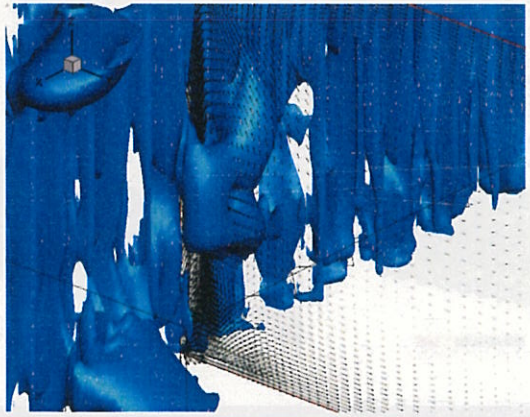

## The waver of secondary flow near the triangul[illegible]oughness

- The non-linear k-ε models can reproduce the waver of secondary flow near the triangular roughness on side walls.

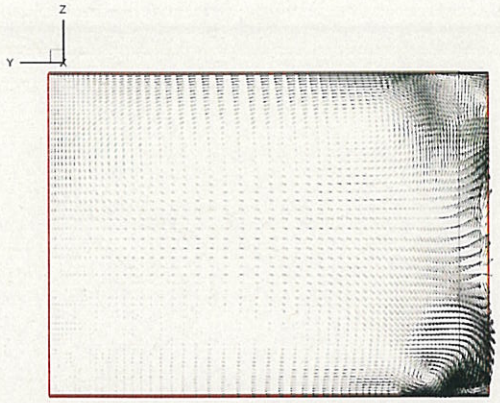


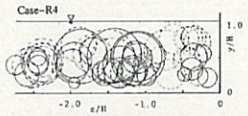


Fig. 6. Distribution of flow cells observed in 35 photographs as shown in Fig. 5.

今本博健，石垣泰輔，塩野耕二：直線開水路流れの二次流について，京都大学防災研究所年報，第35号，B-2,pp.571-579,1993.



## Comparison [illegible] the vortex tube with URANS and LES

- The many vortex tubes from time averaged velocity of LES are seen near the water surface and bottom. We hope URANS can reproduce 3d-structure of turbulence near the trianguler roughness roughly.

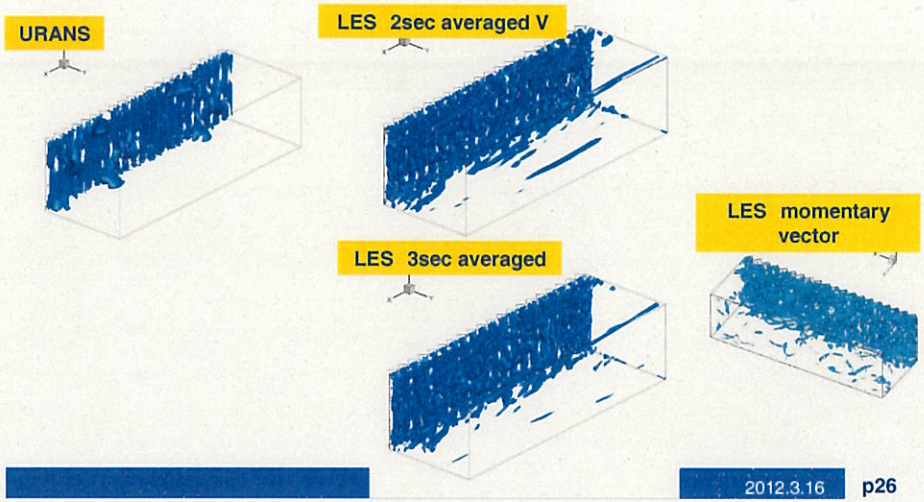




## Concluding remarks

- The computation by URANS and LES reproduce the maximum-velocity-dip phenomenon which was measured in experiment. The computational results of LES agree with the experimental result better than the results of URANS. It is necessary to modify the URANS model and to calculate using various grids in the future work.

- In the future, we plan to apply URANS at the planning stage of hydro-power-plants because URANS require less CPU time than LES and apply LES at the detailed design stage.

Korean Japan mini-simpojium
Kobe Univ.

# Efficient Method for River Surface Flow Measurements

Ichiro FUJITA

Department of Civil Engineering, Graduate School of Engineering, Kobe University,
1-1 Rokkodai, Nada, Kobe, 675-8501, Japan, ifujita@kobe-u.ac.jp

## Background

#1 River flow velocity distribution or river discharge
⇒ one of the most important hydrological parameters in planning rivers

#2 Conventional measurement method for flood (Japan, Korea)
⇒ float method; measure distance along their paths and integrate them over the cross-sectional area

#3 Float method
⇒ robust and simple to use in various conditions
⇒ difficult to employ in huge flood condition or sudden flood
⇒ measurement itself becomes extremely dangerous or impossible
⇒ traceability of floats is questionable

#4 Alternative methods
⇒ acoustic Doppler current profiler (ADCP) , UHF radar radio wave velocity meter, ultrasonic velocity meter
⇒ imaging techniques (LSPIV,STIV)

## Objective

#1 Radar and imaging methods
⇒ assume water surface ripple convection with the surface flow

#2 LSPIV without seeding particles
⇒ tend to yield underestimated value depending on flow condition

# Examine the accuracy of imaging methods with other measurement instrument (ADCP)
# Compare the performance of STIV with LSPIV

- Large-Scale Particle Image Velocimetry (LSPIV)
  1994: Fujita, Komura (JSCE)
  1998: Fujita, Muste, Kruger (J.Hyd,Res.)
- Space-Time Image Velocimetry (STIV)
  2005: Fujita, Tsubaki (IAHR)
  2007: Fujita, et al. (JRBM)

## LSPIV (Large-Scale PIV)

#1 Extension of PIV to free surface velocity measurement
⇒ with or without seeding

#2 Field images are usually taken from riverbank or bridge
⇒ oblique images are obtained

#3 Establish mapping relation between screen coordinates (x,y) and physical coordinates (X,Y,Z)
⇒ use mark points located along riverbank

#4 Generate rectified images
⇒ use water level information

#5 Apply conventional PIV to the rectified images

#6 The size of the template becomes an order of meter or ten meters
⇒ physical scale is different from laboratory experiments

## LSPIV introduced on Hydrolink (IAHR)

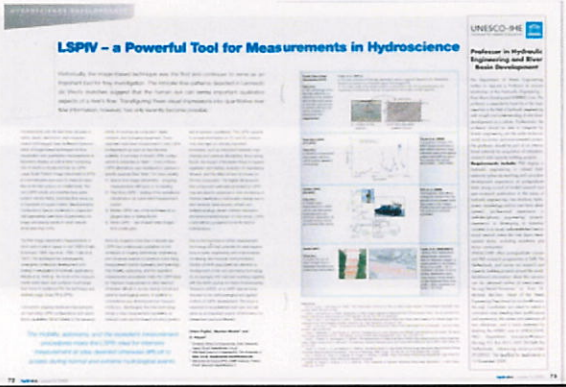


## STIV(Space-Time Image Velocimetry)

The STIV is the algorithm to calculate automatically the mean gradient or image orientation appeared in the space-time image by image analysis.

Generation of space-time image

1. set a search line in the direction of the main surface flow.
2. construct STI by piling up the luminance distribution on the search line.

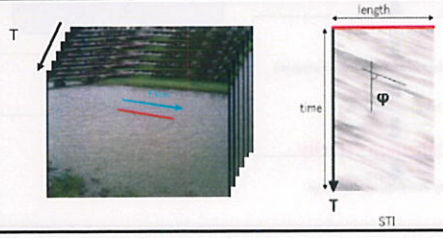

## STIV Procedure (1/5)

①oblique image ②corrected image

Image transformation

Read Bmp files

**Set search lines**

Internal process

Construct STI

Calculate orientation angle from histogram

Calculate coherency

Calculate velocity

Velocity distribution, discharge

**Use LSPIV to set the mean direction**

Transformation

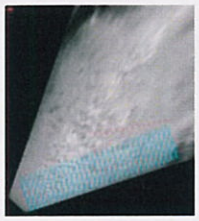

## STIV Procedure(2/5)

①oblique image ②corrected image

Image transformation

Read Bmp files

Set search lines

Internal process

**Construct STI**

Calculate orientation angle from histogram

Calculate coherency

Calculate velocity

Velocity distribution, discharge

Template for calculating orientation vector

length

time

**Gradient tensor method**

*Tensor of image orientation*

$$J_{pq} = \int_A \frac{\partial g}{\partial x_p}\frac{\partial g}{\partial x_q}\,dxdt$$

$$\tan 2\phi = \frac{2J_{12}}{J_{22} - J_{11}}$$

## STIV Procedure(3/5)

①oblique image ②corrected image

Image transformation

Read Bmp files

Set search lines

Internal process

Construct STI

**Calculate orientation angle from histogram**

Calculate coherency

Calculate velocity

Velocity distribution, discharge

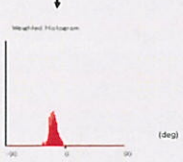


## STIV Procedure(4/5)

①oblique image ②corrected image

Image transformation

Read Bmp files

Set search lines

Internal process

Construct STI

Calculate orientation angle from histogram

**Calculate coherency**

Calculate velocity

Velocity distribution, discharge

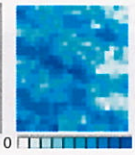


Coherency indicates strength of image pattern

1.0 for ideal pattern

0.0 for white noise

**Definition of coherency**

$$J_{pq} = \int_A \frac{\partial g}{\partial x_p}\frac{\partial g}{\partial x_q}\,dxdt$$

$$C_c = \frac{\sqrt{(J_{22} - J_{11}) + 4J_{12}^2}}{J_{11} + J_{22}}$$

## STIV Procedure(5/5)

①oblique image ②corrected image

Image transformation

Read Bmp files

Set search lines

Internal process

Construct STI

Calculate orientation angle from histogram

Calculate coherency

**Calculate velocity**

Velocity distribution, discharge

**Mean angle with Cc as a weight**

$$\bar{\phi} = \int \phi C(\phi) d\phi / \int C(\phi) d\phi$$

**Mean velocity along search line**

$$U = \frac{S_x}{S_t}\tan\bar{\phi}$$

$Sx$ : length scale (m/pixel)
$St$ : time scale (sec/pixel)
$\varphi$ : orientation angle

## LSPIV vs STIV

**LSPIV:**

- # two-dimensional measurement method
- # usually use seeded image in laboratory experiment
- # tend to yield underestimated value for unseeded image

**STIV:**

- # one-dimensional measurement method
- # need information of flow direction
- # can be used for seeded and unseeded images
- # algorithm is simple

## Setting of measurement panels

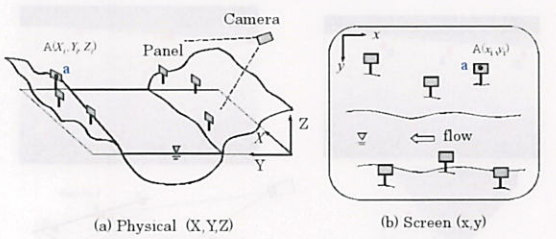


(a) Physical (X,Y,Z) (b) Screen (x,y)

# Note : set the panels in a zigzag manner
# difficult to set the panels nearer to the camera

## Example of panel setting

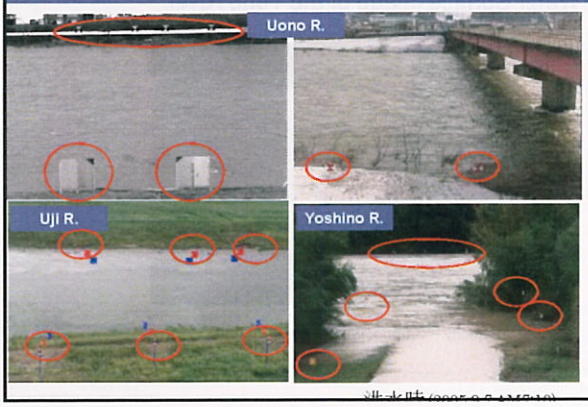


## Mapping relations

Physical coordinates (X,Y,Z) and screen coordinates (x, y)

$$x=\frac{A_1X+A_2Y+A_3Z+A_4}{C_1X+C_2Y+C_3Z+1} \qquad y=\frac{B_1X+B_2Y+B_3Z+B_4}{C_1X+C_2Y+C_3Z+1}$$

Determine 11 variables from more than 6 panel coordinates by the least square method

If we assume the water surface is flat

$$Z=D_1X+D_2Y+D_3$$

Substitution of the above eq. to the original relation

$$x=\frac{(A_1+A_3D_1)X+(A_2+A_3D_2)Y+(A_3D_3+A_4)}{(C_1+C_3D_1)X+(C_2+C_3D_2)Y+(C_3D_3+1)}=\frac{aX+bY+c}{dX+eY+f}$$

$$y=\frac{(B_1+B_3D_1)X+(B_2+B_3D_2)Y+(B_3D_3+B_4)}{(C_1+C_3D_1)X+(C_2+C_3D_2)Y+(C_3D_3+1)}=\frac{gX+hY+i}{dX+eY+f}$$

Another relations

$$x_p-x_c=-f\left[\frac{m_{11}(X_p-X_{c1})+m_{12}(Y_p-Y_{c1})+m_{13}(Z_p-Z_{c1})}{m_{31}(X_p-X_{c1})+m_{32}(Y_p-Y_{c1})+m_{33}(Z_p-Z_{c1})}\right]$$

$$y_p-y_c=-f\left[\frac{m_{21}(X_p-X_{c1})+m_{22}(Y_p-Y_{c1})+m_{23}(Z_p-Z_{c1})}{m_{31}(X_p-X_{c1})+m_{32}(Y_p-Y_{c1})+m_{33}(Z_p-Z_{c1})}\right]$$

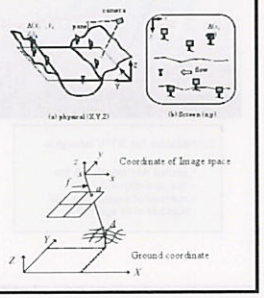


## Measurement site: Tone River

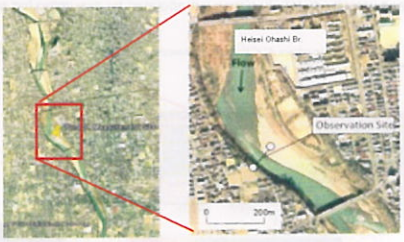


Location of the observation site in the Tone River in Maebashi City, downstream of the Heisei Ohashi Bridge; about 180km from the river mouth

## ADCP: Acoustic Doppler Current Profiler


| | |
|---|---|
| mode | 12 (high speed) |
| layer | 10 cm |
| Number of layer | 50 |
| sampling time at a point | 3.2s |
| Water ping | 3 |
| Bottom ping | 3 |

## Measurement section

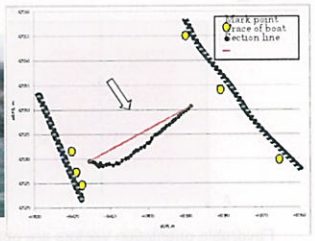


Measurement section and trace of boat-mounted ADCP

## Water Surface image of the Tone River

Velocity ~ 3.5m/s, Water depth ~ 2.0m

## Mark point locations and image transformation

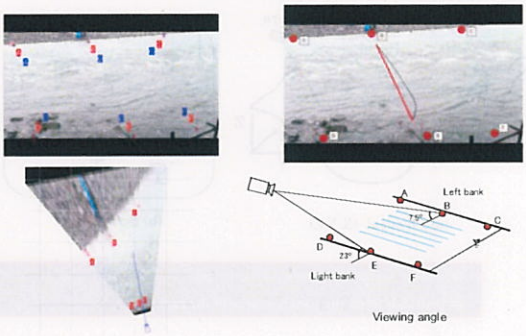


Transformed image used for LSPIV

## Measurement data by ADCP

Water surface velocity distribution was extrapolated by assuming log profile

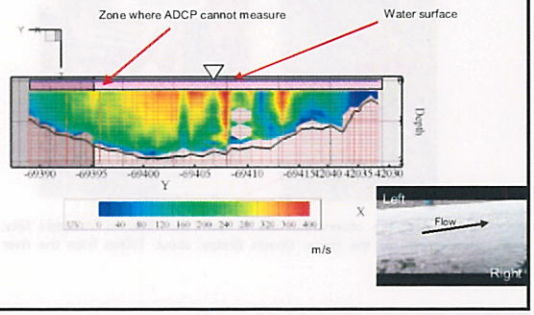


## Measurements by STIV

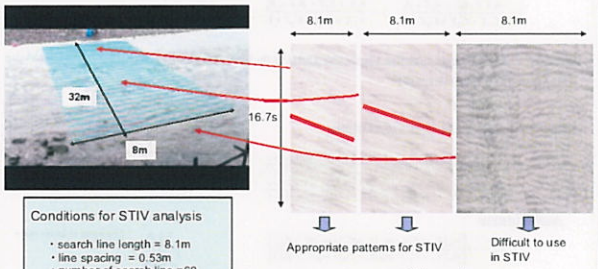


Conditions for STIV analysis

- search line length = 8.1m
- line spacing = 0.53m
- number of search line =60
- number of image = 500

## Application of STIV with 2D-FFT for image filtering

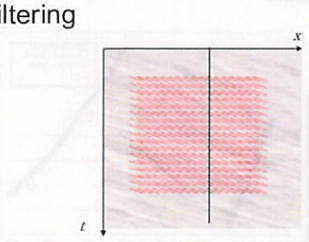


STI is rearranged to a square shape of 256 by 256 pixel

Template size in STIV = 40 by 40

Favorable orientation vectors are obtained

## Measurement by LSPIV

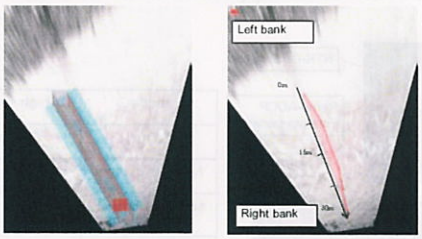


conditions for LSPIV analysis

- template size = 40*40 pixel
- spacing =0.53m
- number of template = 60
- pixel size = 8cm/pixel
- number of image = 500
- dt = 0.0666 s

## Comparison with ADCP (the Tone River)

- Streamwise velocity distributions

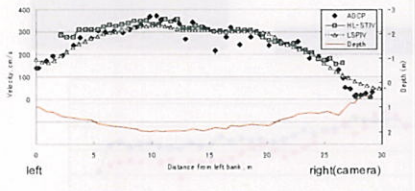


Discharges

| method | Q(m3/s) |
|---|---|
| STIV | 100.48 |
| LSPIV | 98.60 |
| ADCP | 89.64 |

Maximum velocity :
almost the same for each method
Velocity profile :
STIV and LSPIV ⇒ yield smooth variation
ADCP ⇒ data scatter due to almost instantaneous measurement while traversing


## Measurement of the Uono River flow

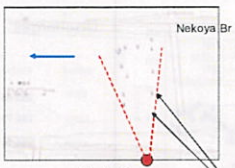


Camera is set on the left bank

Mark points

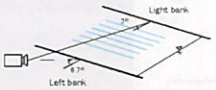


Viewing angle


Setting of mark point at water surdace

## Captured surface image of the Uono River

This video was not captured for the purpose of measurement, but just as a reminder of the flow feature.

## Measurement by STIV

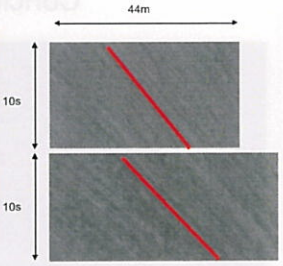


STI samples

Conditions for STIV analysis
- search line length = m
- line spacing = 2m
- number of search line =60
- number of image = 300

Surface features are clearly visible even from a distance!

## Measurement by LSPIV

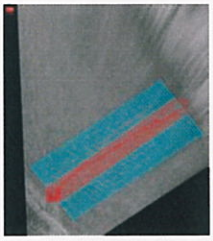

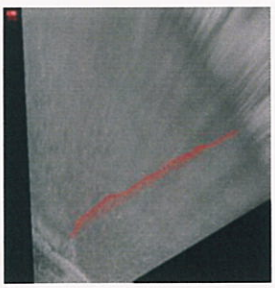

conditions for LSPIV analysis
- template size = 40*40 pixel
- spacing =2.0m
- number of template = 60
- pixel size = 25cm/pixel
- number of image = 300
- dt = 0.13 s

## Measurement by ADCP

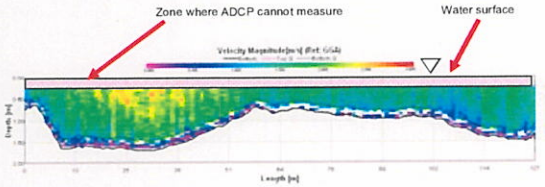

## Comparison with ADCP (the Uono River)

- Streamwise velocity distribution

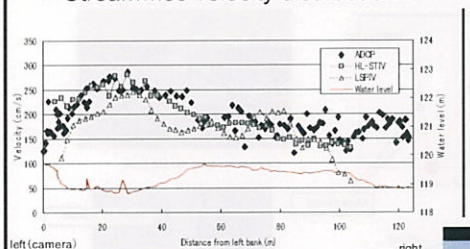


Discharges

| method | Q(m3/s) |
|---|---|
| STIV | 292.45 |
| LSPIV | 186.78 |
| ADCP | 296.79 |


STIV ⇒ similar to ADCP
LSPIV ⇒ underestimated data

## Another flood data of the Uono River

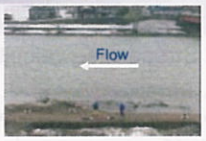


Snow-melt flood of Uono River

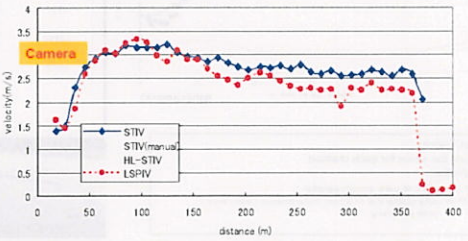


## Conclusion

#1 Measurements of river surface velocity by three different methods, i.e. ADCP, LSPIV and STIV are conducted in the upstream reach of the Tone River and the Uono River.

#2 Despite the difference in measurement techniques, the measured data agreed well with each other in the Tone River measurement, demonstrating the validity of the assumption that the water surface ripples are advected with the surface velocity

#3 In The Uono River measurement, LSPIV yields underestimated value due to the poor image resolution and low viewing angle. On the other hand, STIV successfully measured surface velocity even under such conditions.

#4 Since the above assumption does not hold true in a severe weather condition with wind waves, the effect of the wind on the advection of surface pattern is a further research to investigate.

Thank you for your kind attention!

# *When River Meets Sea*

Development of power generation technology utilizing salinity gradient of fresh and sea water

March 16 2012

Lee, Seung Oh

Hongik University, Korea

홍익대학교 HONGIK UNIVERSITY

HERL Hydro-Environmental Research Laboratory Hongik University

## Contents

Introduction

Background

Technology development

Results

Expectation

Conclusion

# Introduction



## Introduction(1)

- **What are problems facing our earth?**

Hunger

Pollutant

Education


Global warming

Energy Sources

What can engineers do?

# Introduction(1)

- **Who can solve these problems?**

Hunger

Pollutant

Education

⇨ This can be solved with International cooperation.



# Introduction(1)

- **Who can solve these problems?**


Global warming

Energy Sources

⇨ This problem only engineering can be solved.

Before that — For solving the problem, we must know about that.

# Introduction(1)

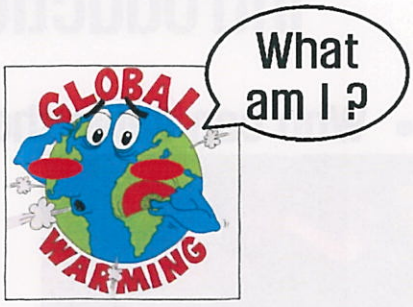


- **What is the Global warming?**
  - Definition
    → Rising average temperature of Earth' s atmosphere and oceans

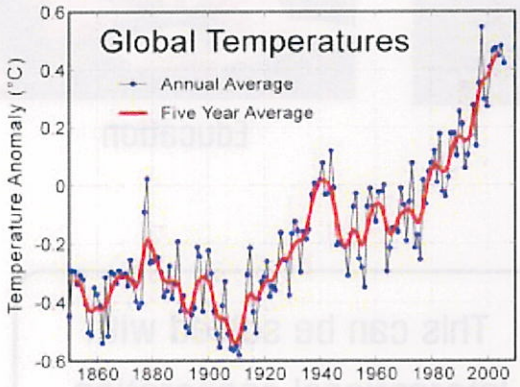


It will cause.....

Rising of Sea levels

Changing precipitation pattern

Expansion of subtropical deserts

Continuing retreat of glaciers

(Occurrence of extreme weather
Changes in crop yields
Extinction of animals)

⇩

There are directly related to human's life.



# Introduction(1)

- **What causes Global warming?**
  - Too many Greenhouse gases that made by human


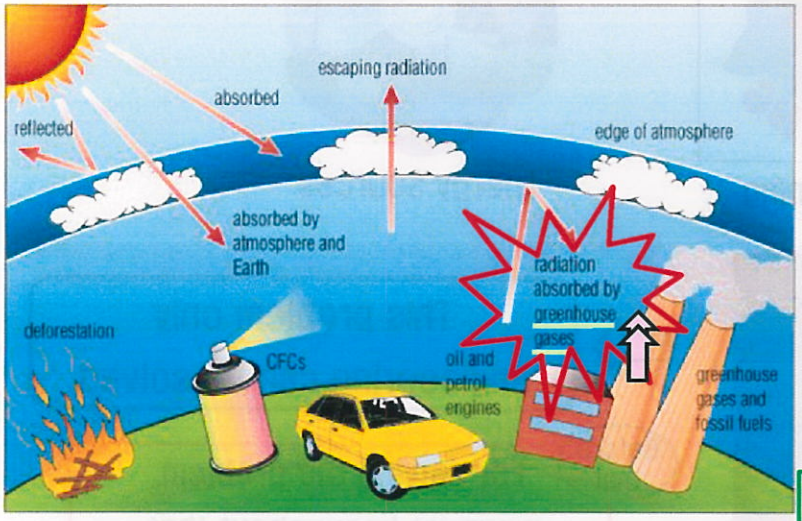


The gases were made by.....

Wood

Coal

Oil

Natural gas

(ethane, propane, butanes, pentanes)

The fossil energy!

⇩

**Source of global warming**

# Introduction(1)

- **Why government can't stop using fossil energy?**

1. Low level of renewable energy technologies
2. Cheaper than other green energy source
3. Stable energy supply

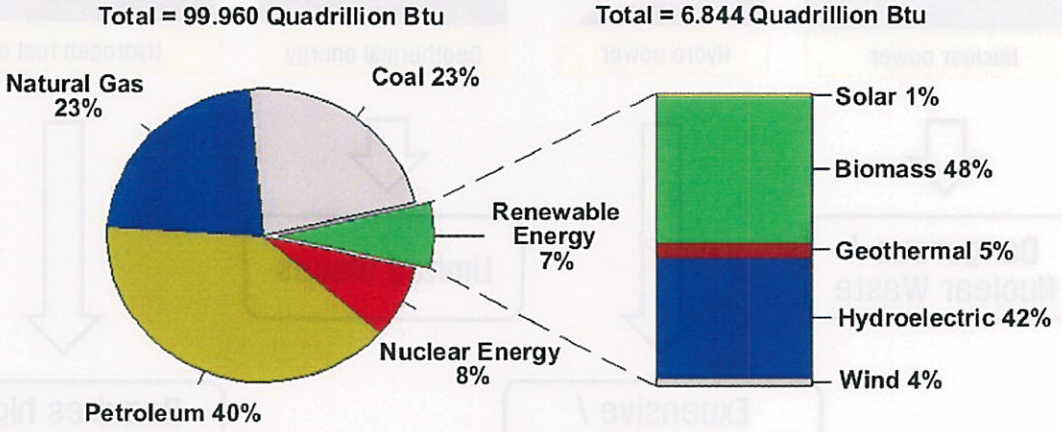




# Introduction(1)

- **But the reality is...**

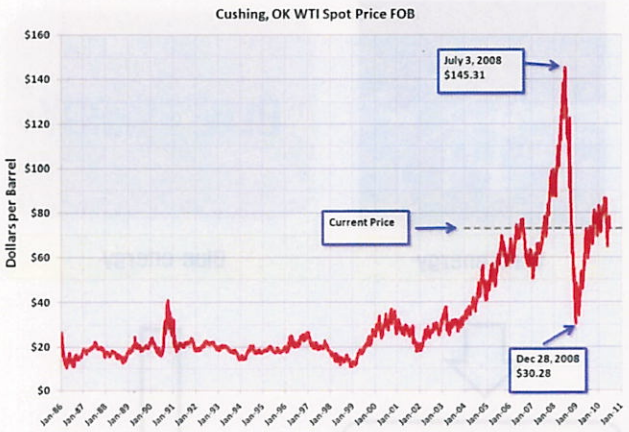


Unstable oil price /
Depletion of fossil energy

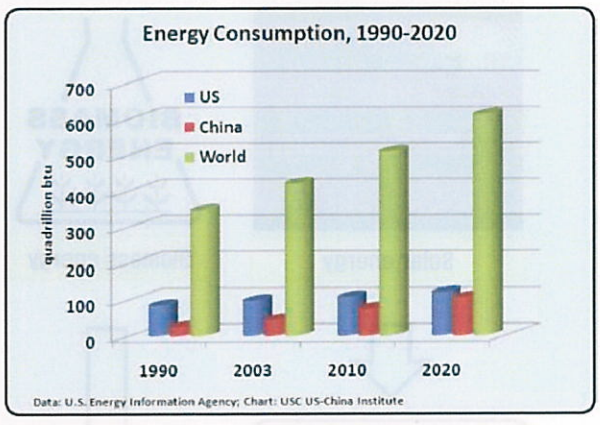


increase in energy demand

**The Alternative Energy should be developed.**

# Introduction(2)

- **Alternative energy**

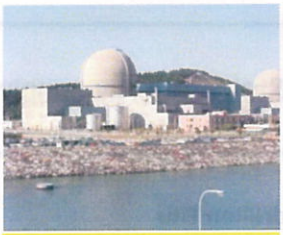

Nuclear power

Hydro power

Geothermal energy

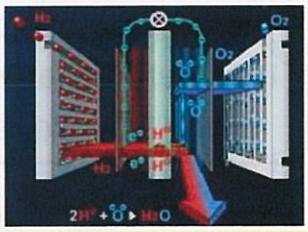

Hydrogen fuel cell

Dangerous / Nuclear Waste

Expensive / Requires the dam

Limited places

Requires highly technology



# Introduction(2)

- **Alternative energy**

Solar energy

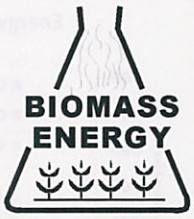


Biomass energy

Wind energy


Blue energy

Limited places

Limited places

Limited places

?

# Blue Energy

- **What is Blue Energy?** → Sometimes called ocean energy
  - Definition : A term for the method of generating electricity through the convergence of both fresh and salt water

Tidal energy

Wave energy

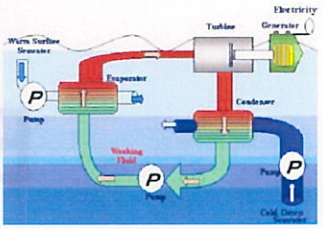


Thermal energy

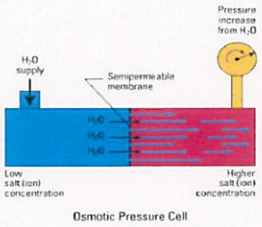


Osmotic Pressure Cell

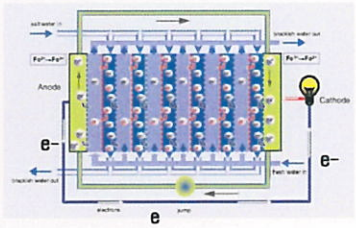


Salinity gradient energy



# Water Cycle & Salinity Gradient Energy

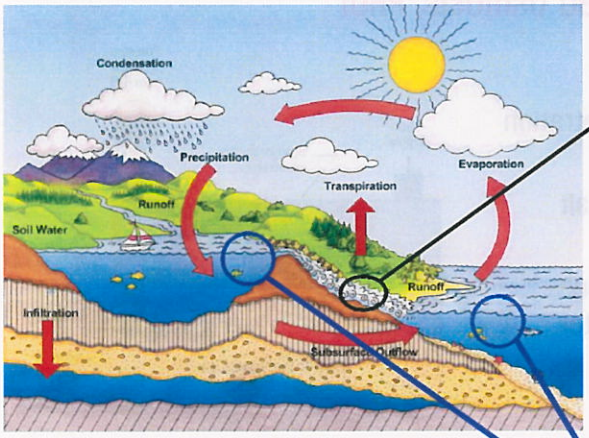


Water Cycle

In Korea, the inflow of seawater is

**38.6 billion tons(31%)**

(Total water resource : 124 billion tons)

## Salinity Gradient Energy

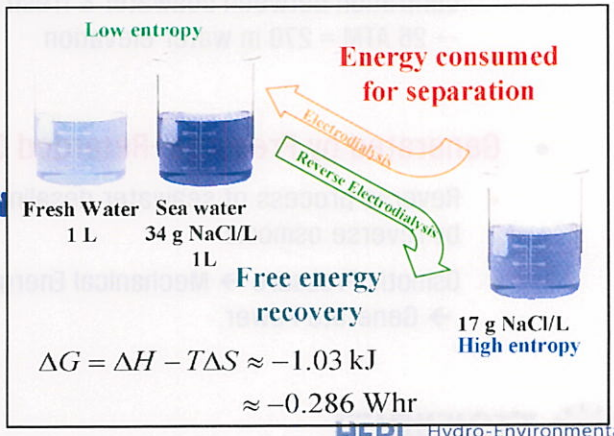

# Background



## PRO system

- The principle of PRO (Pressure-Retarded Osmosis, PRO)
  - Osmotic Pressure
    - Move $H_2O$ molecules from low salt concentration to higher salt concentration
    - Pressure increase from water of higher salt concentration
    - The osmosis pressure of different salt concentration between seawater & fresh water → 26 ATM = 270 m water elevation

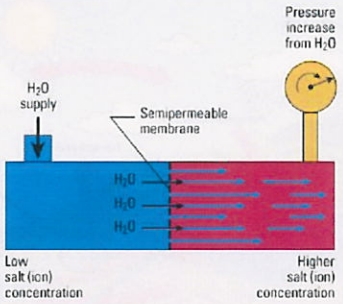

Osmotic Pressure Cell

  - Generated by Pressure-Retarded Osmosis
    - Reverse process of seawater desalination by reverse osmosis
    - Osmotic Pressure → Mechanical Energy → Generate Power

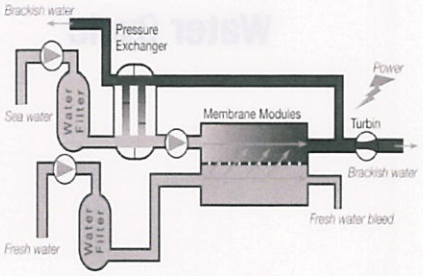

# RED System

- The principle of RED(Reverse Electro-dialysis)
  - Ion exchange membranes

    Constructed to permit selective passage of either anions or cations
  - Electro-dialysis

    Ions are transported through ion permeable membranes Under the influence of an electrical potential gradient
  - Reverse Electro-dialysis

    Electrical potential or ionic currents are induced by controlled mixing of concentrated and dilute solution of electrolytes

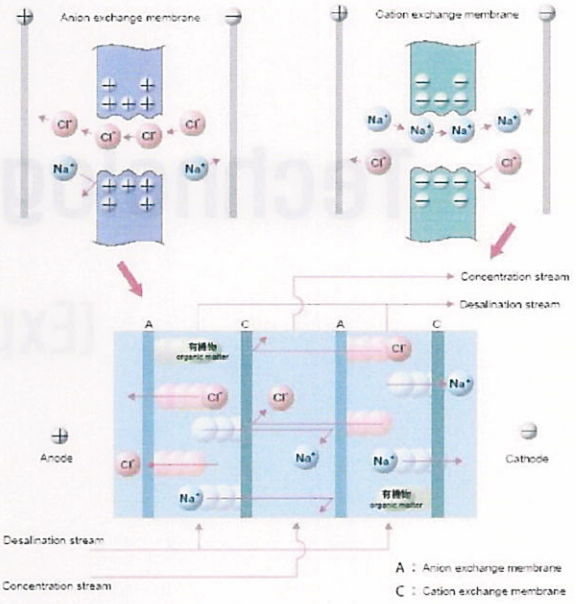




# RED System

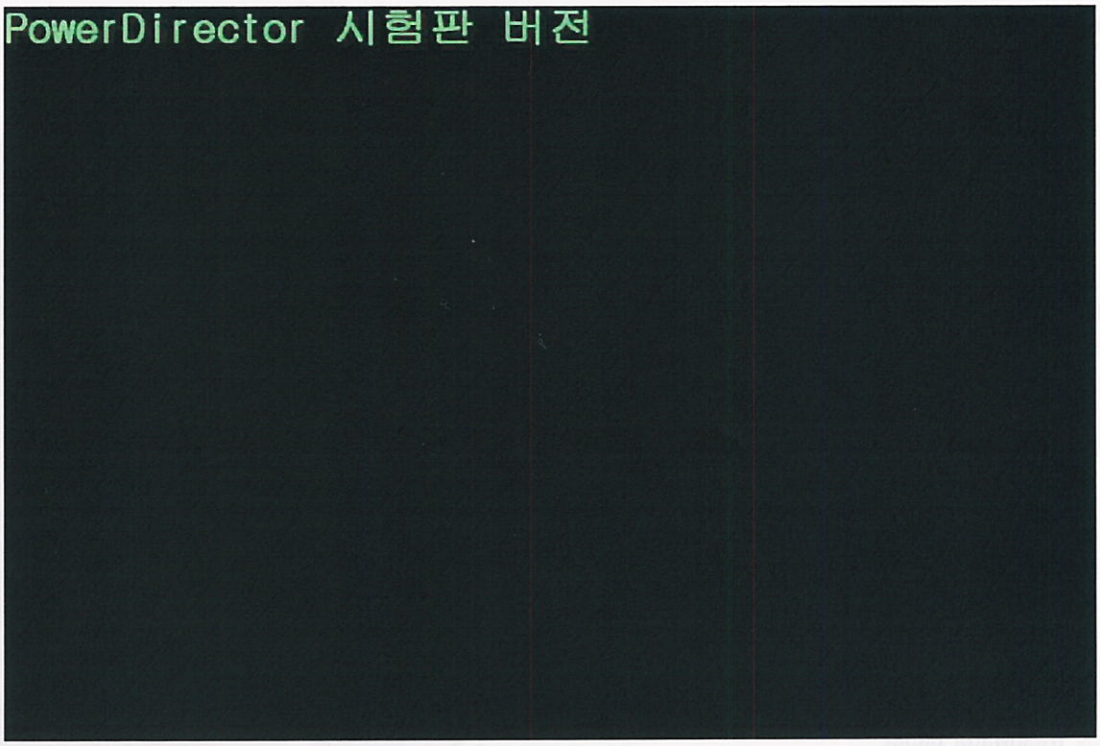

# Technology development

## (Experiment)



## RED Stack Schematic

- Assembling of RED Red stack

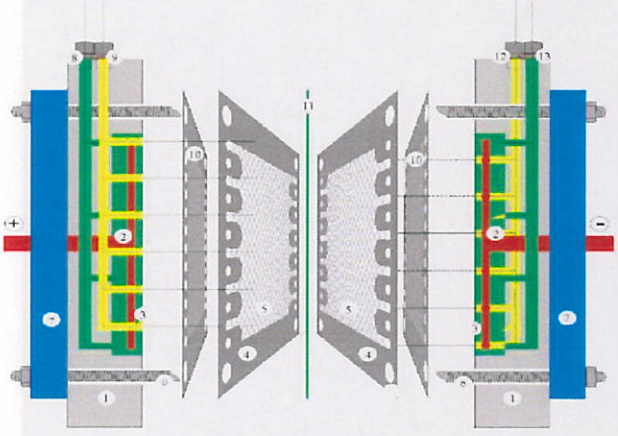

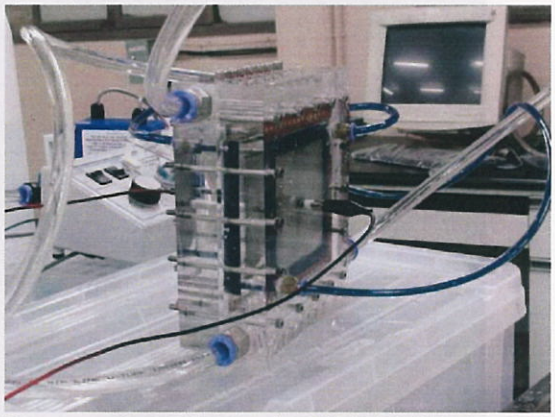

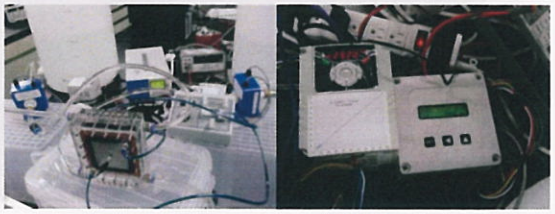

① arcylic board ② electrode ③ electrolyte solution
④ spacer ⑤ grid net ⑥ bolts ⑧ freshwater inlet
⑨ seawater inlet ⑩ chloride change membranes
⑪ anion change membranes ⑫ seawater outlet
⑬ freshwater outlet

# Demo. of RED system

Demonstratoin
of RED system



# Introduction

- Evaluation of RED stack bettery characteristic using electric load
  - Measuring current & voltage
    → For evaluation of Power characteristic of RED stack bettery

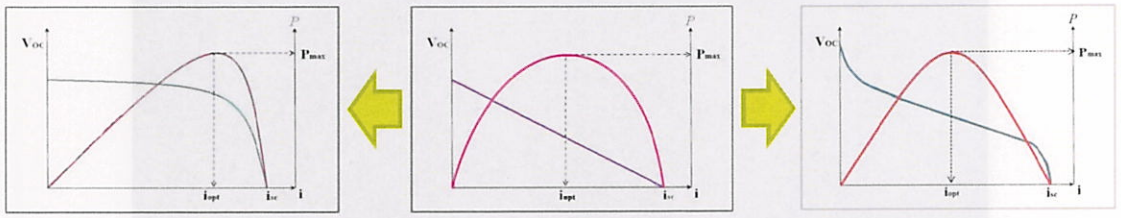


Chemical bettery  General power supply  RED stack bettery

# Terms for Evaluation on Power Characteristics

- Experiment **Condition**

| Membrane | | # of Cells | Sea water Conc. (g/L) | Fresh water Conc. (g/L) | Channel Thickness (mm) | Linear Velocity (cm/s) |
|---|---|---|---|---|---|---|
| CEM | AEM | | | | | |
| CIMS | AFN | 30 | 35 | 0.5 | 0.2 | 0.14 ~ 4.44 |

- **System Schematic**

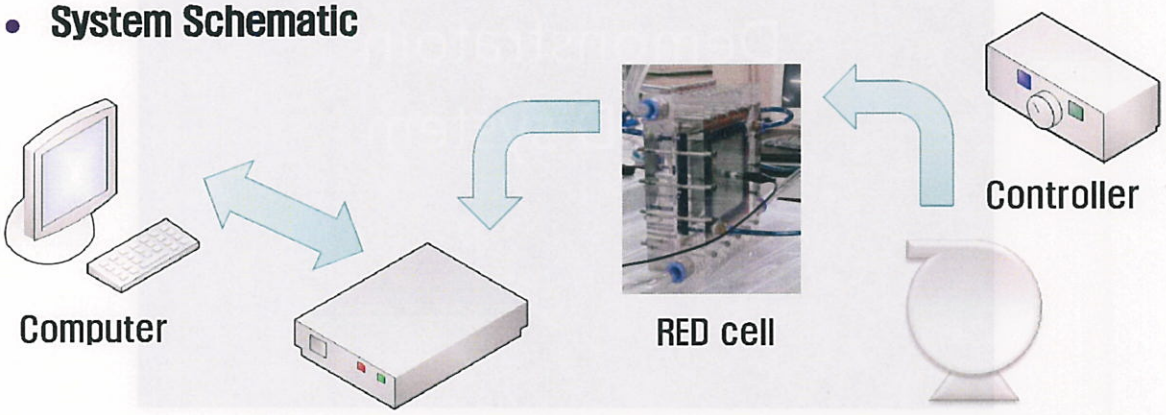




# Experiments of RED system

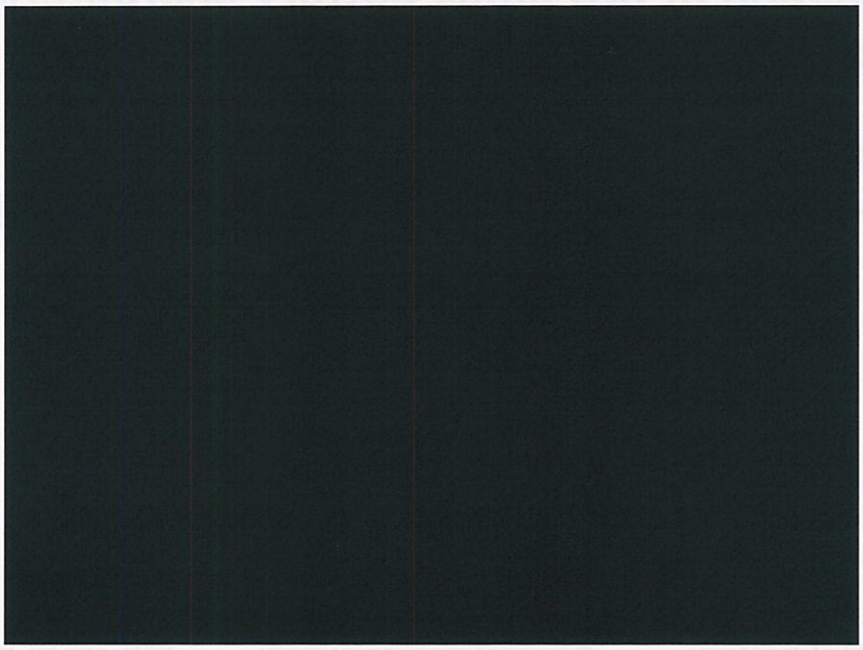

# Voltage-Current Characteristic by Linear Velocity

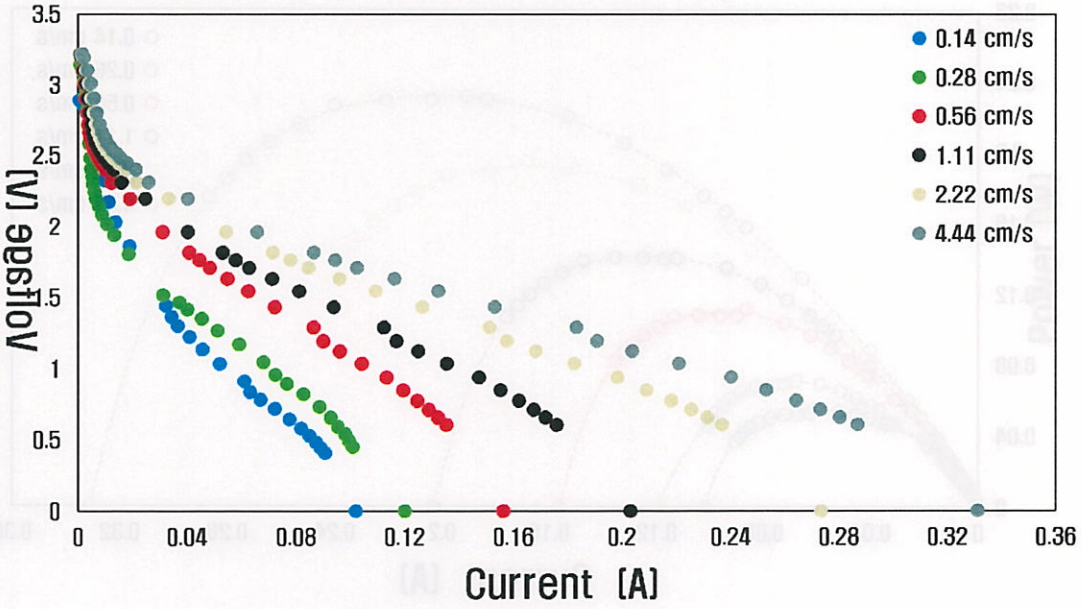


※ No-load voltage : almost constant
(It is not related to Linear velocity)



# Effects of Linear Velocity on Current

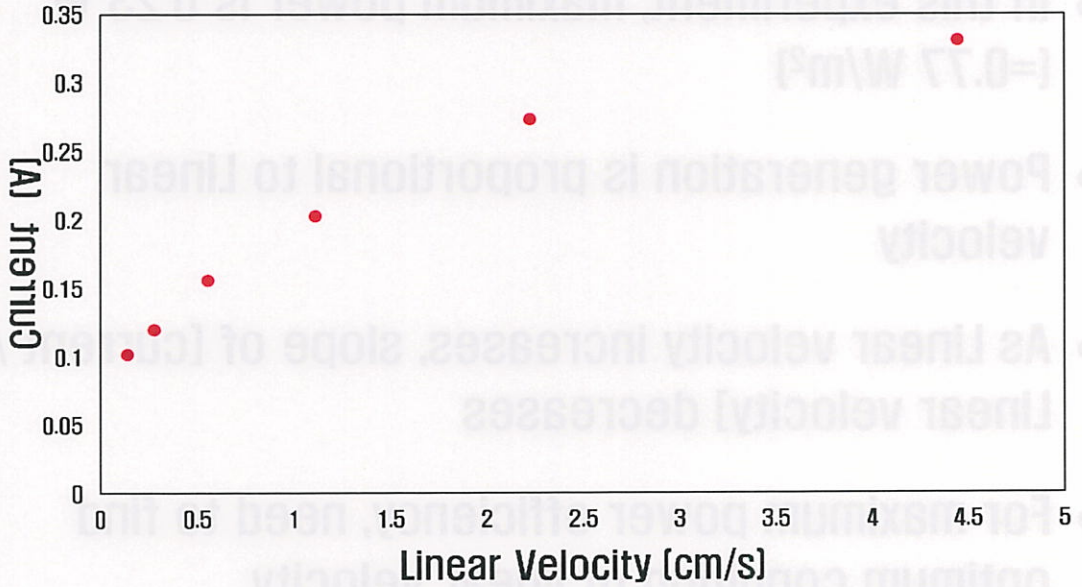


※ As linear velocity increases, current exponentially grows and the rate of it is decreased.

# Power Generation by Linear Velocity

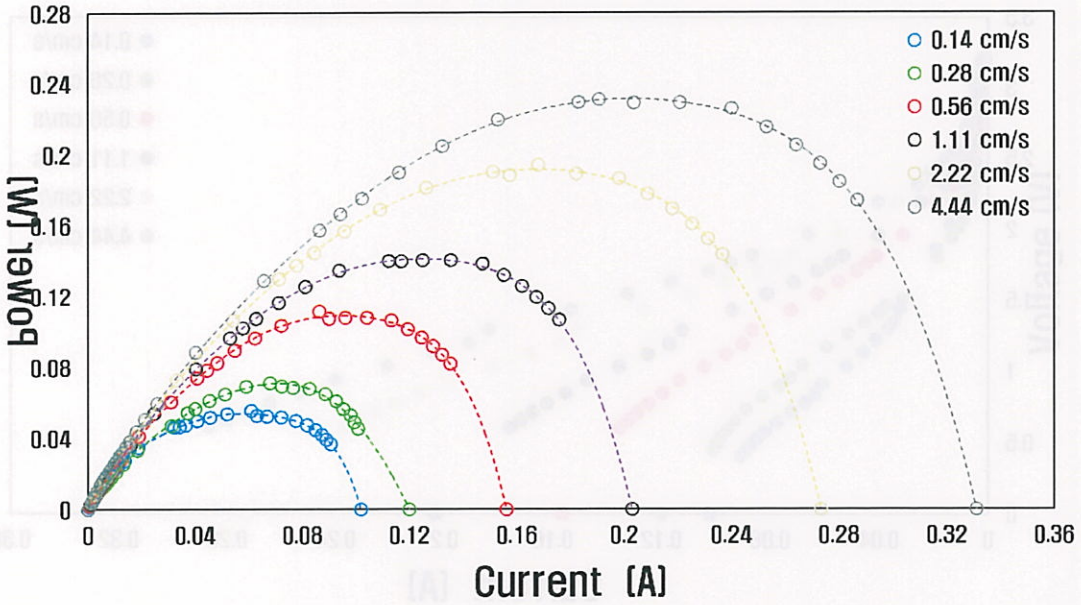


※ The maximum generation power at 4.44 cm/s is 0.23 W → 0.77 W/m²



# Conclusion

- In this experiment, maximum power is 0.23 W (=0.77 W/m²)
- Power generation is proportional to Linear velocity
- As Linear velocity increases, slope of [current / Linear velocity] decreases
- For maximum power efficiency, need to find optimum condition of linear velocity

# Technology development

## (Numerical Analysis)



## Introduction to CFX

- A commercial Computational Fluid Dynamics(CFD) program used to simulate fluid flow in a variety of applications.
  - Water flowing past ship hulls
  - Gas turbine engines (including the compressors, combustion chamber, turbines and afterburners),
  - Aircraft aerodynamics
  - Pumps & fans HVAC
  - HVAC (High-voltage alternating current) systems
  - Mixing vessels
  - Hydrocyclones
  - Vacuum cleaners, and more.

# Introduction to CFX

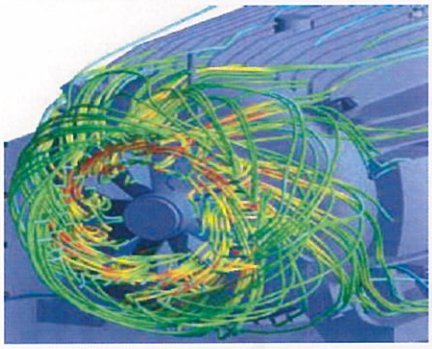

Cooling air flow predictions to optimize heat transfer around electric motor

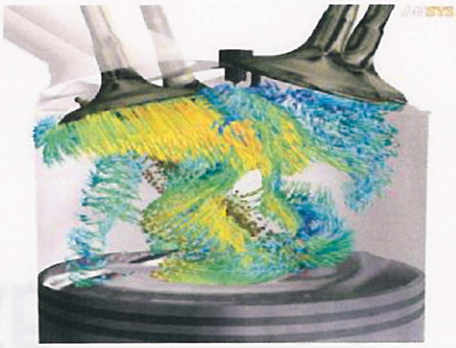

Vortex structures in a four-stroke engine just after injection of fuel and intake valve opening

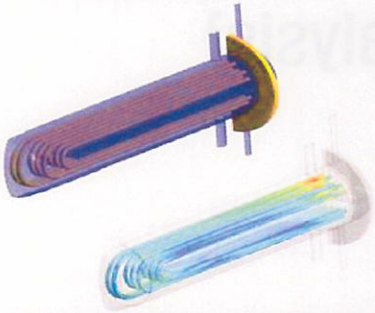

Prediction of heat transfer distribution in a shell and tube heat exchanger

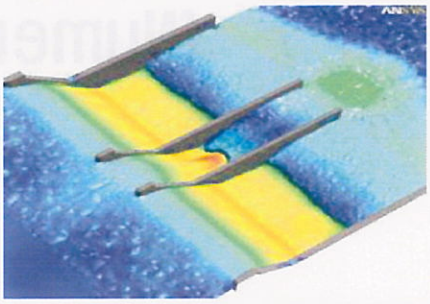

Flow velocities on the free surface water flow across a dam with a sluice, showing hydraulic jump just past the base



# Introduction

## Need for analysis using CFX about internal flow of RED module

- For PRO+RED system, need to find the characteristics of RED Module

- The gap between cells are extremely small (~$10^{-5}$ m) so internal flow characteristic cannot be measured by experiment.

**Numerical analysis is needed for internal flows.**

# Approach of Research

- Good agreement between FDM model and CFX results for pulse flow
- As verification of CFX, comparison with results form 2D FDM will be conducted under same conditions to proceed 3D simulations
- Comparative study about steady and pulse situation will be carried out in terms of electric power generation



# Literature review

- Reverse Electrodialysis (RED) and Power Generation

| | | | |
|---|---|---|---|
| Process : | RED (Mixing) | ↔ | Desalination (Separation) |
| Energy : | Generation | ↔ | Consumption |

- Diagram for RED generator

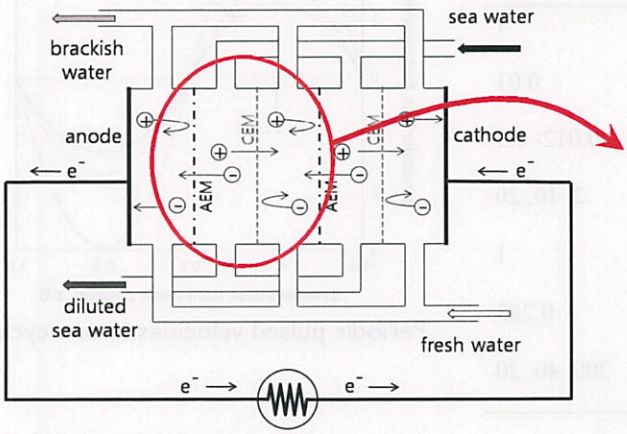


- Model Framework
  - ✓ Single Unit Analysis
  - ✓ Pulsatile Flow
  - ✓ Ion Transport Theories

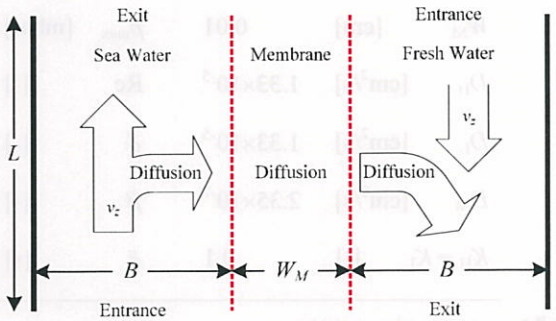

# Construction of Model

- Countercurrent flows (sea and fresh water)
- Both streams with time-dependent Pulsed Form
- Pseudo steady-state in semi-permeable membrane

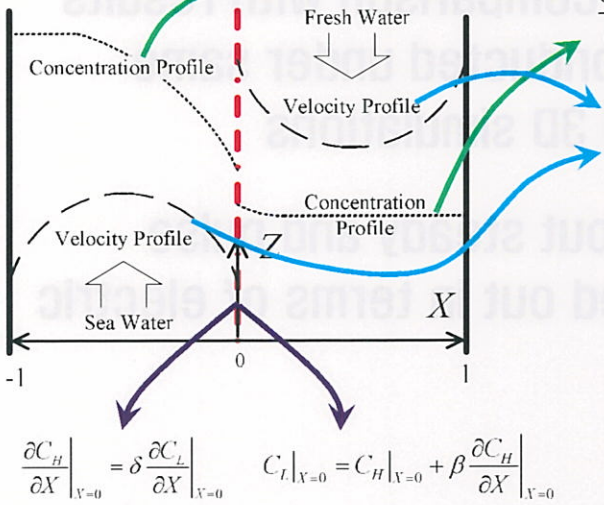


$$\frac{\partial C_i}{\partial \tau} = \Gamma \frac{\partial^2 C_i}{\partial X^2} - V_i \frac{\partial C_i}{\partial Z} \qquad i = \begin{cases} H \text{ (Sea Water Side)} \\ L \text{ (Fresh Water Side)} \end{cases}$$

$$\frac{\partial V_i}{\partial \tau} = \frac{(L/B)}{\mathrm{Re}} \left\{ 12(-\Delta P) + \frac{\partial^2 V_i}{\partial X^2} \right\}$$

$$\Delta P = \begin{cases} -1 + \cos\left[2\pi (f\xi)\tau\right] & \text{Sea Water} \\ 1 - \cos\left[2\pi (f\xi)\tau\right] & \text{Fresh Water} \end{cases}$$

$$\left.\frac{\partial C_H}{\partial X}\right|_{X=0} = \delta \left.\frac{\partial C_L}{\partial X}\right|_{X=0} \qquad C_I|_{X=0} = C_H|_{X=0} + \beta \left.\frac{\partial C_H}{\partial X}\right|_{X=0}$$

- Dimensionless variables

$$X = x/B \qquad Z = z/L \qquad \tau = v_m t/L$$

$$C_H = c_H/c_0 \qquad C_L = c_L/c_0 \qquad V_i = v_i/v_m$$

$$\Gamma = \left(D_i/B^2\right)/\left(v_m/L\right) \qquad \delta = D_L/D_H$$

$$\beta = \left(K_H D_H/B\right)/\left(D_M/W_M\right) \qquad \mathrm{Re} = \rho v_m B/\mu$$



# Results (1)

Numerical scheme

- Orthogonal collocation on finite element method (OCFEM)
- Mesh grids: 2,178 (= 11x11x9x2)
- NDSolve in Mathematica

Simulation Parameters

| Parameters | | Values | Parameters | | Values |
|---|---|---|---|---|---|
| $B$ | [cm] | 0.2 | $\rho$ | [g/cm$^3$] | 1 |
| $L$ | [cm] | 20 | $\mu$ | [g/cm·s] | 0.01 |
| $W_M$ | [cm] | 0.01 | $p_{max}$ | [mbar] | 0.012- 1.2 |
| $D_H$ | [cm$^2$/s] | $1.33\times10^{-5}$ | Re | [-] | 2, 10, 20 |
| $D_L$ | [cm$^2$/s] | $1.33\times10^{-5}$ | $\delta$ | [-] | 1 |
| $D_M$ | [cm$^2$/s] | $2.35\times10^{-7}$ | $\beta$ | [-] | 0.283 |
| $K_H = K_L$ | [-] | 0.1 | $\xi$ | [s] | 200, 40, 20 |

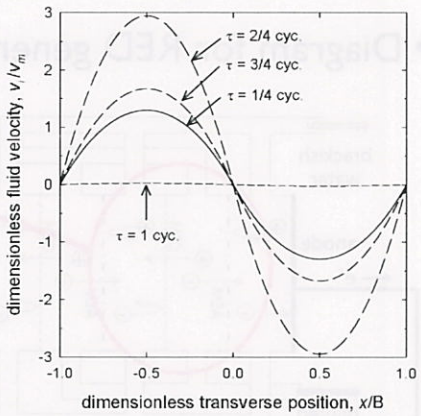


Periodic pulsed velocities in one cycle

# Result (2)

- Voltage of open circuit

$$\Phi_{OC} = \alpha \frac{RT}{\Delta F} \ln\left(\frac{C_H}{C_L}\right)$$

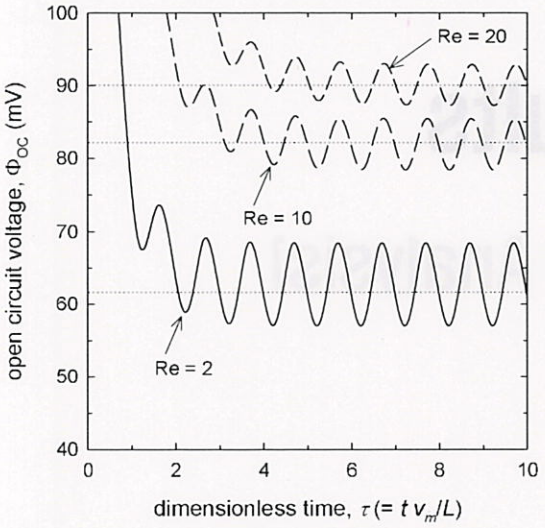


- Current of short circuit

$$I_{SC} = \frac{i_{SC}}{c_0 A} = -\frac{FD_M}{W_M}\frac{\int_A \Delta C dA}{A}$$

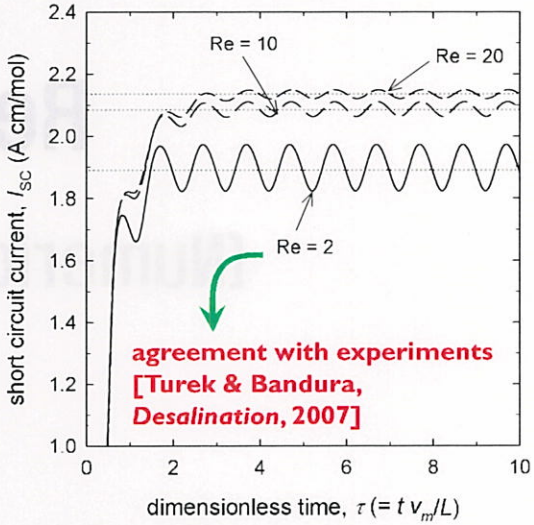




# Convert from ion flux to short circuit current

$$i_{sc} = \frac{\int (\text{ion flux})\, dA \times F}{M_{NaCl} \times \rho \times C_p} = \frac{[J \cdot s^{-1} \cdot kg \cdot m^{-3} \cdot K^{-1}]\ [C \cdot mol^{-1}]}{[kg \cdot mol^{-1}]\ [kg \cdot m^{-3}]\ [J \cdot kg^{-1} \cdot K^{-1}]} = [C \cdot s^{-1}] = [A]$$

Where, $i_{sc}$ : Short circuit current [A]

ion flux : [W · kg · m$^{-3}$ · K$^{-1}$]

$F$ : Faraday constant = 96,485 [C/mol]

$M_{NaCl}$ : Molecular weight of NaCl = 0.05844 [kg/mol]

$\rho$ : Density = 1,000 [kg/m$^3$]

$C_p$ : Specific heat = 4,184 [J · kg$^{-1}$ · K$^{-1}$]

$$I_{sc} = \frac{i_{sc}}{C_0 A} = [A\ cm/mol]$$

Where, $C_0$ : Inlet concentration of sea water [g/l]

$A$ : Area of membrane [cm$^2$]

# Results

## (Numerical Analysis)



## Input Boundary Condition

| Input variable | | Value |
|---|---|---|
| Concentration of seawater[g/L] | | 35 |
| Concentration of freshwater[g/L] | | 0 |
| Effective ion diffusivity of freshwater [$cm^2/s$] | | $1.13 \times 10^{-5}$ |
| Effective ion diffusivity of seawater [$cm^2/s$] | | $1.13 \times 10^{-5}$ |
| Effective ion diffusivity of membrane [$cm^2/s$] | | $7.94 \times 10^{-7}$ |
| Reynolds number | Pulse | 2 |
| | | 10 |
| | | 20 |
| | Steady | 2 |
| | | 10 |

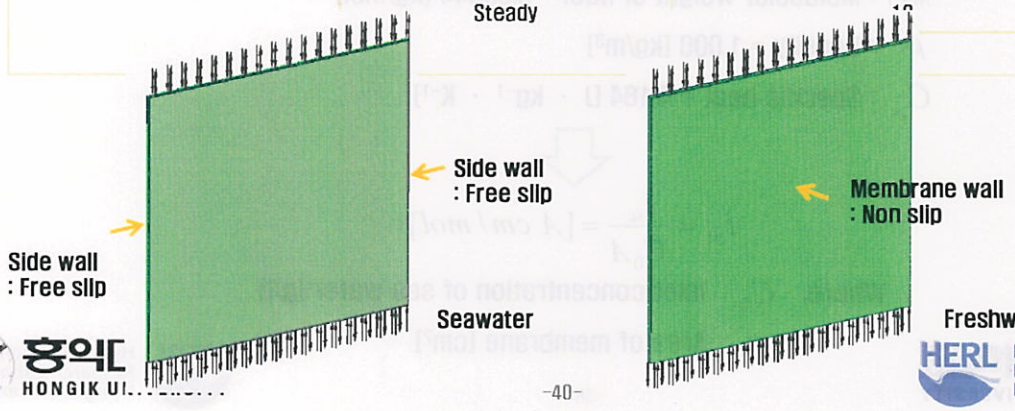

# Mesh

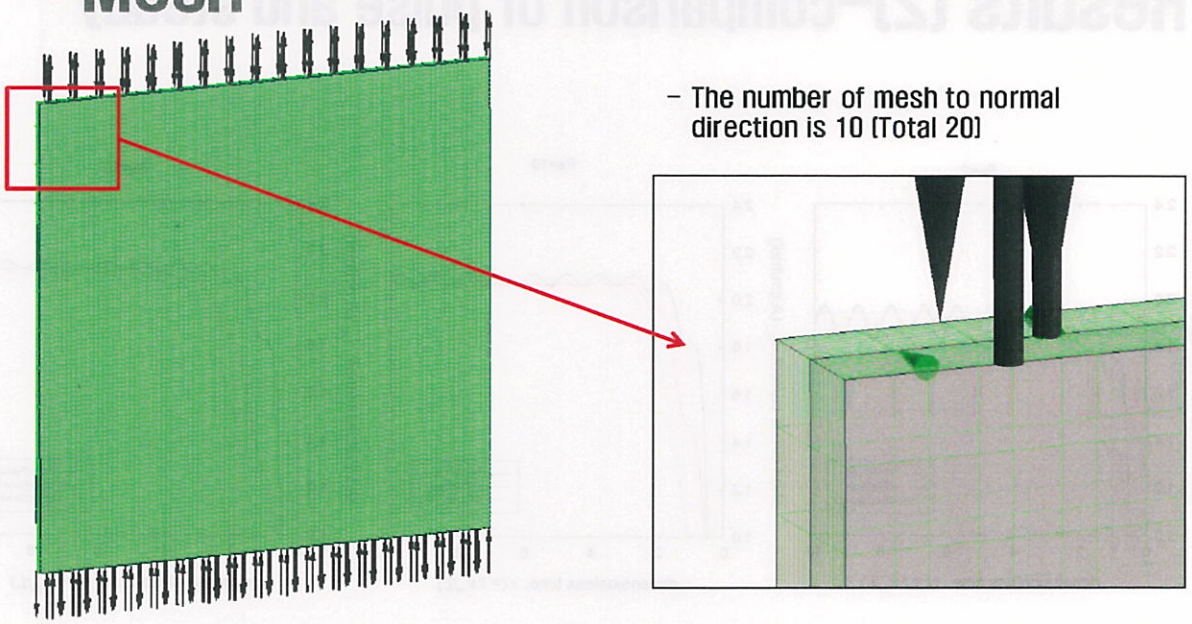

- The number of mesh to normal direction is 10 (Total 20)

| Thickness of channel | Width & height of membrane | # of Node | # of Element | Cell size | | |
|---|---|---|---|---|---|---|
| | | | | dx | dy | dz |
| 0.002m | 0.1m | 214,221 | 200,000 | | | |



# Results (1)–comparison with 2D FDM

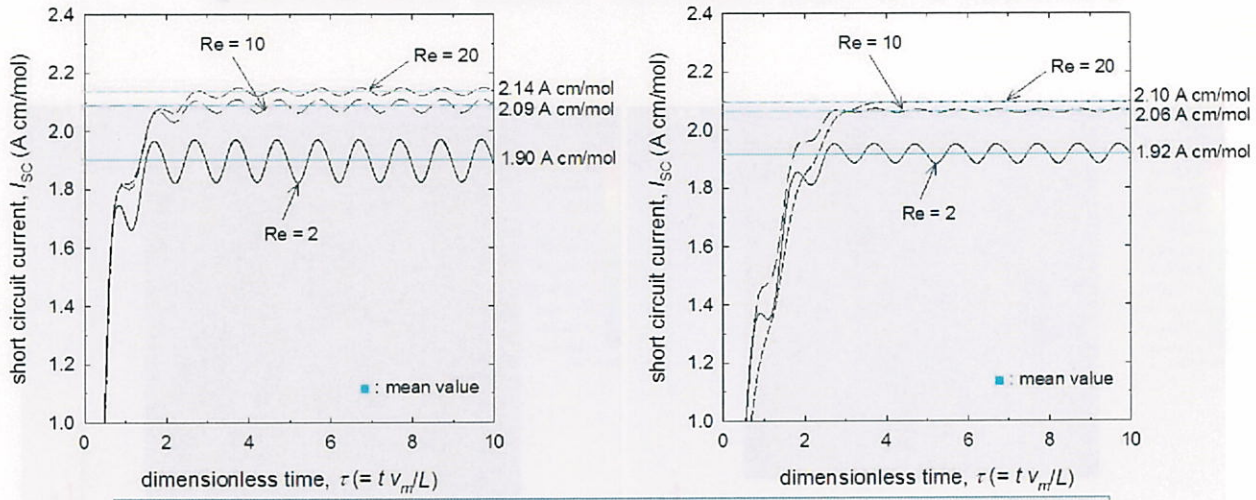


| | Mean value of $I_{sc}$ | | |
|---|---|---|---|
| Reynolds Number | 2 | 10 | 20 |
| FDM | 1.900 | 2.087 | 2.135 |
| CFX | 1.918 | 2.064 | 2.095 |
| Relative error | 0.96% | 1.11% | 1.86% |

# Results (2)–comparison of pulse and steady

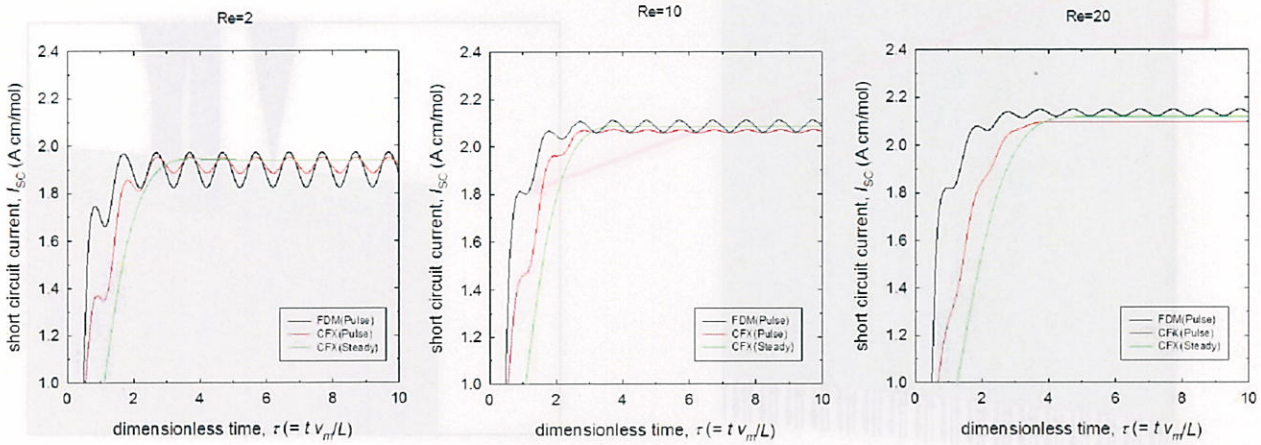




# Results (3)

- Contours of Ion Flux for Pulse and Steady

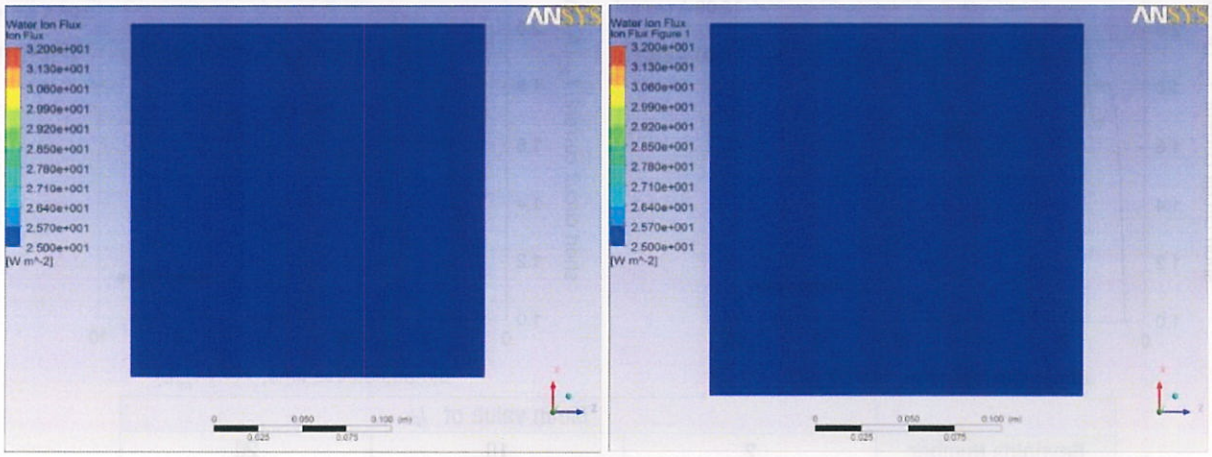


Pulse steady

# Conclusion

- **Experiment Results**
  - As aspect Ratio increases, Short Circuit Current linearly increases
  - As flowrate increases, Short Circuit Current increases but, slope is decreased
- **Conclusion**
  - We can calculate current by using conversion equation
  - Possible to analysis interaction flow characteristics



# Expectation

# Expectation

- Annually 3.9 × $10^{10}$ $m^3$ of water runs to sea in Korea
  → Future blue energy source
- Convergence of PRO and RED module
  → Improve Energy efficiency & optimize module system
- Possession of key technology (PRO+RED System) & blue energy generation technology
- Generation of technological synergy by convergence with Ocean Plant & Seawater desalination
- As connecting the smart grid, PRO+RED system can play the role of decentralized power supply system



# PRO+RED System

- The principle of PRO+RED
  - RED module → Demanding high hydraulic pressure
  - PRO module → Demanding pump, turbine and additional mechanical work
  - Proposed the Integrated power generation system of PRO and RED

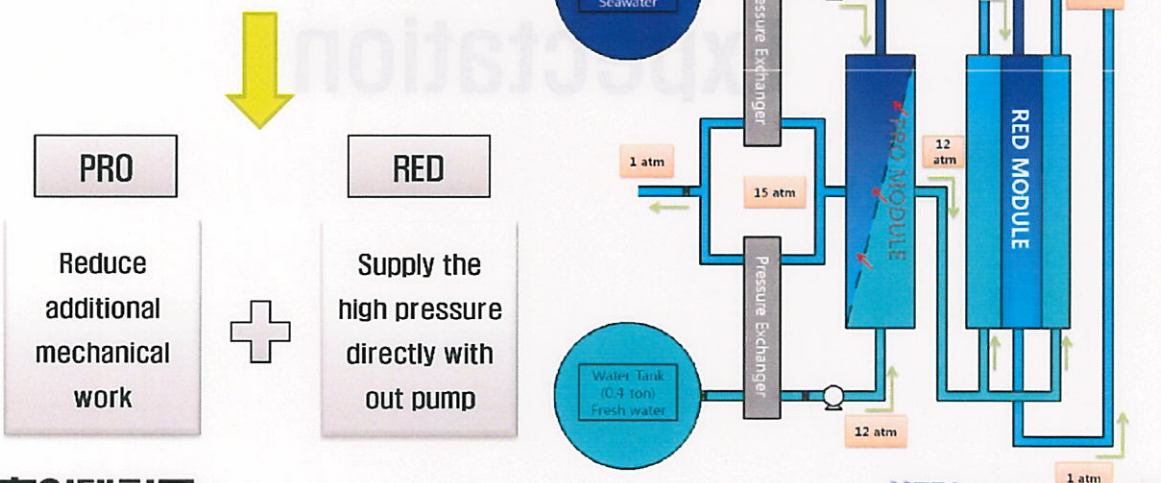

# Future Study

- Various types of Spacer
  - In order to increase turbulence intensity, installation of spacer will be investigated as below.
  - Using the periodic conditions will be asked to analysis of complicated and repeated shapes of internal structure of membrane

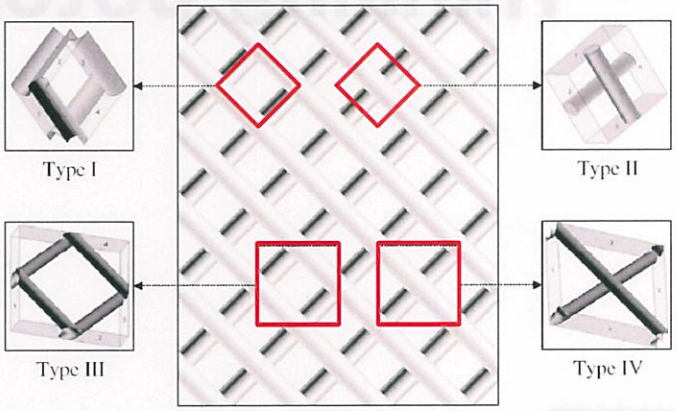




# Marketability

- **Marketability of salient gradient energy**
  - The global salient gradient energy output from estuaries ☞ 2.6 TW
  - 2.6 TW ☞ 20% of the present world wide energy demand
  - But, membrane-based conversion techniques → high price

Decreasing prices of membranes & Increasing prices of fossil fuels

Salinity-gradient power will be attractive in near future

# Thinking potential



## Thinking potential

- Generation of technological synergy by convergence with Seawater desalination

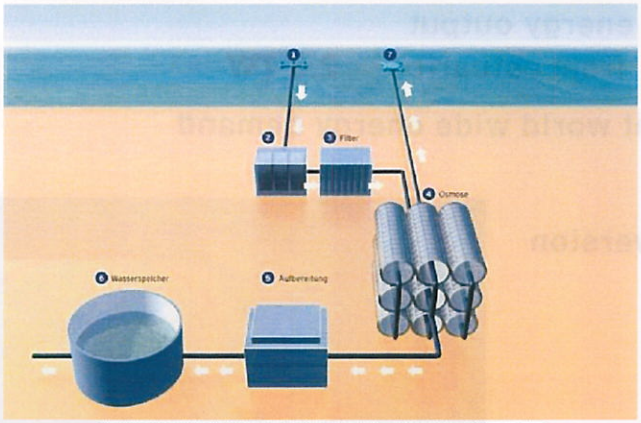

Seawater desalination plant

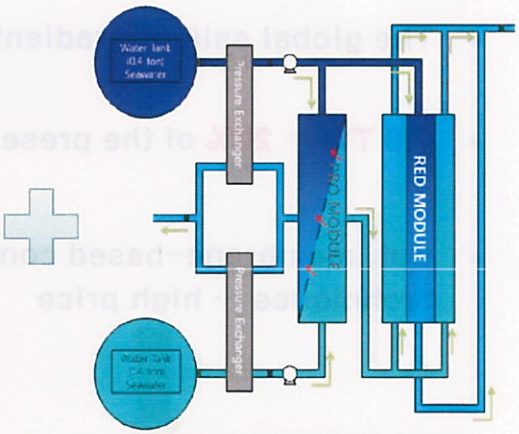


PRO+RED Module

Seawater desalination Plant
→ Production of high salinity sea water & Fresh water
→ High salinity sea water → Employing PRO+RED Module

# Thinking potential

- **Connection to Smart Grid**

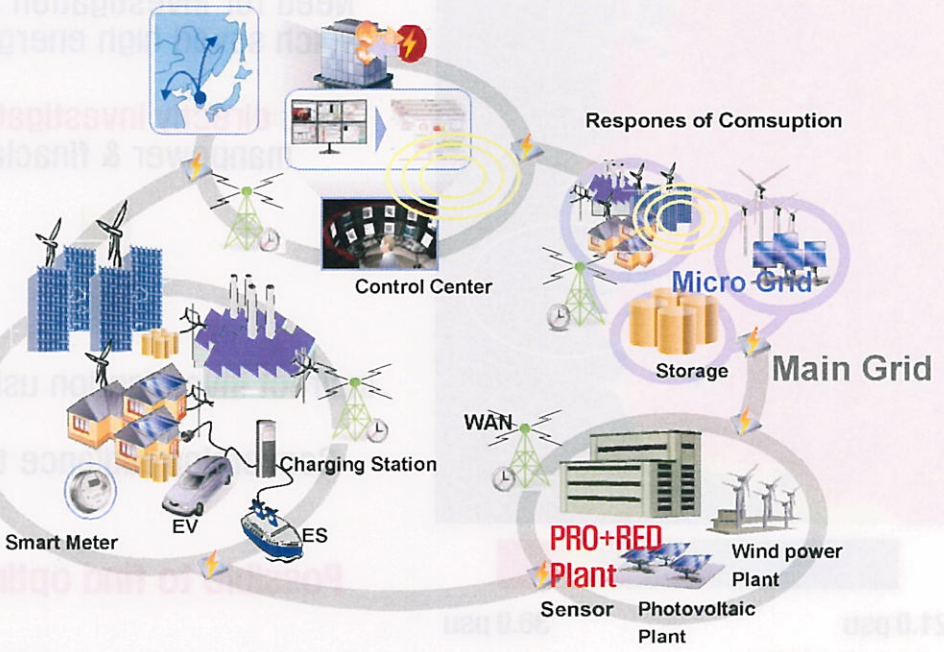





# Thinking potential

- **Connection to Smart Grid**


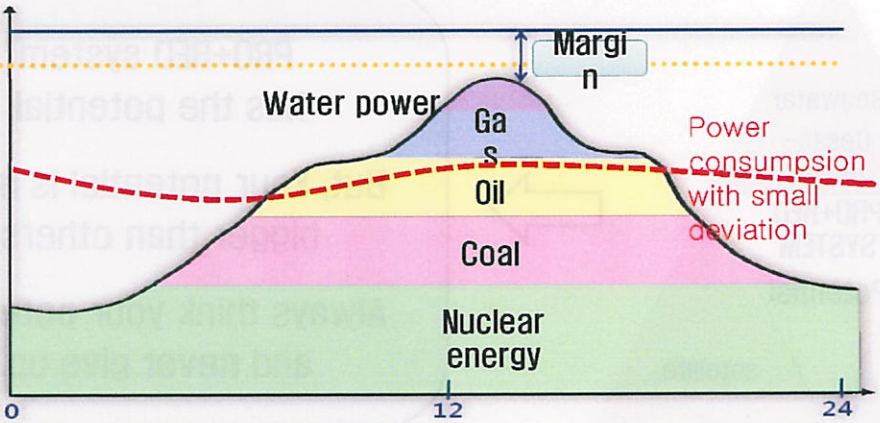


We can reduce facilities which construct for reserve power by using PRO+RED system

# Thinking potential

- **Study for optimum site**

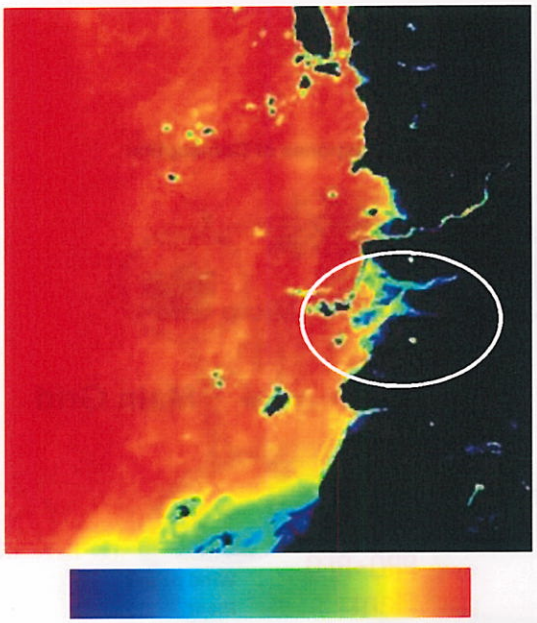

21.0 psu 36.0 psu

Need for investigation about site which saved high energy potential

But, directly investigation bring manpower & finacial loss

Indirect investigation using satellite

Conversion radiance to salinity

**Possible to find optimum site**



# Conclusion

- **Thinck potential**

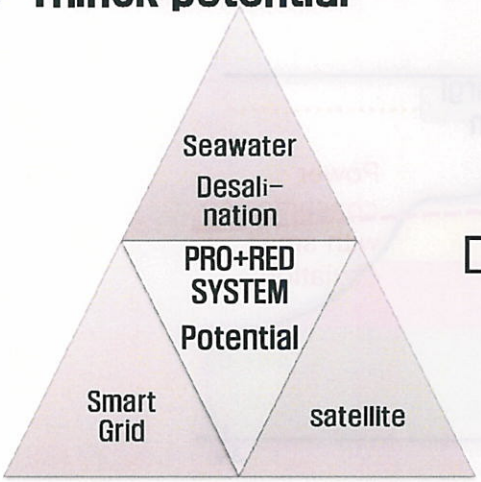


PRO+RED system has the potential.

But, Your potential is much bigger than others.

Always think your potential and **never give up.**

**YOU WILL GET WHAT YOU WANT TO GET !**

# Thank you
# Q & A

# Collision statistics of Lagrangian particles in isotropic turbulence

S. Yokojima[1] · T. Mashiko[2] · T. Matsuzaka[1] · T. Miyahara[1]

[1] Dept. Systems Engineering, Shizuoka University

[2] Dept. Mechanical Engineering, Shizuoka University



## Motivation

- Coagulation, collision & contact of small particles, droplets & microorganisms in turbulent flows play an important role in many natural & industrial processes
  - growth of liquid droplets in turbulent clouds
  - spray atomization process
  - prey-predator relationship in water environment

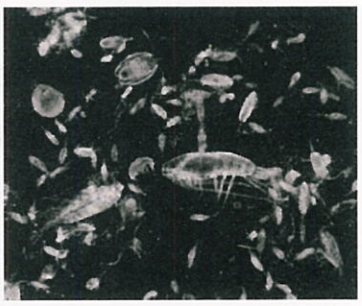

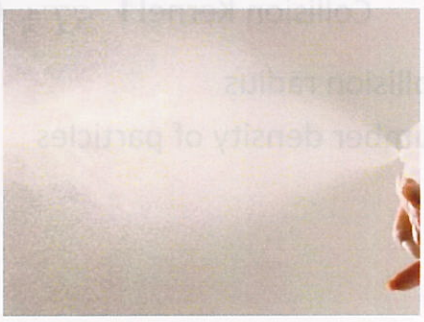

# Objectives

- Collision statistics of Lagrangian particles in homogeneous isotropic turbulence (HIT) are examined
  - collision rate
  - contact duration (period of time during which two particles keep in contact)
- Careful comparison with Saffman-Turner theory [JFM 1 1956]
- Reynolds number dependence



# Saffman-Turner theory (1)

- Assumptions:
  - Zero-inertia particles - particles follow the local fluid motion
  - Particles do not modify the flow field
  - Particle concentration field is uniform and time independent
- Collision rate $N_c$ (# of collisions per unit time per unit volume)

$$N_c = \underbrace{2\pi R^2 \overline{|w_r|}}_{\Gamma_{ST1}} \frac{\bar{n}^2}{2} \qquad (1)$$

Collision Kernel $\Gamma_{ST1}$ (Wang et al., PoF 10 1998)

where $R$ the collision radius

$\bar{n}$ the number density of particles

# Radial component of relative velocity $w_r$

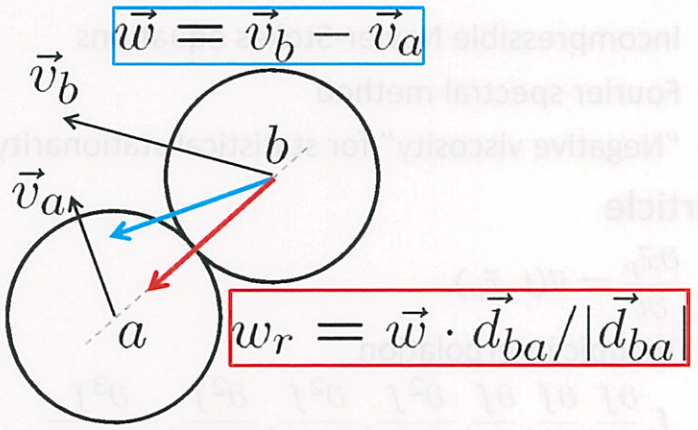


For more details, look at Wang et al.(JFM 415 2000)



# Saffman-Turner theory (2)

- Assumed further:
  - $\overline{|w_r|} \sim R\overline{|\partial u/\partial x|}$
  - $\overline{(\partial u/\partial x)^2} \sim \bar{\varepsilon}/15\nu$
  - Probability distribution of velocity gradient is Gaussian

$$N_c = \underbrace{\left(\frac{8\pi\bar{\varepsilon}}{15\nu}\right)^{1/2} R^3}_{\text{Collision Kernel } \Gamma_{ST2}} \frac{\bar{n}^2}{2} \qquad (2)$$

# Numerical strategies

- Fluid
  - Incompressible Navier-Stokes equations
  - Fourier spectral method
  - "Negative viscosity" for statistical stationarity
- Particle
  - $\frac{\partial \vec{x}_p}{\partial t} = \vec{u}(t, \vec{x}_p)$
  - Tricubic interpolation

$$f, \frac{\partial f}{\partial x}, \frac{\partial f}{\partial y}, \frac{\partial f}{\partial z}, \frac{\partial^2 f}{\partial x \partial y}, \frac{\partial^2 f}{\partial y \partial z}, \frac{\partial^2 f}{\partial z \partial x}, \frac{\partial^3 f}{\partial x \partial y \partial z}$$

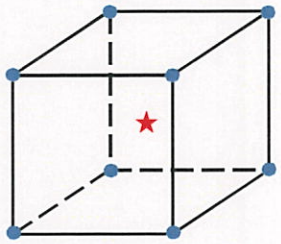



# HIT: Run parameters & statistics

N: total number of Fourier nodes
$\Delta x$: grid spacing
$\Delta t$: time increment
$T$: total simulation period
$Re_\lambda = u'\lambda/\nu$: Taylor Reynolds number
$L_e = u'^3/\varepsilon$: large-eddy length scale
$T_e = u'^2/\varepsilon$: large-eddy turnover time
$u' = (2K/3)^{1/2}$: turbulence intensity
$\eta$: Kolmogorov length scale
$\tau_\eta$: Kolmogorov time scale
$u_\eta$: Kolmogorov velocity scale

| | R20 | R25 | R31 | R37 | R48 | R53 |
|---|---|---|---|---|---|---|
| N | $48^3$ | $64^3$ | $96^3$ | $128^3$ | $192^3$ | $256^3$ |
| $\Delta x/\eta$ | 1.06 | 1.00 | 0.85 | 0.77 | 0.70 | 0.61 |
| $\Delta t/\tau_\eta$ | 0.053 | 0.052 | 0.042 | 0.030 | 0.023 | 0.016 |
| $T/\tau_\eta$ | 422 | 414 | 421 | 412 | ~400 | ~400 |
| $Re_\lambda$ | 20.1 | 24.8 | 30.6 | 37.4 | 47.8 | 53.4 |
| $L_e/\eta$ | 11.8 | 16.2 | 22.2 | 29.9 | 43.4 | 51.1 |
| $T_e/\tau_\eta$ | 5.19 | 6.40 | 7.90 | 9.64 | 12.4 | 13.8 |
| $u'/u_\eta$ | 2.28 | 2.53 | 2.81 | 3.11 | 3.51 | 3.71 |

# Collision, separation & contact duration

- Collision & separation

  IF $d_{AB}(t_1-\Delta t)>R$ & $d_{AB}(t_1)<=R$ THEN A & B collide at $t=t_1$

  IF $d_{AB}(t_2-\Delta t)<=R$ & $d_{AB}(t_2)>R$ THEN A & B separate at $t=t_2$

  $R$ : contact radius ($R/\eta$=1,2,3)

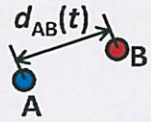


- Contact duration

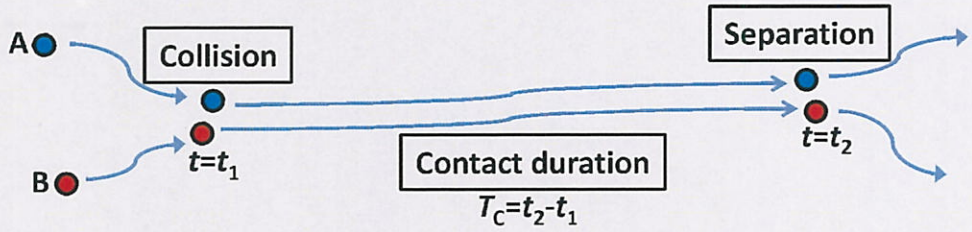




# Number of particles & collisions

| $Re_\lambda$ | $R/\eta$ | $N_P$ | Particle volume fraction | $N_C$ |
|---|---|---|---|---|
| 20.1 | 1 | 7,000 | 2.8% | 98,107 |
| 24.8 | 1 | 10,000 | 2.0% | 98,864 |
| | 1 | 14,000 | 1.4% | 94,666 |
| 30.6 | 2 | 5,000 | 3.9% | 95,303 |
| | 3 | 2,500 | 6.5% | 79,877 |
| 37.4 | 1 | 19,000 | 1.1% | 97,491 |

# 1. Collision rate
## Comparison with ST theory



## Reynolds number effect

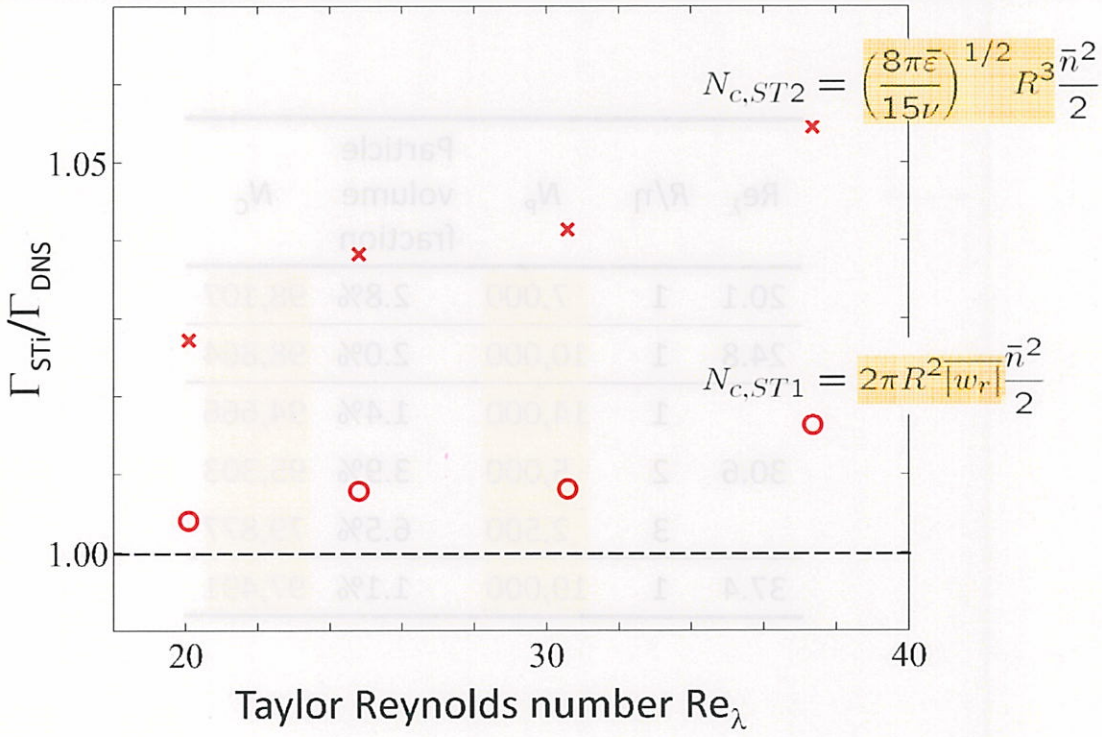

# Collision radius effect

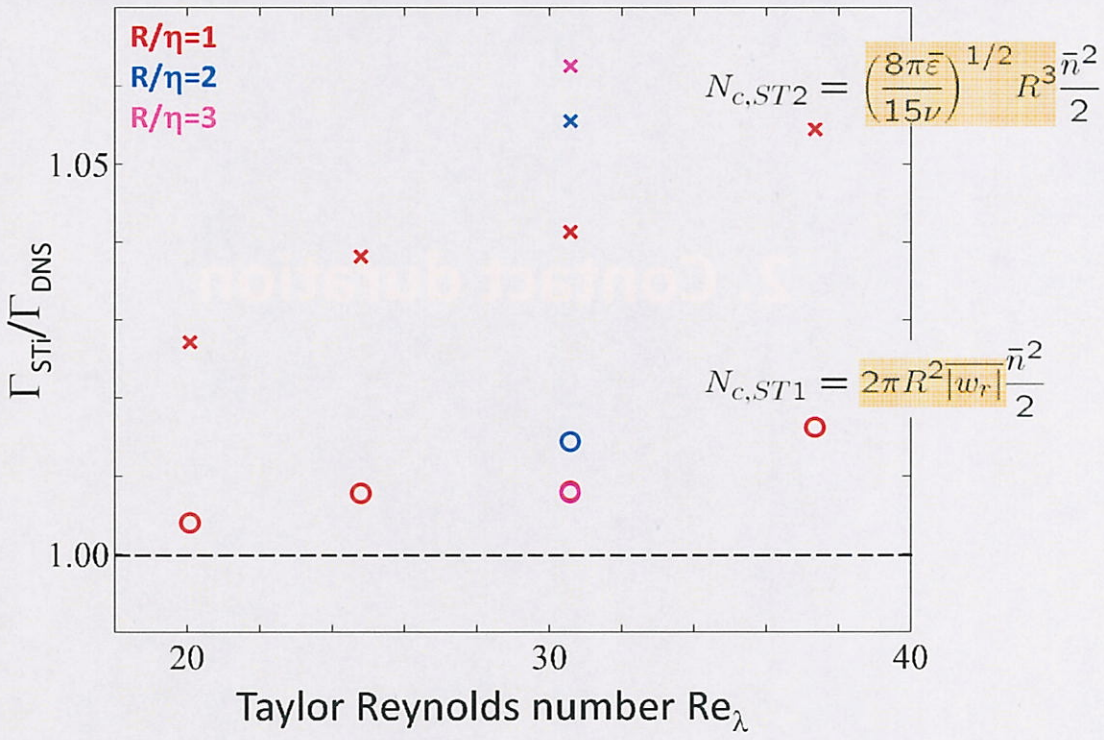




# Distributions of $w_r$

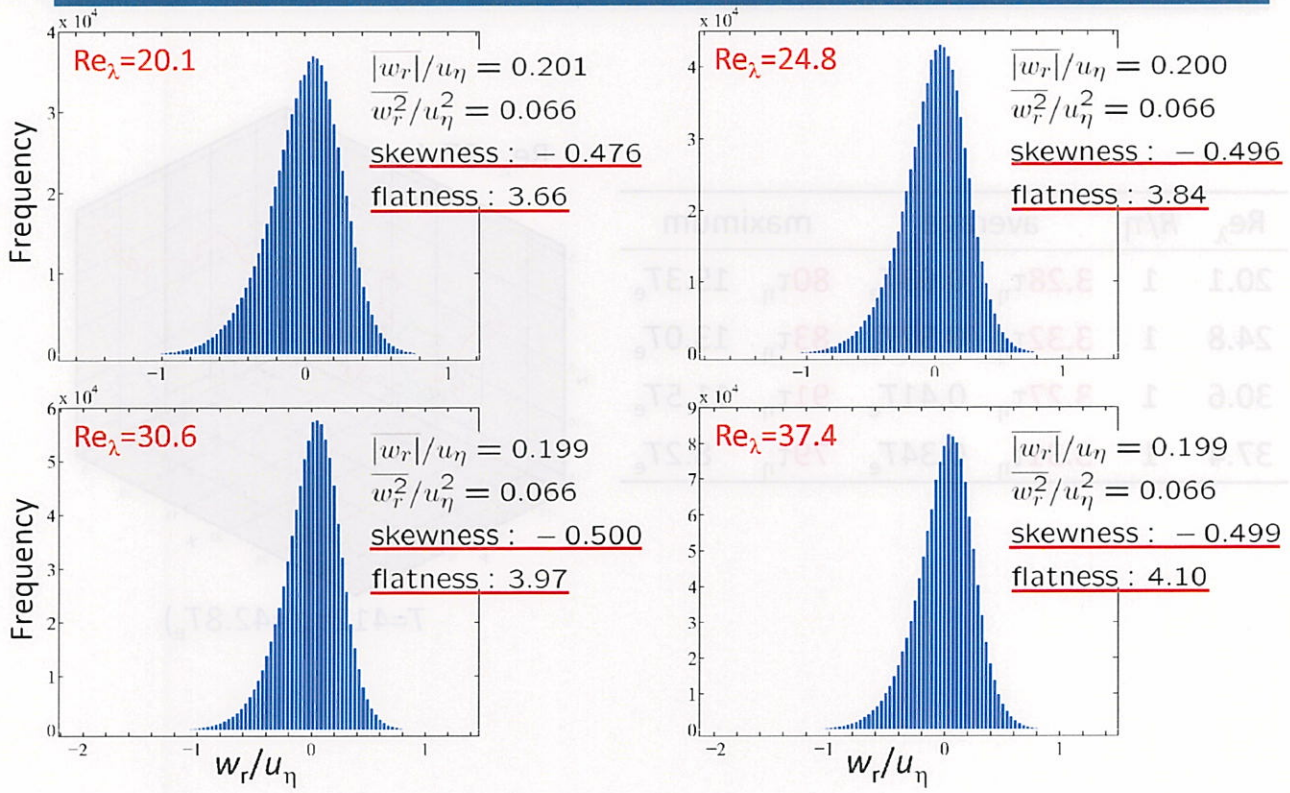

# 2. Contact duration



## Statistics of contact duration

| $Re_\lambda$ | $R/\eta$ | average | | maximum | |
|---|---|---|---|---|---|
| 20.1 | 1 | $3.28\tau_\eta$ | $0.63T_e$ | $80\tau_\eta$ | $15.3T_e$ |
| 24.8 | 1 | $3.32\tau_\eta$ | $0.52T_e$ | $83\tau_\eta$ | $13.0T_e$ |
| 30.6 | 1 | $3.27\tau_\eta$ | $0.41T_e$ | $91\tau_\eta$ | $11.5T_e$ |
| 37.4 | 1 | $3.31\tau_\eta$ | $0.34T_e$ | $79\tau_\eta$ | $8.2T_e$ |

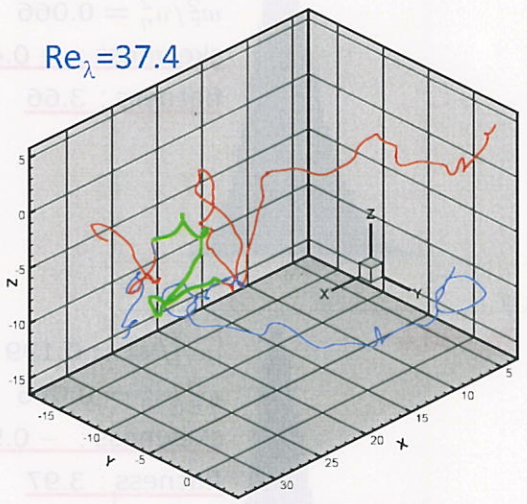

# PDF & CDF of contact duration

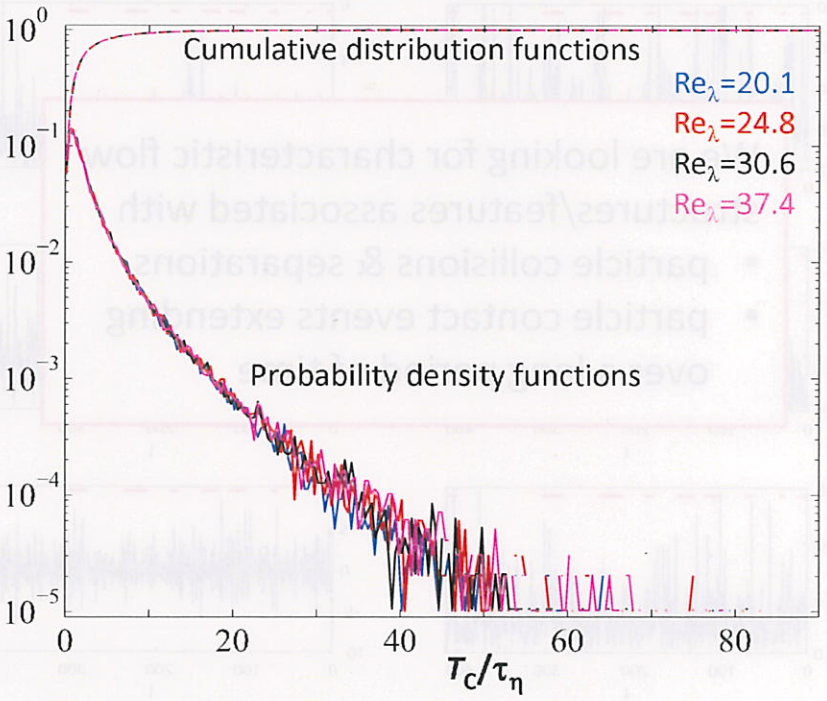




# 3. Ongoing attempt

# Looking at Lagrangian time histories…

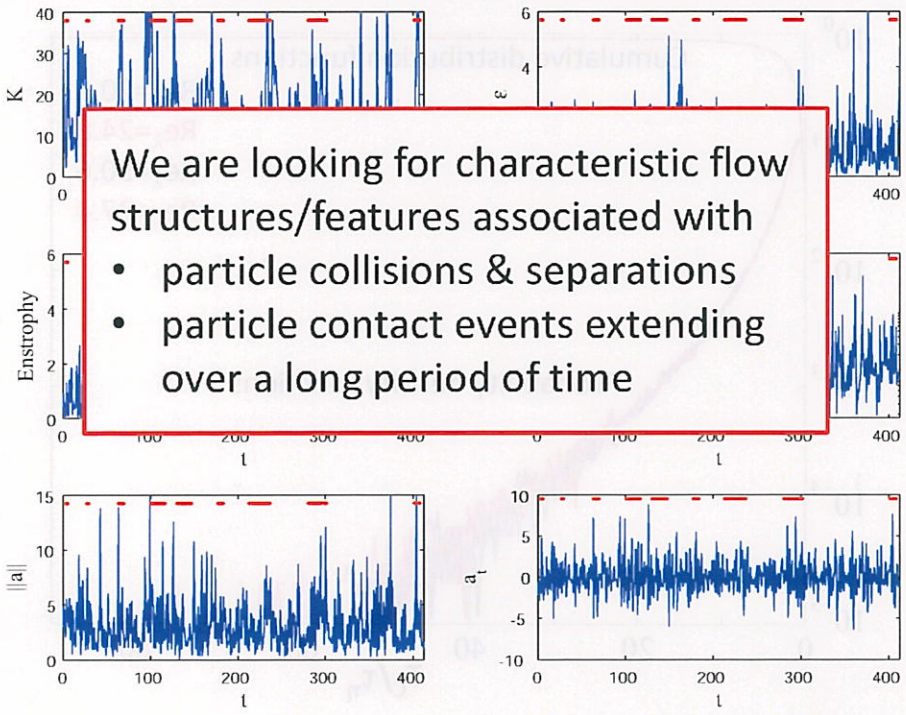


We are looking for characteristic flow structures/features associated with

- particle collisions & separations
- particle contact events extending over a long period of time



# Summary

- Collision statistics of tracer particles in isotropic turbulence has been studied
  - Both collision rate and contact duration can be scaled with Kolmogorov scales
  - Saffman-Turner theory well predicts DNS results

The phenomena is expected to be ubiquitous in more practical flows as well, since turbulence is locally more isotropic at higher Reynolds number